GD | C-63-021

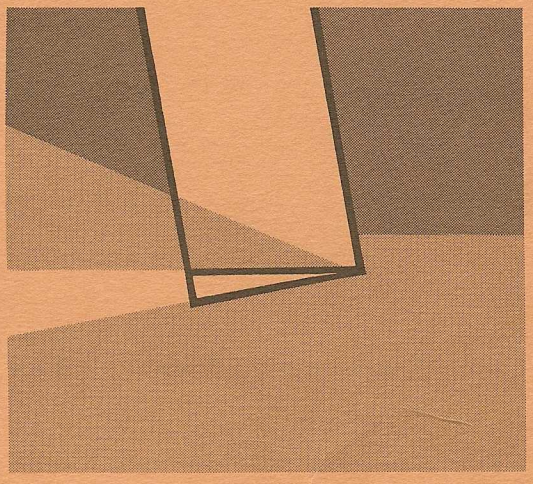

SUPERCAVITATING HYDROFOIL STUDIES

FEBRUARY 1963

GENERAL DYNAMICS | CONVAIR
Post Office Box 1950, San Diego 12, California

GDC-63-021

SUPERCAVITATING HYDROFOIL STUDIES

C. E. Jones, Jr.

February 1963

U. S. Navy Bureau of Ships

Contract NObs 84615

ABSTRACT

This report describes an experimental investigation to determine the hydrodynamic characteristics of a flat-plate supercavitating hydrofoil and a two-term supercavitating hydrofoil, both foils having an aspect ratio of 3.0. Force and moment measurements were made for a range of angles of attack from 9.65° to 15.5° and for depths of submersion of 0.333, 0.666, and 1.0 chord in supercavitating flow. Speed varied from 18 to 89 feet per second.

The experimental measurements showed that at $\sigma_v = 0.3$ and $h/c = 0.333$, the two-term foil has an L/D of 5.9 at the design C_L of 0.275. For the same conditions, the flat-plate foil has an L/D of 4.06. The lowest set angle of attack at which either foil can operate with its upper surface unwetted is 9.65°.

CONTENTS

INTRODUCTION

The objective of the experimental investigation described in this report was to furnish the Bureau of Ships with information on the force characteristics of two finite aspect ratio, supercavitating hydrofoils; i. e., a flat-plate foil and a two-term foil cambered to a design lift coefficient of $C_{Ld} = 0.275$. The section offsets for both hydrofoils were specified by BuShips.

The scope of the investigation was confined to obtaining data, and discussing the test results and flow behavior. Correlation with theory is not presented, inasmuch as the program was devoted to obtaining fundamental engineering data for design use and to providing results which would be compared with the experimental findings of other tanks.

The names "flat-plate" and "two-term", dealing with camber of the lower hydrofoil surface, stem from the initial work of Tulin and Burkart (Reference 1). In 1955 they presented a theory for steady, two-dimensional cavity flow about hydrofoil sections at zero cavitation number. They reported that supercavitating hydrofoil force and moment coefficients could be obtained through a mathematical transformation from thin airfoil theory. Linearized results for the two-dimensional flat-plate hydrofoil at infinite submergence were presented. In addition, Tulin and Burkart derived a two-dimensional family of minimum-drag hydrofoil sections whose lower surfaces were cambered to the mean lines of equivalent airfoils having two terms specified in their vorticity series expansion. These sections are known as two-term hydrofoils.

Section 6 of this report contains certain terms which designate the flow conditions encountered and, for the information of the reader, they are now defined.

Supercavitating flow denotes the flow regime where the upper surface of the hydrofoil is bounded by a cavity which forms at the leading edge of the foil and extends rearward a distance equal to or greater than the chord of the hydrofoil. Supercavitating flow may be achieved by increasing the speed of the hydrofoil causing a vapor cavity to form over its upper surface with the resultant condition designated as *vapor-cavitating flow.* In many cases, the upper surface cavity may become atmosphere-connected either by spontaneous natural air entrainment or by controlled air (or gas) feeding. At any rate, by either method the cavity pressure approaches atmospheric pressure and the resultant condition is designated as *ventilated flow.*

At certain foil positions or speeds, a cavity may not develop or it may partially develop (i. e., have a length less than the foil's chord). Under these circumstances the flow is designated as *non-cavitating*; no distinction is made between partially cavitating and non-cavitating flow.

While supercavitating force and moment characteristics were the prime concern of this program, there were many instances where non-cavitating flow did occur. Plots of non-cavitating lift, drag, and pitching moment coefficients are included for information.

Ventilated flow data by natural air entrainment was obtained at a submergence ratio $h/c = 0.333$ on both hydrofoils. Attempts to obtain ventilated flow using trip wires, probes, etc. were made; but, this data is not listed because of its unknown influence upon the hydrofoil force and moment characteristics. However, brief remarks about the observed effectiveness are included in this report.

1 | MODEL DESCRIPTION

Each hydrofoil model had a projected planform area of 27 sq. in. (3 in. by 9 in.), and was rectangular in planform, without twist, taper or dihedral.

Figure 1 shows a flat-plate hydrofoil section, and includes a tabulation of the section offsets. The figure shows the flat, lower surface of the section coinciding with the nose-tail line (the straight line drawn between the leading edge of the foil and the lower trailing edge). The upper surface of this foil was beveled at the leading edge. The bevel extended back to one-tenth of the hydrofoil chord at an angle of 9° 33' with the nose-tail line. Behind the bevel, the upper surface extended linearly back to a trailing edge thickness of 0.3519 in.

Figure 2 shows the section of the two-term foil, together with its offsets measured from the nose-tail line. This section does not represent the product of any optimization study; rather, it was recommended to BuShips by DTMB as one having a reasonable shape for practical use. It was designed (on the basis of two-dimensional flow at zero cavitation number) to operate at an angle of attack of 3.695° measured from the nose-tail line. At that design angle it was predicted to develop a design lift coefficient of 0.275.

Figure 2 shows a "foil reference line" which makes an angle of 0.973° with the nose-tail line. By the definition given in Reference 2, the foil reference line lies on the x-axis such that it is parallel to U_∞, and the two-term foil is ordinarily constructed with reference to this line. On this basis, when the foil is rotated to its design angle of attack, the reference line will be 3.695° minus 0.973° or 2.722° below the x-axis.

The single supporting strut (Figure 3) had a 3-inch chord and was parabolic in shape, terminating in a blunt trailing edge. The blunt trailing edge provided an air entrainment path from the atmosphere to the upper surface of the hydrofoil.

The model foils and the supporting strut were contour-cut from ARMCO 17-4PH steel blocks and finished to template dimensions by hand filing and polishing. After polishing, the foils and strut were heat-treated to increase their yield strength.

2 | INSTRUMENTATION

Figures 4 and 5 show the model in position for test, and the carriage with associated instrumentation.

Figure 6 is a closeup of the combined depth and angle of attack assembly box with the model mounted under it. This combined arrangement made it possible to vary model depth and angle of attack rapidly. To set an angle of attack on the model, the adjustment block (Figure 6) rotated the foil until a hole lined up with a corresponding prepositioned hole in the side of the assembly box. A tapered pin was driven through the two holes, thus setting the angle of attack of the model quite accurately. Each setting was checked with an angle block set between the strut and the lower horizontal surface of the assembly box. Following each angle of attack change, the depth of the model required adjustment. This was quickly accomplished by manually turning the jack screw mechanism (shown on top of the assembly box) until the leading edge of the model was at the desired depth.

The forces and moments of the foil were obtained by moment-type strain gage balances mounted in a "stacked" arrangement on the upper end of the strut. These balances were used in the same manner as in a previous program (Reference 3). All electrical signals generated by balance deflection during the test runs were transmitted via amplifiers to a recording oscillograph. The amplifiers and oscillograph were mounted on the carriage (Figures 4 and 5).

Figure 7 shows one of the hydrofoil models with the bending and torsion strain gage beams installed. One beam is shown with its contact point at 0.9c,

the other with its contact point at 0.5c. With this arrangement it was possible to measure tip deflection at these two points. Both beams were cantilevered from a point near the root at the trailing edge where their respective strain gages were situated. The strain gages were calibrated and equations established to convert the strain gage deflections of both gages to bending and torsional deflections of the foil tip, relative to the foil root.

Shore-mounted hangers positioned at five-foot intervals along the tank rails interrupted a light path to a carriage-mounted photo cell. The interruption — which was recorded as a sharp trace deflection on the oscillograph — furnished the distance-time history needed to compute the velocity at any instant during each run.

Motion pictures were taken periodically to observe flow behavior. Figures 4 and 5 show the mounting platform for the Bell & Howell 35mm Eyemo camera. The lighting arrangement used is also shown.

3 | TEST PROCEDURE

The tests were conducted in the Convair Towing Basin using the high-speed carriage and the hydraulic drive system. Normal force, axial force, and pitching moment about the midchord were measured over a range of speeds from 18.65 to 89.0 ft./sec. These speeds correspond to Reynold's numbers ranging from 3.85×10^5 to 1.83×10^6, based upon foil chord.

For each test speed, the cavitation number (based on vapor pressure) was computed using $\rho = 1.94$ slugs/ft.^{3}. Cavitation number varied between 0.27 and 7.45, which embraced all flow conditions from non-cavitating to ventilated flow.

The foils were tested at set angles of attack ranging from 7.8° to 15.5°. These angles were called "set" angles due to the manner in which the foils were mounted to the strut. The set angle of attack used throughout this report is defined as the angle formed by the intersection of the nose-tail line and the line parallel to the flow, U_∞. Therefore, in the case of the two-term foil, which has a reference line 0.973° above its nose-tail line, one must subtract 0.973° from the "set" angles listed in the data of this report to obtain the true angles of attack of the foil.

Measurements of foil tip deflection and tip twist were obtained for each two-term foil test run, and corrections for the effect of twist were applied to obtain its "rigid wing" lift coefficient. The correction for twist was found to be so small that no correction to the drag coefficient or pitching moment coefficient was made. Unfortunately, about halfway through the flat-plate foil tests, the

deflection strain gages failed. But, since the twist effect had been found earlier to be so small, it was decided in the interest of expediency to continue the flat-plate tests without taking deflection readings. This assumed that no serious error would result if an estimated correction — based upon deflection data recorded before the failure — were applied.

4 | DATA REDUCTION

Equations for the force and deflection strain gages were established for both models, and the equation constants were determined by model calibration in a static test rig. These constants were checked throughout the test program by periodic calibration checks.

The strain gage equations were programmed on the IBM 1620 computer. During the tests, all strain gage oscillograph traces for each run were manually read and card punched. Computer output consisted of hydrofoil bending and torsion deflections, cavitation number based on assumed vapor pressure, and lift, drag, and pitching moment in coefficient form based on projected foil planform of 27 sq. in. and a foil chord of 3 in.

Due to the method of mounting the force balances, normal force and axial force were recorded on the oscillograph roll. Coordinate-axis resolution was accomplished by the computer to obtain lift and drag using the formulas:

$$L = N \cos \alpha - A \sin \alpha$$

$$D = N \sin \alpha + A \cos \alpha$$

A preliminary series of test runs with the strut was conducted without the hydrofoils mounted. Tares obtained for drag and pitching moment were reduced to coefficient form and thereafter applied to the test results to eliminate strut effects.

5 | RESULTS

The lift, drag, and pitching moment coefficients (Tables 1 and 3), plotted against σ_v, are presented for both hydrofoils in Figures 13 through 30 and 39 through 56. These figures constitute the basic plots and are discussed in Section 6. In addition, a number of derived plots are presented to show clearly the variation of certain coefficients with selected parameters.

The major results of this study are listed as follows:

a. The superiority of the two-term foil was shown. This study shows that the two-term foil has a lift-drag ratio of 5.9 when operating at its design lift coefficient of 0.275 at $\sigma_v = 0.3$ and $h/c = 0.333$. At the same lift coefficient, the flat-plate foil has a lift-drag ratio of 4.06.

b. It was not possible to operate either foil at set angles of attack below 9.65° without wetting their upper surfaces.

c. Ventilated flow by natural air entrainment could be obtained only at $h/c = 0.333$. Vapor-cavitating flow was obtained at all submergence ratios.

6 | DISCUSSION OF RESULTS

6.1 FLOW CHARACTERISTICS

6.1.1 NON-CAVITATING FLOW — Figure 8 shows the two-term foil with its upper surface wetted. The trailing edge cavity extends the full span of the foil; at the foil tip, the tubular vortex cavity is shown with its apex touching the trailing edge. Each cavity forms at low speed, independently of the other. The trailing edge cavity originates at the surface behind the strut at low speeds. As the model accelerates to test speed, this cavity moves down the strut and spreads along the trailing edge. On the other hand, the vortex cavity originates in the wake of the foil and moves to the trailing edge as speed increases. It remains there until the model reaches a certain critical speed. At that point, it leaps forward to the leading edge in a shift that appears to initiate supercavitating flow.

Figure 9 shows the flat-plate foil in non-cavitating flow. This photograph is a print of a 16mm frame taken on reversal film. Consequently, in this negative print the white trailing edge cavity appears black, rather than white. During this test run, a cavitation bubble formed on the beveled leading edge. The appearance and rearward growth of this bubble were common occurrences during tests of this foil.

All non-cavitating runs exhibited stable flow patterns.

6.1.2 SUPERCAVITATING FLOW — Figures 10a through 10e are reproductions of 35mm motion picture frames showing the progressive change from vapor-cavitating flow to ventilating flow at ventilation inception speed.

Figure 10a shows the foil in a vapor-cavitating flow, a flow condition characterized by the frothy upper-surface cavity boundary which obscures the foil. The tip vortex cavity may be seen with its apex at the foil leading edge. Spray generation in vapor-cavitating flow was light.

In general, vapor-cavitating runs were not as stable as the non-cavitating flow runs; instead, the flow boundaries tended to pulsate.

The remaining photographs in the sequence (Figures 10b through 10e) depict the transition to ventilated flow. In this transition, the tip vortex momentarily becomes indistinguishable in the flow and, at the same time, the slope of the upper-surface cavity boundary increases markedly.

Figure 10e marks the end of the transition and shows the foil in fully ventilated flow. In this flow condition, the cavity boundary over the foil was stable. Flow separation was clean and the entire top surface of the foil was easily visible from above. Spray generation was extremely heavy, varying between three and four feet in height. A roaring noise accompanied the ventilated runs — in contrast to the whining sound characteristic of the vapor-cavitating runs.

6.1.3 VENTILATION DEVICES — Early in the test program, a series of tests was conducted to achieve ventilated flow at submergence ratios greater than $h/c = 0.333$ and at set angles of attack lower than $9.65°$.

During these tests, it became evident that water intended to "fill in" behind the strut and throttle the airflow. In an attempt to remedy this effect, a metal "glove" (Figure 11) was devised to fit over the strut leading edge and extend from the free surface down to the hydrofoil. This was intended to enlarge the air path by flow separation at the "step" created by the glove. The glove was not effective, however, as the air still was unable to make its way out over the foil span.

Trip wires and air probes were tested, both separately and simultaneously. Of the two, the trip wire appeared the most effective, but program limitations did not permit enough testing to arrive at definite conclusions concerning either

the trip wire or the air probe. Figure 12 shows the two-term foil in ventilated flow with a 0.017-in. diameter trip wire on its leading edge and air probes at the quarter-span points.

6.2 LIFT COEFFICIENT

Figures 13 through 15 and 22 through 24 illustrate the variation of lift coefficient with σ_v for both foils in supercavitating flow. The lowest set angle of attack at which supercavitating flow was achieved was 9.65°. At this angle, flow conditions were unstable and tended to vary between the limiting conditions of supercavitating and fully wetted flow. This instability occurred at all submergence ratios and is reflected in the test point scatter for that angle of attack.

The scatter on the two-term foil at a 9.65° angle of attack and submergence ratio of 1.0 is evident in Figure 24. Four vapor-cavitation test points are shown; the three high points were taken in one series of runs. The low point was obtained in another series of runs, many of which were rejected for lack of supercavitating flow. The trend of the test points was in complete opposition to the trend at higher angles of attack. The resultant curve — shown as a dashed line — is weighted between the limiting points and is aligned to be compatible with curves for higher angles of attack.

At h/c = 0.333, ventilated flow data was obtained successfully for both foils. Figures 13 and 22 indicate the ventilated test points as flagged symbols and the ventilated curves as dashed lines — this notation is also used for ventilated flow drag and pitching moment data in subsequent figures. The curves illustrate the hydrofoil force coefficients' virtual independence of σ_v in ventilated flow.

Cross-plots of the C_L versus σ_v curves (Figures 31 and 32) show the variation of the lift coefficient with angle of attack at constant cavitation number for each foil. The figures also indicate the effect of cavitation numbers on C_{L_α} and that the C_{L_α} decreases with the decreasing cavitation number.

The C_L curves for the two-term foil exhibit a fair degree of linearity with changing angle of attack. The flat-plate foil, unlike the two-term foil, has a reflex in its C_L curve which occurs at about a 12° angle of attack. Below 12°, the C_L curve has an extremely shallow slope; but, at some angle of attack above 12°, the lift increases rapidly with the angle of attack until at high angles of attack there is little difference between the corresponding C_L of the flat-plate and two-term foils (although the absolute values of C_L on the two-term foil are generally higher). The reflex in the flat-plate foil lift curve has been attributed to the beveled leading edge. At low angles of attack, it is believed that flow separation does not occur at the leading edge; instead, it takes place at the bevel, resulting in rather low lift coefficients. At an angle of attack of about 12°, the cavity jumps clear of the beveled region; this, it is felt, causes the marked increase in C_L as the angle of attack increases.

The effect of depth is shown in Figures 31 and 32. Generally, the lift curve slope at each angle of attack increased with decreasing submergence ratio. The average increase in lift coefficient (Figure 33) between h/c = 1.0 and 0.333 is approximately 0.04 for both foils at σ_v = 0.3.

6.3 DRAG COEFFICIENT

Plots of drag coefficient against σ_v for supercavitating flow are shown in Figures 16 through 18 for the flat-plate foil, and in Figures 25 through 27 for the two-term foil. From these figures, faired cross-plots (Figures 34 and 35) were prepared for selected cavitation numbers and for three submergence ratios to show the variation of drag coefficient with angle of attack. Ventilated drag coefficient curves are shown for h/c = 0.333.

The figures show the effect of σ_v on drag coefficient. Generally, the drag coefficient curves for both foils exhibited a divergent pattern with increasing σ_v and an increasing degree of variation with σ_v as angle of attack increased.

In the case of the two-term foil, Figures 25 and 26 show that below 11.7°

the drag coefficient increased with decreasing σ_V at h/c = 0.666 and 1.000. At h/c = 0.333, however, the test point dispersion tended to obscure this trend.

Comparing Figures 34 and 35 shows that, while the families of curves for each foil at all submergence ratios follow a generally consistent pattern, there is a marked difference in families. The curves for the two-term foil are almost flat in appearance, whereas, the drag coefficient curves for the flat foil are bowed and exhibit a marked decrease in slope at the low angles of attack. This rapid slope decrease or "leveling off" of the drag coefficient is believed to be caused by wetting of the beveled surface of the flat foil near the leading edge.

Ventilated drag coefficients for both models at h/c = 0.333 are shown in Figures 16 and 25. As in the case of the lift coefficient, each ventilated drag coefficient curve is lower than its vapor-cavitating counterpart and is essentially independent of σ_V.

6.4 PITCHING MOMENT COEFFICIENT

The extreme sensitivity of the force balances used in the test setup made the pitching moment (about 0.50c) by far the most difficult reaction to measure precisely. This difficulty is illustrated by the rather severe scatter of test points in Figures 19 through 21 and 28 through 30. In general, the pitching moment coefficient was positive for all submergence ratios tested. For both foils, it increased in magnitude as the submergence ratio increased. Further, at each submergence ratio, a slight increase in pitching moment was noted as the angle of attack increased. At equal conditions of depth and angle of attack, the flat-plate foil experienced higher positive pitching moments than the two-term foil.

The positive pitching moment values obtained in the study indicate that the center of pressure (C_M/C_L) for both models was forward of 0.50c. Estimates of center of pressure position indicated that the center of the flat-plate foil was approximately 0.24c forward of 0.50c at h/c = 1.0; whereas, the center of pressure of the two-term foil was about 0.03c forward of 0.50c at h/c = 1.0.

6.5 LIFT-DRAG RATIO COMPARISON

Variation of L/D with depth for three selected cavitation numbers is illustrated in Figures 36 and 37. Comparative plots of L/D against C_L at $\sigma_v = 0.3$ for the three submergence ratios are shown in Figures 38a through 38c.

Figures 36 and 37 indicate that in supercavitating flow there is little change in L/D between h/c = 0.333 and 1.000 for a fixed angle of attack. Within the σ_v range shown in the figures, L/D changes only slightly as σ_v varies, although lift and drag are dependent upon σ_v.

Figures 38a through 38c show the L/D increase as angle of attack decreases for each submergenc ratio. With both foils operating at the same angle of attack, there is little difference in their L/D ratios. But, compared on the basis of equal lift coefficient, the L/D of the two-term foil is considerably higher. Figure 38a indicates that, at the design C_L of 0.275, the two-term has an L/D of 5.9, compared to the flat-plate foil L/D of 4.06.

Ventilated values of L/D for both foils appear in Figure 38a. On the basis of equal lift coefficient, the ventilated L/D ratio for each foil was lower than the corresponding vapor-cavitating L/D ratio.

6.6 NON-CAVITATING FLOW

A number of test runs were conducted at low speeds where supercavitation did not occur. Plots of the non-cavitating data are included in Figures 38 through 56. The supercavitating test points discussed earlier are included in the plots to emphasize the force coefficient variation at the transition from non-cavitating to supercavitating flow.

Test points in the non-cavitating region are sparse — a result of the concentration upon supercavitating flow data. Consequently, rather extreme fairing was necessary to draw some of the lift and drag coefficient plots. The pitching moment coefficient points were plotted, but curves were not faired through highly scattered points.

Figures 38 through 56 show the transition $1.0 < \sigma_v < 2.0$. In certain cases, the force coefficients increased slightly at the inception of cavitation and fell off as σ_v decreased; in other cases, no coefficient increase was noted.

6.7 CORRECTION FOR THE EFFECT OF HYDROFOIL TWIST

Foil tip deflections and tip twist measurements were recorded to ascertain the degree of foil elastic deformation. It was anticipated that the twist, in particular, would be appreciable since measurements of each foil indicated that the center of twist was near the trailing edge. Test data, however, revealed rather modest values for deflections and twist. Consequently, the only correction made was for the effect of spanwise twist on the lift coefficient.

Foil-span twist effect can be stimated by using the classical solution for the torsional deflection of a rectangular, cantilevered wing (Reference 4). The differential equation for the torsion is:

$$\frac{d^2\Theta}{dz^2} = -\mu^2\Theta \tag{1}$$

where

$$\mu^2 = \frac{1}{GJ} C_{L_\alpha} (ec) \text{ eq.}$$

The general solution of Equation 1 is

$$\Theta = A_T \sin \mu z + B_R \cos \mu z. \tag{2}$$

Applying the boundary condition

$$\Theta = 0, \quad z = 0.$$

The solution is

$$\Theta = A_T \sin \mu z. \tag{3}$$

Where A_T is a constant (for a particular flow condition) which can be evaluated by applying the boundary condition at the tip.

Equation 1 indicates that estimating the effect of twist is complicated by the number of variables present; for example, Equation 1 depends upon C_{L_α} which in vapor-cavitating flow varies with σ_v and depth. The factor, (ec), which represents the distance between the foil center of twist and center of pressure, also varies with σ_v and depth. Presence of dynamic pressure, q, shows the dependency of Equation 1 upon the speed.

To reduce the computational labor without seriously degrading the results, certain assumptions were made:

a. The variation of lift slope with depth of submergence is ignored.

b. The distance between the center of twist and the center of pressure, symbolized by (ec), is constant along the span and is independent of the depth of submergence.

c. The dynamic pressure, q, is approximately equal to $2,000/\sigma_v$.

On the basis of these assumptions, the basic load distribution and the incremental load distribution of the "rigid" foil due to foil twist were estimated by Multhopp's method based upon Prandtl's lifting line theory. In applying this method, the section lift slopes were obtained by multiplying their experimental values by: $\frac{AR + 1}{AR}$. Refer to Reference 5.

Assuming symmetrical loading, the lift distribution for the rigid foil and the incremental load distribution were computed using four Multhopp stations:

$$z = \frac{b}{2} \begin{Bmatrix} 0.92388 \\ 0.70711 \\ 0.38268 \\ 0 \end{Bmatrix}$$

Before computing the load distribution due to twist, the function Θ_T/A_T as a function of σ_v was determined using Equation 3 and the following foil characteristics:

Flat-Plate Foil	Two-Term Foil
$J = 0.2676$ in.^{4}	$J = 0.1812$ in.^{4}
$G = 10.5 \times 10^6$ psi	$G = 10.5 \times 10^6$ psi
(ec) = 1.40 in.	(ec) = 1.07 in.
n = 0.550 in.	n = 0.669 in.

Calculations of Θ_T/A_T were made for $\sigma_v = 0.3$, 0.5, 0.7, and 0.9 for arbitrary values of Θ_T; the results are plotted in Figure 57. Then, using Figure 57 and Equation 3, the twist angles at interior span points were determined and the incremental lift distribution was computed for selected values of σ_v and Θ_T. This lift distribution curve is shown in Figure 58. This curve applies to both hydrofoils over the range $0.3 < \sigma_v < 0.7$. In the calculations, the foregoing foil characteristics combined in such a manner that twist angles at corresponding interior span points were found to be nearly identical for the same flow conditions.

With Figure 58 and the basic lift distribution curves (Figures 59 and 60) which vary with α, a corrective function, K, was computed and applied to the experimental lift coefficients to give the corrected values in the data. This corrective function is plotted in Figures 61 and 62 as a function of tip twist for various angles of attack.

The twist deflection data for the flat-plate foil, given in Table 2, was obtained during the first part of the program. This data, in conjunction with the curve in Figure 61, was used to obtain the corrected values of lift coefficient given in Table 1.

Table 3 contains the corrected values of lift coefficient for the two-term foil.

Figures 61 and 62 show that for $0.3 < \sigma_v < 0.7$, the maximum correction for twist did not exceed 5.5 per cent.

7 | CONCLUSIONS AND RECOMMENDATIONS

Judging from the results of experimental study, successful operation of a supercavitating hydrofoil in vapor-cavitating or ventilated flow at low angles of attack will depend largely upon the design of the foil's upper surface. Flow separation must occur at the foil leading edge. In this regard, the beveled upper surface (near the leading edge) is considered detrimental to hydrofoil performance as it encourages upper-surface wetting.

If supercavitating flow is desired at lower angles of attack, it is recommended that the slope of the bevel be reduced. Although the upper surface of the two-term foil did not have a bevel, it is recommended that the slope of the upper surface be reduced to achieve supercavitating flow at low angles of attack. This can be accomplished — at some sacrifice of lift-drag ratio — by modifying the foil camber.

It is concluded that, within the 20- to 85-fps speed range covered by these tests, the parabolic strut alone cannot provide a satisfactory air path at submergence ratios equal to or greated than two-thirds. To achieve and maintain ventilated flow at submergence ratios equal to or greater than two-thirds, the strut must be assisted by other devices.

8 | REFERENCES

1. Tulin, M. P. and Burkart, M. P., "Linearized Theory for Flows About Lifting Surfaces at Zero Cavitation Number," DTMB Report C-638, 1955.

2. Auslaender, J., "Low Drag Supercavitating Hydrofoil Sections, "Hydronautics Technical Report 001-7, April 1962.

3. Jones, C. E., "Flapped Hydrofoils in Smooth Water - Subcavitating Flow," General Dynamics/Convair Report ZH-153, November 1961.

4. Fung, Y. C., "An Introduction to the Theory of Aero-Elasticity," John Wiley and Sons, Inc.

5. Johnson, V. E., "Theoretical and Experimental Investigation of Arbitrary Aspect Ratio, Supercavitating Hydrofoils Operating Near the Free Water Surface," NACA Report RM L57I16, 12 December 1957.

9 | SYMBOLS

A	Axial force (parallel to nose-tail line), lb.
A_T	Arbitrary constant
AR	Aspect ratio, b/c
b	Hydrofoil span, ft.
B_R	Arbitrary constant
c	Chord, ft.
C_D	Drag coefficient, D/qS
C_{D_α}	Drag curve slope, $\partial C_D/\partial_\alpha$
C_L	Lift coefficient, L/qS
C_{L_α}	Lift curve slope, $\partial C_L/\partial_\alpha$
$\frac{C_L}{C_D}$	Lift-drag ratio
C_M	Pitching moment coefficient about 0.5c, M/qSc. A positive moment causes the leading edge to be displaced upward.
C_{M_α}	Pitching moment curve slope, $\partial C_M/\partial_\alpha$
$\frac{C_M}{C_L}$	Distance of the center of pressure from midchord, expressed as a fraction of the chord.
D	Drag, lb.
e	Distance between the hydrofoil's center of twist and center of pressure, expressed as a fraction of the chord.

G	Shear modulus of rigidity, psi
h	Depth of leading edge of foil below the static free surface, ft.
h/c	Submergence ratio
J	Polar moment of inertia, $in.^4$
L	Lift, lb.
M	Pitching moment about 0.5c, ft.-lb.
N	Normal force (normal to nose-tail line), lb.
n	Horizontal distance between the trailing edge and the center of twist.
p_v	Vapor pressure, $lb./ft.^2$
p_∞	Free stream pressure, $lb./ft.^2$
q	Dynamic pressure, $lb./ft.^2$
S	Planform area, $ft.^2$
t	Thickness of the foil at any distance x
U_∞	Speed of model, ft./sec.
x	Distance from leading edge along x-axis (nose-tail line is the x-axis)
y	Distance along y-axis
z	Distance along the hydrofoil span, measured from the midspan
α	Angle of attack, degrees
σ_v	Cavitation number based on vapor pressure, $\frac{p_\infty - p_v}{q}$
ρ	Density, $slugs/ft.^3$
Θ	Geometric twist of any point on the hydrofoil span relative to the root, degrees
Θ_T	Geometric twist of the tip of the hydrofoil relative to the root, degrees
δ_T	Deflection of the tip of the hydrofoil (at 0.9c) relative to the root, in.

10 | TABLES

Table 1. Test Data
Flat-Plate Hydrofoil

Run	h/c	α	U_∞	σ_v	C_L	C_D	$C_{M_{\frac{1}{2}c}}$
12596	0.333	15.50	20.5	5.12	0.272	0.079	- 0.141
12597	0.333	15.50	29.4	2.49	0.289	0.085	+ 0.059
12600	0.333	15.50	27.2	2.91	0.279	0.084	- 0.073
12602	0.333	15.50	36.4	1.62	0.281	0.082	+ 0.017
12604	0.333	15.50	47.9	0.938	0.281	0.082	+ 0.021
12606	0.333	15.50	58.5	0.629	0.280	0.081	+ 0.037
12609	0.333	15.50	67.2	0.477	0.290	0.084	+ 0.028
12611	0.333	15.50	78.5	0.349	0.286	0.084	+ 0.019
12613	0.333	15.50	86.6	0.287	0.289	0.083	+ 0.032
12618	0.333	15.50	88.2	0.277	0.292	0.086	+ 0.026
12572	0.666	15.50	54.2	0.735	0.439	0.132	+ 0.045
12574	0.666	15.50	58.5	0.631	0.409	0.124	+ 0.035
12576	0.666	15.50	65.6	0.501	0.387	0.119	+ 0.048
12578	0.666	15.50	64.2	0.524	0.396	0.121	+ 0.049
12580	0.666	15.50	78.5	0.350	0.372	0.114	+ 0.051
12583	0.666	15.50	54.6	0.724	0.454	0.137	+ 0.060
12589	0.666	15.50	63.2	0.540	0.399	0.122	+ 0.071
12592	0.666	15.50	79.7	0.340	0.360	0.111	+ 0.059
12552	1.000	15.50	58.0	0.643	0.415	0.130	+ 0.080
12554	1.000	15.50	63.4	0.538	0.395	0.124	+ 0.091
12556	1.000	15.50	73.8	0.397	0.357	0.112	+ 0.095
12558	1.000	15.50	80.7	0.332	0.351	0.109	+ 0.081
12570	1.000	15.50	52.4	0.788	0.421	0.129	+ 0.011
12572	1.000	15.50	53.7	0.750	0.422	0.130	+ 0.088
12522	0.333	13.89	18.9	6.03	0.403	0.105	+ 0.013
12524	0.333	13.89	19.8	5.49	0.220	0.057	- 0.026
12526	0.333	13.89	29.4	2.49	0.258	0.068	+ 0.018
12528	0.333	13.89	35.9	1.67	0.262	0.070	+ 0.008
12530	0.333	13.89	43.8	1.22	0.255	0.068	- 0.069
12532	0.333	13.89	59.2	0.614	0.366	0.099	+ 0.028
12534	0.333	13.89	66.0	0.494	0.262	0.070	+ 0.027
12536	0.333	13.89	77.3	0.360	0.260	0.069	+ 0.023
12538	0.333	13.89	83.8	0.307	0.335	0.091	+ 0.040
12540	0.333	13.89	85.5	0.294	0.256	0.067	+ 0.019

Table 1. Test Data (Continued)
Flat-Plate Hydrofoil (Continued)

Run	h/c	α	U_∞	σ_v	C_L	C_D	$C_{M_{\frac{1}{2}c}}$
13612	0.333	13.89	67.4	0.474	0.258	0.068	+ 0.030
13614	0.333	13.89	67.6	0.471	0.252	0.065	+ 0.026
13616	0.333	13.89	67.6	0.471	0.254	0.066	+ 0.031
13618	0.333	13.89	67.9	0.467	0.253	0.066	+ 0.039
12504	0.666	13.89	18.65	6.20	0.339	0.075	- 0.683
12510	0.666	13.89	51.4	0.817	0.391	0.106	+ 0.035
12512	0.666	13.89	54.8	0.719	0.372	0.103	+ 0.044
12514	0.666	13.89	63.7	0.532	0.338	0.096	+ 0.030
12516	0.666	13.89	74.9	0.385	0.317	0.087	+ 0.057
12518	0.666	13.89	83.4	0.310	0.307	0.085	+ 0.047
12492	1.000	13.89	58.5	0.632	0.341	0.097	+ 0.087
12494	1.000	13.89	63.2	0.542	0.316	0.089	+ 0.089
12496	1.000	13.89	75.5	0.379	0.169	0.055	- 0.070
12498	1.000	13.89	79.5	0.342	0.290	0.081	+ 0.079
12604	1.000	13.89	67.8	0.471	0.291	0.084	+ 0.037
12606	1.000	13.89	69.0	0.454	0.280	0.078	+ 0.057
12608	1.000	13.89	68.3	0.464	0.285	0.080	+ 0.048
12610	1.000	13.89	67.6	0.473	0.289	0.081	+ 0.050
12294	0.333	11.70	55.3	0.707	0.221	0.045	- 0.008
12300	0.333	11.70	58.3	0.633	0.261	0.059	+ 0.001
12302	0.333	11.70	65.2	0.506	0.218	0.046	+ 0.023
12306	0.333	11.70	75.8	0.375	0.220	0.048	+ 0.016
12308	0.333	11.70	83.4	0.309	0.220	0.051	+ 0.013
12390	0.333	11.70	55.4	0.701	0.183	0.040	- 0.031
12392	0.333	11.70	62.0	0.560	0.219	0.048	+ 0.002
12394	0.333	11.70	78.2	0.352	0.212	0.049	+ 0.010
12396	0.333	11.70	84.4	0.302	0.224	0.052	+ 0.017
12399	0.333	11.70	84.8	0.299	0.227	0.048	- 0.011
12278	0.666	11.70	55.9	0.691	0.253	0.061	+ 0.007
12280	0.666	11.70	59.9	0.601	0.247	0.058	+ 0.043
12282	0.666	11.70	64.5	0.519	0.251	0.059	+ 0.043
12284	0.666	11.70	77.0	0.364	0.237	0.056	+ 0.042
12286	0.666	11.70	85.9	0.292	0.243	0.057	+ 0.035
12386	0.666	11.70	52.8	0.774	0.264	0.062	+ 0.048

Table 1. Test Data (Continued)
Flat-Plate Hydrofoil (Continued)

Run	h/c	α	U_∞	σ_v	C_L	C_D	$C_{M_{\frac{1}{2}c}}$
12218	1.000	11.70	58.4	0.634	0.228	0.055	+ 0.046
12220	1.000	11.70	62.2	0.559	0.228	0.054	+ 0.059
12222	1.000	11.70	67.6	0.473	0.229	0.054	+ 0.053
12224	1.000	11.70	77.0	0.364	0.231	0.055	+ 0.062
12226	1.000	11.70	85.1	0.298	0.235	0.056	+ 0.060
12228	1.000	11.70	89.0	0.273	0.226	0.054	+ 0.070
12376	1.000	11.70	54.4	0.731	0.241	0.061	+ 0.021
12380	1.000	11.70	62.5	0.554	0.238	0.057	+ 0.051
12382	1.000	11.70	76.4	0.371	0.234	0.057	- 0.126
12460	0.333	9.65	76.0	0.373	0.189	0.036	+ 0.014
12462	0.333	9.65	84.4	0.302	0.195	0.036	+ 0.019
13554	0.333	9.65	73.5	0.398	0.185	0.034	+ 0.006
13556A	0.333	9.65	83.7	0.307	0.132	0.031	- 0.047
13556B	0.333	9.65	83.7	0.272	0.139	0.028	- 0.058
12440	0.666	9.65	64.5	0.519	0.201	0.041	+ 0.041
12442	0.666	9.65	75.5	0.379	0.200	0.040	+ 0.035
12444	0.666	9.65	83.6	0.309	0.195	0.039	+ 0.034
13542	0.666	9.65	70.2	0.438	0.197	0.038	+ 0.021
13546	0.666	9.65	71.8	0.419	0.200	0.039	+ 0.025
13548	0.666	9.65	66.7	0.485	0.176	0.033	+ 0.005
12410	1.000	9.65	65.0	0.498	0.195	0.039	+ 0.064
12412	1.000	9.65	76.4	0.371	0.185	0.032	+ 0.062
12414	1.000	9.65	83.5	0.310	0.195	0.040	- 0.081
12470	1.000	9.65	72.8	0.408	0.192	0.039	+ 0.068
12473	1.000	9.65	85.2	0.298	0.187	0.038	+ 0.063

Non-Cavitating Data - Flat-Plate Hydrofoil

Run	h/c	α	U_∞	σ_v	C_L	C_D	C_M
12564	0.666	15.5	19.26	5.82	0.655	0.156	- 0.108
12566	0.666	15.5	27.40	2.87	0.689	0.162	+ 0.040
12568	0.666	15.5	34.60	1.80	0.531	0.131	+ 0.745
12570	0.666	15.5	45.20	1.06	0.550	0.160	- 0.646
12588	0.666	15.5	46.90	0.98	0.550	0.159	- 0.571

Table 1. Test Data (Continued)
Non-Cavitating Data - Flat-Plate Hydrofoil

Run	h/c	α	U_∞	σ_v	C_L	C_D	C_M
12544	1.000	15.5	20.10	5.35	0.728	0.173	+ 0.200
12546	1.000	15.5	27.05	2.96	0.697	0.161	+ 0.140
12548	1.000	15.5	34.80	1.79	0.695	0.168	- 0.657
12550	1.000	15.5	41.40	1.26	0.724	0.170	+ 0.173
12565	1.000	15.5	29.60	2.47	0.632	0.164	- 0.278
12568	1.000	15.5	33.20	1.96	0.677	0.159	+ 0.059
13562	0.333	13.89	66.70	0.483	0.214	0.057	- 0.027
12506	0.666	13.89	29.30	2.51	0.466	0.118	- 0.416
12508	0.666	13.89	36.40	1.63	0.572	0.119	+ 0.067
12478	1.000	13.89	28.70	2.63	0.581	0.110	+ 0.231
12480	1.000	13.89	19.60	5.63	0.580	0.115	+ 0.200
12486	1.000	13.89	25.50	3.33	0.571	0.116	+ 0.159
12488	1.000	13.89	34.20	1.85	0.571	0.119	+ 0.144
12490	1.000	13.89	43.10	1.16	0.583	0.121	+ 0.193
12290	0.333	11.70	28.40	2.67	0.296	--	+ 0.165
12292	0.333	11.70	41.00	1.28	0.311	0.052	+ 0.275
12296	0.333	11.70	44.70	1.08	0.308	0.055	+ 0.301
12298	0.333	11.70	36.70	1.60	0.299	0.075	- 0.065
12274	0.666	11.70	30.10	2.38	0.346	0.077	- 0.259
12276	0.666	11.70	37.70	1.50	0.351	0.077	- 0.219
12288	0.666	11.70	45.00	1.07	0.300	0.070	+ 0.026
12095	1.000	11.70	28.40	2.68	0.370	0.083	- 0.477
12097	1.000	11.70	40.70	1.31	0.352	0.079	- 0.387
12099	1.000	11.70	46.30	1.01	0.366	0.084	- 0.338
12450	0.333	9.65	29.70	2.44	0.313	0.047	- 0.092
12452	0.333	9.65	36.70	1.60	0.316	0.047	- 0.026
12454	0.333	9.65	53.10	0.76	0.320	0.049	+ 0.046
12456	0.333	9.65	55.30	0.704	0.324	0.050	+ 0.043
12458	0.333	9.65	63.90	0.527	0.328	0.050	+ 0.049
12430	0.666	9.65	26.00	3.19	0.321	0.044	+ 0.012
12432	0.666	9.65	35.20	1.74	0.320	0.044	+ 0.065
12434	0.666	9.65	49.00	0.899	0.308	0.050	+ 0.045
12436	0.666	9.65	57.00	0.664	0.277	0.033	+ 0.583
12438	0.666	9.65	63.50	0.535	0.288	0.053	- 0.280
13538	0.666	9.65	38.60	1.45	0.329	0.041	+ 0.067
13540	0.666	9.65	57.20	0.660	0.258	0.030	+ 0.471

Table 1. Test Data (Continued)
Non-Cavitating Data - Flat-Plate Hydrofoil

Run	h/c	α	U_∞	σ_v	C_L	C_D	C_M
12402	1.000	9.65	29.90	2.42	0.324	0.047	+ 0.090
12404	1.000	9.65	36.40	1.63	0.299	0.042	+ 0.086
12406	1.000	9.65	46.50	1.00	0.338	0.048	+ 0.165
12408	1.000	9.65	56.40	0.68	0.281	0.037	+ 0.529
12466	1.000	9.65	56.50	0.677	0.323	0.050	+ 0.103
12468	1.000	9.65	62.70	0.550	0.270	0.034	+ 0.595
12350	0.333	7.80	30.60	2.30	0.248	0.029	+ 0.012
12352	0.333	7.80	37.70	1.51	0.236	0.029	- 0.009
12354	0.333	7.80	46.50	0.996	0.249	0.030	+ 0.048
12356	0.333	7.80	61.60	0.567	0.242	0.029	+ 0.070
12358	0.333	7.80	65.60	0.500	0.253	0.032	+ 0.020
12360	0.333	7.80	75.80	0.375	0.259	0.031	+ 0.077
12362	0.333	7.80	85.10	0.297	0.159	0.025	+ 0.023
12332	0.666	7.80	31.30	2.203	0.222	0.024	- 0.006
12334	0.666	7.80	37.80	1.51	0.237	0.024	+ 0.074
12336	0.666	7.80	46.50	1.00	0.239	0.027	+ 0.083
12338	0.666	7.80	60.60	0.588	0.242	0.028	+ 0.088
12340	0.666	7.80	62.50	0.552	0.249	0.029	+ 0.065
12342	0.666	7.80	72.70	0.408	0.257	0.030	+ 0.071
12344	0.666	7.80	72.70	0.408	0.260	0.031	+ 0.071
12346	0.666	7.80	80.70	0.331	0.217	0.031	- 0.147
12316	1.000	7.80	29.50	2.48	0.222	0.035	- 1.130
12318	1.000	7.80	38.10	1.49	0.233	0.024	+ 0.094
12320	1.000	7.80	44.40	1.10	0.236	0.024	+ 0.126
12322	1.000	7.80	60.60	0.589	0.234	0.027	+ 0.107
12324	1.000	7.80	64.50	0.520	0.246	0.029	+ 0.092
12326	1.000	7.80	74.10	0.394	0.257	0.029	+ 0.124
12328	1.000	7.80	83.30	0.312	0.219	0.033	- 0.209

Table 2. Deflection and Twist Data — Flat-Plate Foil

Run	h/c	α Deg.	U_∞ Ft./Sec.	σ_v	δ_T Inches	Θ_T Degrees
13944	0.333	11.81	19.04	5.94	0.0037	- 0.0064
13946	0.333	11.81	48.80	1.12	0.0076	- 0.1104
13948	0.333	11.81	47.80	0.94	0.0093	- 0.1577
13951	0.333	11.81	55.6	0.70	0.0130	- 0.0772
13953	0.333	11.81	69.3	0.45	0.0259	- 0.1184
13960	0.333	11.81	81.2	0.33	0.0241	- 0.1613
13963	0.666	11.81	27.0	5.04	0.0047	+ 0.0221
13965	0.666	11.81	50.5	0.85	0.0101	- 0.1185
13967	0.666	11.81	53.6	0.75	0.0147	- 0.3209
13969	0.666	11.81	77.0	0.36	0.312	+ 0.1413
13974	1.000	11.81	20.45	5.17	0.0039	+ 0.0169
13976	1.000	11.81	45.40	1.05	0.0114	+ 0.0295
13978	1.000	11.81	54.30	0.73	0.0174	+ 0.0671
13980	1.000	11.81	77.50	0.36	0.0289	+ 0.0938
13989	0.333	9.77	17.00	7.45	0.0019	+ 0.0956
14042	0.333	9.77	20.60	5.07	0.0047	+ 0.1409
14044	0.333	9.77	42.60	1.19	0.0097	+ 0.0761
14046	0.333	9.77	54.4	0.73	0.0167	+ 0.1261
14048	0.333	9.77	72.5	0.41	0.0203	+ 0.1056
14024	0.666	9.77	20.6	5.08	0.0030	+ 0.0853
14026	0.666	9.77	37.4	1.54	0.0080	+ 0.0565
14028	0.666	9.77	52.1	0.80	0.0161	+ 0.0988
14030	0.666	9.77	62.4	0.55	0.0246	+ 0.0897
14032	0.666	9.77	79.3	0.34	0.0168	- 0.0276
14062	1.000	9.77	21.30	4.77	0.0031	+ 0.0933
14064	1.000	9.77	35.50	1.72	0.0070	+ 0.0641
14066	1.000	9.77	62.90	0.55	0.0243	+ 0.1139
14068	1.000	9.77	72.00	0.42	0.0184	+ 0.1042
14106	1.000	9.77	73.50	0.40	0.0200	+ 0.110
14095	1.000	9.77	72.50	0.412	0.0198	+ 0.067
14142	1.000	9.77	72.20	0.415	0.0223	+ 0.113
14140	1.000	9.77	73.20	0.404	0.0226	+ 0.117
14150	1.000	9.77	73.90	0.396	0.0213	+ 0.081
14148	1.000	9.77	71.40	0.424	0.0204	+ 0.131
14130	1.000	9.77	70.70	0.433	0.0046	+ 0.181
14126	1.000	9.77	67.40	0.476	0.0167	+ 0.110

Table 2. Deflection and Twist Data — Flat-Plate Foil (Continued)

Run	h/c	α Deg.	U_∞ Ft./Sec.	σ_v	δ_T Inches	Θ_T Degrees
14128	1.000	9.77	70.20	0.439	0.0018	- 0.177
14075	1.000	9.77	71.70	0.421	0.0182	+ 0.098
14087	1.000	9.77	76.90	0.366	0.0213	+ 0.117
14131	1.000	9.77	50.80	0.838	0.0162	+ 0.116
14134	1.000	9.77	57.20	0.661	0.0224	+ 0.160
14099	1.000	9.77	72.20	0.415	0.217	+ 0.0658
14097	1.000	9.77	72.20	0.415	0.0227	+ 0.0943
14104	1.000	9.77	72.90	0.407	0.0241	+ 0.1640
14184	0.333	7.76	21.50	4.661	0.0030	+ 0.0773
14186	0.333	7.76	37.00	1.572	0.0077	+ 0.0693
14188	0.333	7.76	58.90	0.621	0.0158	+ 0.0949
14194	0.333	7.76	79.70	0.339	0.0308	+ 0.2409
14172	0.666	7.76	20.98	4.903	0.0015	+ 0.1017
14174	0.666	7.76	35.40	1.722	0.0047	+ 0.0701
14176	0.666	7.76	38.60	1.449	0.0070	+ 0.0895
14178	0.666	7.76	60.10	0.597	0.0195	+ 0.2007
14180	0.666	7.76	78.00	0.355	0.0318	+ 0.2553
14156	1.000	7.76	23.00	4.091	0.0030	+ 0.0853
14158	1.000	7.76	37.80	1.514	0.0065	+ 0.0509
14160	1.000	7.76	39.20	1.408	0.0073	+ 0.0594
14162	1.000	7.76	42.30	1.209	0.0079	+ 0.0619
14164	1.000	7.76	65.40	0.506	0.0211	+ 0.1589
14166	1.000	7.76	77.90	0.357	0.0321	+ 0.2145
14196	0.333	5.89	21.60	4.615	0.0005	+ 0.107
14198	0.333	5.89	41.20	1.268	0.0061	+ 0.092
14202	0.333	5.89	61.40	0.571	0.0134	+ 0.109
14204	0.333	5.89	81.40	0.325	0.0231	- 0.008
14210	0.666	5.89	23.55	3.891	0.0016	+ 0.097
14212	0.666	5.89	42.20	1.212	0.0051	+ 0.029
14214	0.666	5.89	62.20	0.558	0.0126	+ 0.042
14217	0.666	5.89	79.90	0.338	0.0217	- 0.046
14224	1.000	5.89	23.90	3.787	0.0018	+ 0.101
14226	1.000	5.89	43.10	1.165	0.0053	+ 0.055
14228	1.000	5.89	62.80	0.549	0.0118	+ 0.033
14230	1.000	5.89	84.00	0.307	0.0216	+ 0.009

Table 3. Test Data
Two-Term Hydrofoil

Run	h/c	α	U_∞	σ_v	C_L	C_D	$C_{M_{\frac{1}{2}c}}$	δ_T Inches	Θ_T Deg.
13044	0.333	15.5	28.0	2.74	0.372	0.100	-0.017	0.0100	-0.1371
13048	0.333	15.5	43.2	1.15	0.388	0.108	+0.014	0.0239	-0.0937
13050	0.333	15.5	56.4	0.677	0.569	0.167	+0.005	0.0540	0.0359
13052	0.333	15.5	62.2	0.556	0.526	0.152	+0.025	0.0603	0.1361
13054	0.333	15.5	72.8	0.406	0.471	0.140	+0.020	0.0724	0.2524
13056	0.333	15.5	79.1	0.344	0.469	0.141	+0.033	0.0761	0.5947
13032	0.666	15.5	56.6	0.674	0.541	0.158	+0.033	0.0535	0.0854
13034	0.666	15.5	63.8	0.530	0.485	0.144	+0.018	0.0603	0.1599
13036	0.666	15.5	72.0	0.416	0.479	0.145	+0.034	0.0707	0.3727
13038	0.666	15.5	80.7	0.331	0.453	0.138	+0.041	0.0850	0.4475
13012	1.000	15.5	53.5	0.756	0.551	0.163	+0.015	0.0487	0.0557
13014	1.000	15.5	60.7	0.587	0.512	0.155	+0.058	0.0573	0.1233
13016	1.000	15.5	70.5	0.435	0.485	0.149	+0.072	0.0703	0.2744
13018	1.000	15.5	80.0	0.338	0.436	0.138	+0.062	0.0781	0.7865
12984	0.333	13.89	25.4	3.34	0.475	0.118	-0.169	0.0102	-0.0474
12986	0.333	13.89	35.1	1.75	0.378	0.094	-0.074	0.0138	0.0056
12988	0.333	13.89	47.8	0.942	0.335	0.081	-0.006	0.0225	0.0159
12990	0.333	13.89	54.8	0.717	0.340	0.083	-0.007	0.0307	-0.0289
12992	0.333	13.89	55.6	0.696	0.435	0.112	-0.017	0.0397	0.0420
12994	0.333	13.89	61.2	0.575	0.467	0.120	+0.004	0.0517	0.0826
12996	0.333	13.89	71.8	0.418	0.443	0.118	-0.006	0.0682	0.1539
12998	0.333	13.89	79.5	0.341	0.422	0.112	+0.006	0.0772	0.2820
12972	0.666	13.89	57.5	0.653	0.463	0.125	+0.035	0.0493	-0.0034
12974	0.666	13.89	63.1	0.542	0.449	0.120	+0.043	0.0556	0.0159
12976	0.666	13.89	72.5	0.410	0.412	0.112	+0.038	0.0651	0.2651
12978	0.666	13.89	77.0	0.364	0.424	0.116	+0.037	0.0739	0.3370
12956	1.000	13.89	58.0	0.643	0.467	0.125	+0.060	0.0508	-0.0375
12958	1.000	13.89	62.7	0.550	0.458	0.124	+0.054	0.0551	0.1032
12960	1.000	13.89	70.7	0.433	0.436	0.118	+0.068	0.0652	0.1226
12962	1.000	13.89	77.9	0.356	0.405	0.111	+0.049	0.0738	0.1330
13624	0.333	11.7	60.3	0.592	0.298	0.064	+0.011	--	--
13626	0.333	11.7	60.3	0.592	0.290	0.061	+0.006	--	--
13628	0.333	11.7	59.9	0.600	0.294	0.061	+0.029	--	--
13636	0.333	11.7	62.9	0.544	0.296	0.062	+0.012	--	--
13638	0.333	11.7	64.1	0.524	0.293	0.061	+0.012	--	--

Table 3. Test Data (Continued)
Two-Term Hydrofoil (Continued)

Run	h/c	α	U_∞	σ_v	C_L	C_D	$C_{M_{\frac{1}{2}c}}$	δ_T Inches	Θ_T Deg.
13648	0.333	11.7	66.7	0.484	0.387	0.087	+0.024	--	--
13650	0.333	11.7	65.1	0.508	0.385	0.086	+0.024	--	--
12896	0.333	11.7	25.2	3.39	0.289	0.062	-0.211	0.0077	-0.0526
12900	0.333	11.7	52.7	0.775	0.278	0.057	-0.029	0.0243	0.0187
12902	0.333	11.7	55.9	0.689	0.381	0.083	-0.012	0.0355	0.0957
12904	0.333	11.7	57.2	0.658	0.377	0.083	-0.023	0.0365	0.1014
12906	0.333	11.7	65.9	0.496	0.292	0.061	-0.004	0.0354	0.1529
12908	0.333	11.7	76.0	0.373	0.343	0.078	-0.007	0.0558	0.2999
12910	0.333	11.7	82.0	0.320	0.375	0.085	-0.001	0.0746	0.1872
12920	0.666	11.7	59.9	0.601	0.371	0.084	+0.028	0.0392	0.1531
12922	0.666	11.7	66.7	0.485	0.368	0.084	+0.034	0.0470	0.2236
12924	0.666	11.7	77.0	0.364	0.348	0.081	+0.011	0.0607	0.2486
12926	0.666	11.7	82.7	0.315	0.364	0.085	+0.012	0.0715	0.3460
12938	1.000	11.7	59.4	0.613	0.384	0.088	+0.038	0.0424	-0.0014
12940	1.000	11.7	65.2	0.509	0.370	0.085	+0.049	0.0479	0.0112
12942	1.000	11.7	74.1	0.394	0.377	0.088	+0.019	0.0616	0.0599
12944	1.000	11.7	81.6	0.325	0.360	0.084	+0.011	0.0693	0.1596
12802	0.333	9.65	53.5	0.752	0.272	0.048	+0.004	0.0208	0.0888
12804	0.333	9.65	56.4	0.677	0.319	0.058	+0.012	0.0281	0.1041
12806	0.333	9.65	58.5	0.629	0.304	0.055	+0.016	0.0297	0.0744
12816	0.333	9.65	66.0	0.494	0.310	0.057	-0.001	0.0373	0.1363
12818	0.333	9.65	75.8	0.375	0.279	0.049	+0.004	0.0443	0.0910
12820	0.333	9.65	86.6	0.287	0.289	0.051	+0.008	0.0582	0.1819
12884	0.666	9.65	58.5	0.631	0.368	0.046	+0.558	0.0455	0.1389
12886	0.666	9.65	66.7	0.485	0.297	0.055	+0.003	0.0406	-0.0754
12888	0.666	9.65	77.2	0.362	0.326	0.060	+0.006	0.0576	-0.0202
13504	0.666	9.65	59.4	0.612	0.340	0.057	-0.287	--	--
13508	0.666	9.65	66.1	0.494	0.261	0.047	+0.023	--	--
13510	0.666	9.65	80.0	0.337	0.287	0.056	+0.008	--	--
13512	0.666	9.65	87.8	0.280	0.312	0.061	0		
12768	1.000	9.65	29.7	2.45	0.344	0.053	+0.042	0.00899	0.0472
12770	1.000	9.65	37.4	1.55	0.343	0.054	+0.064	0.0144	0.0792
12772	1.000	9.65	50.1	0.862	0.366	0.060	+0.012	0.0275	0.1255
12774	1.000	9.65	58.9	0.624	0.368	0.063	+0.003	0.0391	0.1012
12776	1.000	9.65	64.5	0.520	0.263	0.054	-0.021	0.0328	0.0106
12834	1.000	9.65	69.5	0.448	0.327	0.063	+0.006	0.0450	0.1172
12836	1.000	9.65	80.0	0.338	0.341	0.065	+0.022	0.0610	0.1904
12838	1.000	9.65	86.3	0.290	0.344	0.065	+0.046	0.0711	0.2811

Table 3. Test Data (Continued)
Non-Cavitating — Two-Term Foil

Run	h/c	α	U_∞	σ_v	C_L	C_D	C_M
13046	0.333	15.5	28.10	2.73	0.604	0.168	0
13026	0.666	15.5	27.30	2.90	0.803	0.188	+0.015
13028	0.666	15.5	33.60	1.91	0.714	0.180	-0.245
13030	0.666	15.5	42.30	1.21	0.645	0.176	-0.543
13004	1.000	15.5	25.80	3.25	0.779	0.177	+0.040
13006	1.000	15.5	33.60	1.92	0.681	0.167	+0.662
13010	1.000	15.5	42.10	1.22	0.762	0.189	-0.019
12966	0.666	13.89	27.90	2.77	0.583	0.137	-0.115
12968	0.666	13.89	34.60	1.80	0.570	0.131	-0.009
12970	0.666	13.89	41.80	1.24	0.542	0.132	-0.013
12950	1.000	13.89	25.30	3.38	0.696	0.142	+0.072
12952	1.000	13.89	35.30	1.74	0.573	0.139	+0.024
12954	1.000	13.89	43.10	1.16	0.642	0.159	-0.031
12898	0.333	11.70	35.80	1.68	0.416	0.091	-0.086
13528	0.333	11.70	29.50	2.47	0.239	0.047	-0.531
13530	0.333	11.70	37.60	1.52	0.181	0.040	-0.103
13532	0.333	11.70	45.00	1.06	0.154	0.037	-0.152
13534	0.333	11.70	58.40	0.631	0.205	0.046	-0.107
13630	0.333	11.70	59.20	0.614	0.238	0.051	--
13632	0.333	11.70	59.00	0.618	0.184	0.041	--
12914	0.666	11.70	28.00	2.75	0.426	0.075	+0.279
12916	0.666	11.70	35.20	1.74	0.454	0.084	+0.333
12918	0.666	11.70	42.30	1.21	0.455	0.095	0
12932	1.000	11.70	24.70	3.55	0.538	0.091	+0.105
12934	1.000	11.70	34.50	1.82	0.545	0.093	+0.147
12936	1.000	11.70	43.50	1.14	0.420	0.091	+0.069
12798	0.333	9.65	29.50	2.47	0.415	0.055	+0.011
12800	0.333	9.65	36.40	1.62	0.414	0.056	+0.019
12878	0.666	9.65	27.40	2.87	0.430	0.056	+0.089
12880	0.666	9.65	37.60	1.53	0.425	0.056	+0.111
12882	0.666	9.65	48.90	0.903	0.434	0.063	+0.116
13498	0.666	9.65	30.80	2.27	0.412	0.055	-0.005
13500	0.666	9.65	38.40	1.46	0.407	0.056	+0.081
13502	0.666	9.65	50.00	0.863	0.408	0.062	+0.140

Table 3. Test Data (Continued)
Non-Cavitating — Two-Term Foil (Continued)

Run	h/c	α	U_∞	σ_v	C_L	C_D	C_M
13506	0.666	9.65	47.90	0.941	0.414	0.059	+0.147
13516	0.666	9.65	30.00	2.40	0.400	0.055	+0.047
13518	0.666	9.65	35.80	1.68	0.396	0.058	+0.054
13520	0.666	9.65	49.60	0.877	0.400	0.059	+0.062
12826	1.000	9.65	29.40	2.50	0.417	0.053	+0.057
12828	1.000	9.65	36.60	1.62	0.419	0.057	+0.132
12830	1.000	9.65	42.80	1.18	0.428	0.061	+0.131
12832	1.000	9.65	59.40	0.613	0.397	0.062	+0.385
12060	1.000	7.76	25.60	3.30	0.434	0.048	+0.070
12062	1.000	7.76	35.90	1.67	0.332	0.035	+0.075
12064	1.000	7.76	43.20	1.16	0.345	0.038	+0.047
13066	1.000	7.76	58.80	0.626	0.353	0.057	-0.219
13068	1.000	7.76	65.20	0.509	0.342	0.054	+0.065
13070	1.000	7.76	74.70	0.388	0.355	0.054	+0.071
13072	1.000	7.76	81.70	0.324	0.383	0.055	+0.099

11 | ILLUSTRATIONS

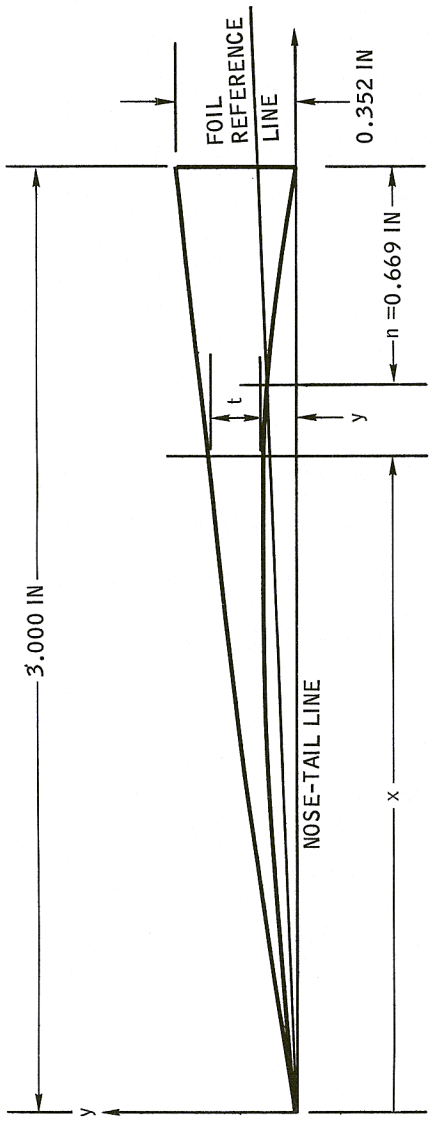

x/c	x (in.)	y/c	y (in.)	t/c	t (in.)
0.0075	0.0225	0.00056	0.0017	0.00147	0.0044
0.0125	0.0375	0.0010	0.0030	0.00210	0.0063
0.050	0.150	0.00441	0.0132	0.00520	0.0156
0.100	0.300	0.00905	0.0272	0.00801	0.0240
0.200	0.600	0.01759	0.0528	0.01272	0.0382
0.300	0.900	0.02436	0.0731	0.01815	0.0545
0.400	1.200	0.02893	0.0868	0.02505	0.0752
0.500	1.500	0.03104	0.0931	0.03422	0.1072
0.550	1.650	0.03112	0.0934	0.03960	0.1188
0.600	1.800	0.03053	0.0916	0.04557	0.1367
0.700	2.100	0.02726	0.0818	0.05944	0.1783
0.800	2.400	0.02112	0.0634	0.07595	0.2279
0.900	2.700	0.01207	0.0362	0.09521	0.2856
0.950	2.850	0.00642	0.0193	0.10591	0.3177
1.000	3.000	0	0	0.11734	0.3520

TWO-TERM

Figure 1. Ordinates for ~~Flat Plate~~ Supercavitating Hydrofoil Model

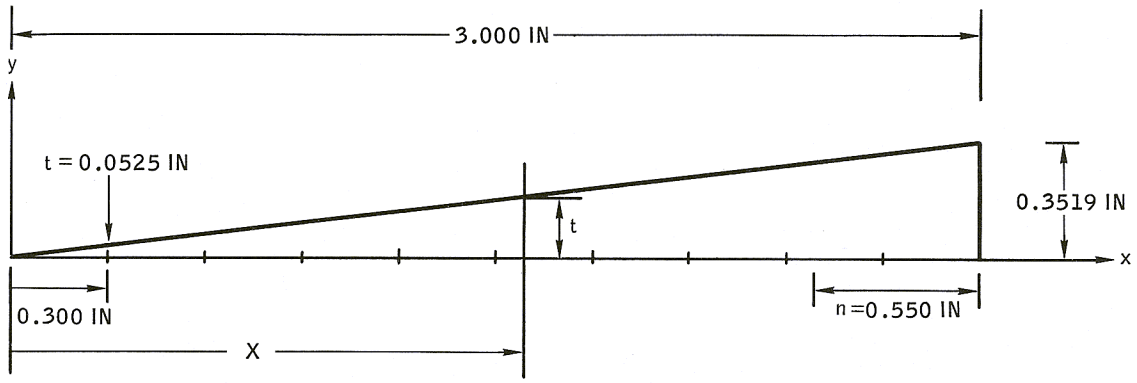

x/c	x (in.)	t/c	t (in.)
0.100	0.300	0.0175	0.0525
0.200	0.600	0.0286	0.0858
0.300	0.900	0.0397	0.1190
0.400	1.200	0.0508	0.1523
0.500	1.500	0.0619	0.1856
0.600	1.800	0.0729	0.2188
0.700	2.100	0.0840	0.2521
0.800	2.400	0.0951	0.2854
0.900	2.700	0.1062	0.3186
1.000	3.000	0.1173	0.3519

NOTE: THE UPPER SURFACE HAS A STRAIGHT BEVEL FROM THE LEADING EDGE (X = 0, t = 0.0020 IN) TO X = 0.300 IN. FROM X = 0.300 IN, t = 0.0525 IN. TO THE TRAILING EDGE, X = 3.000 IN, t = 0.3519 IN, THE UPPER SURFACE IS A STRAIGHT LINE.

FLAT PLATE

Figure 2. Ordinates for ~~Two-Term~~ Supercavitating Hydrofoil Model

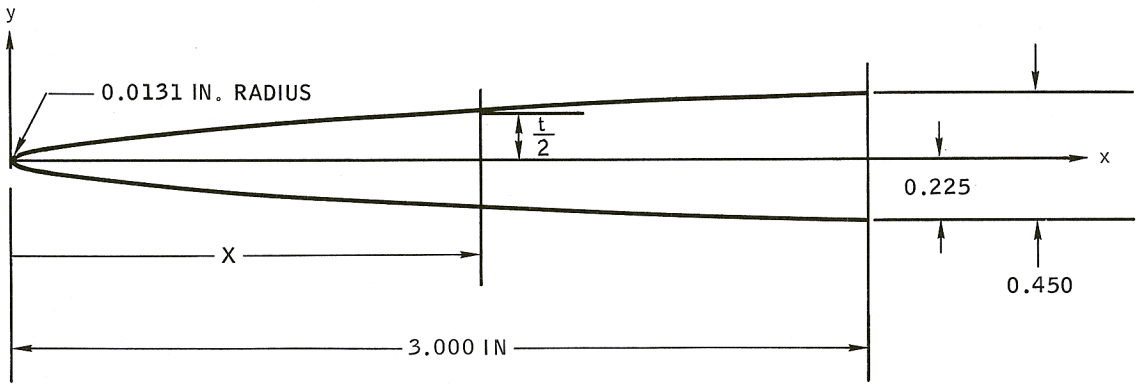

x/c	x (in.)	$\frac{t}{2c}$	$\frac{t}{2}$ (in.)
0	0	0	0
0.0125	0.0375	0.00839	0.025
0.025	0.0750	0.01186	0.036
0.075	0.2250	0.02054	0.062
0.100	0.3000	0.02372	0.071
0.150	0.450	0.02905	0.087
0.200	0.600	0.03354	0.101
0.300	0.900	0.04108	0.123
0.400	1.200	0.04744	0.142
0.500	1.500	0.05303	0.159
0.600	1.800	0.05810	0.174
0.700	2.100	0.06275	0.188
0.800	2.400	0.06708	0.201
0.900	2.700	0.07115	0.213
1.000	3.000	0.07500	0.225

Figure 3. Ordinates of Parabolic Strut Section

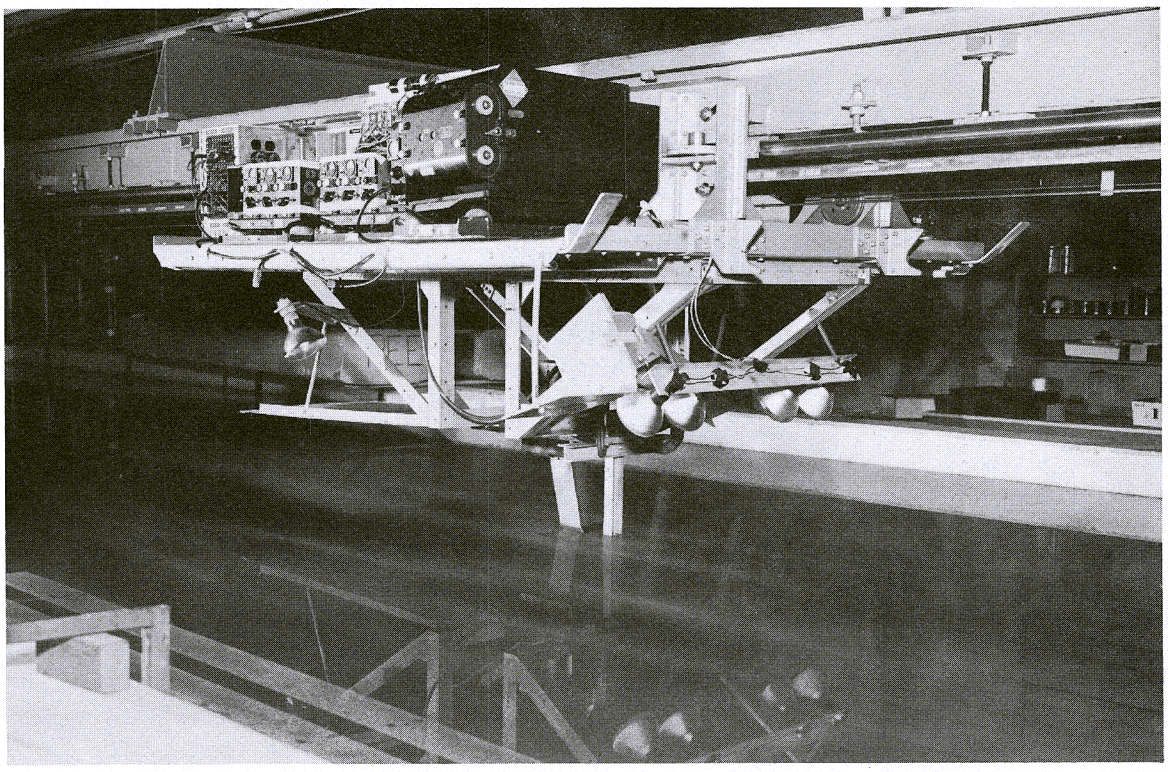

Figure 4. Front View of Test Setup

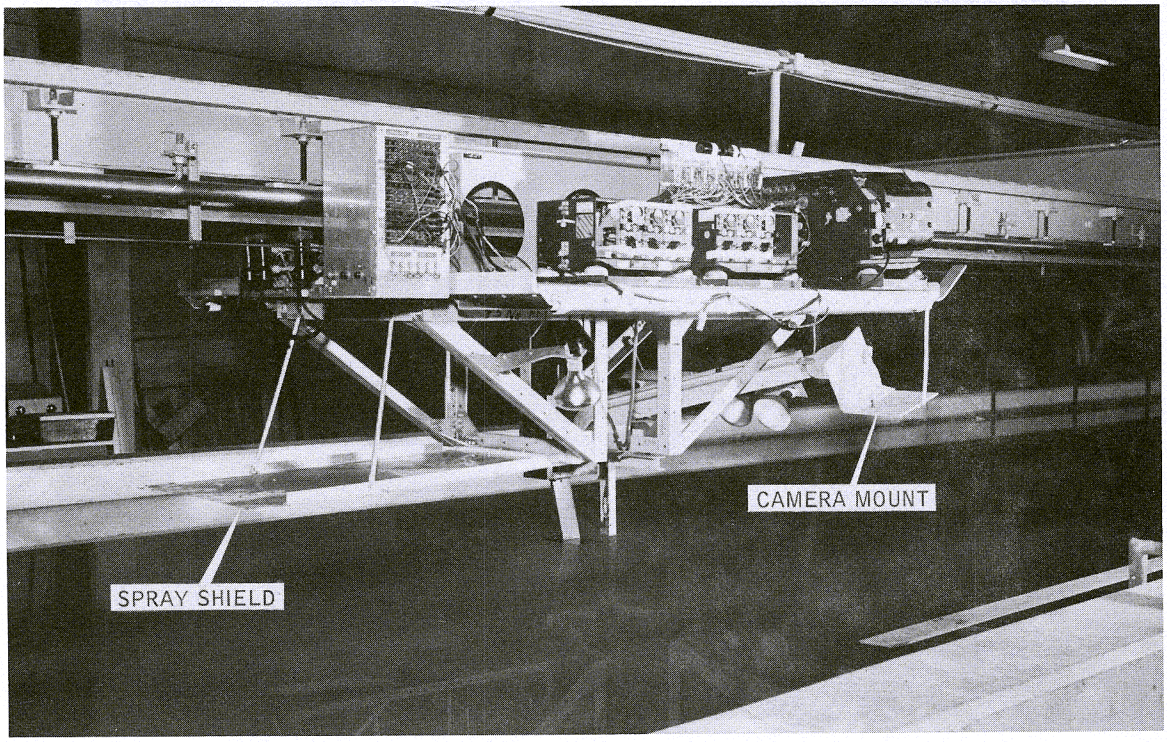

Figure 5. Rear View of Test Setup

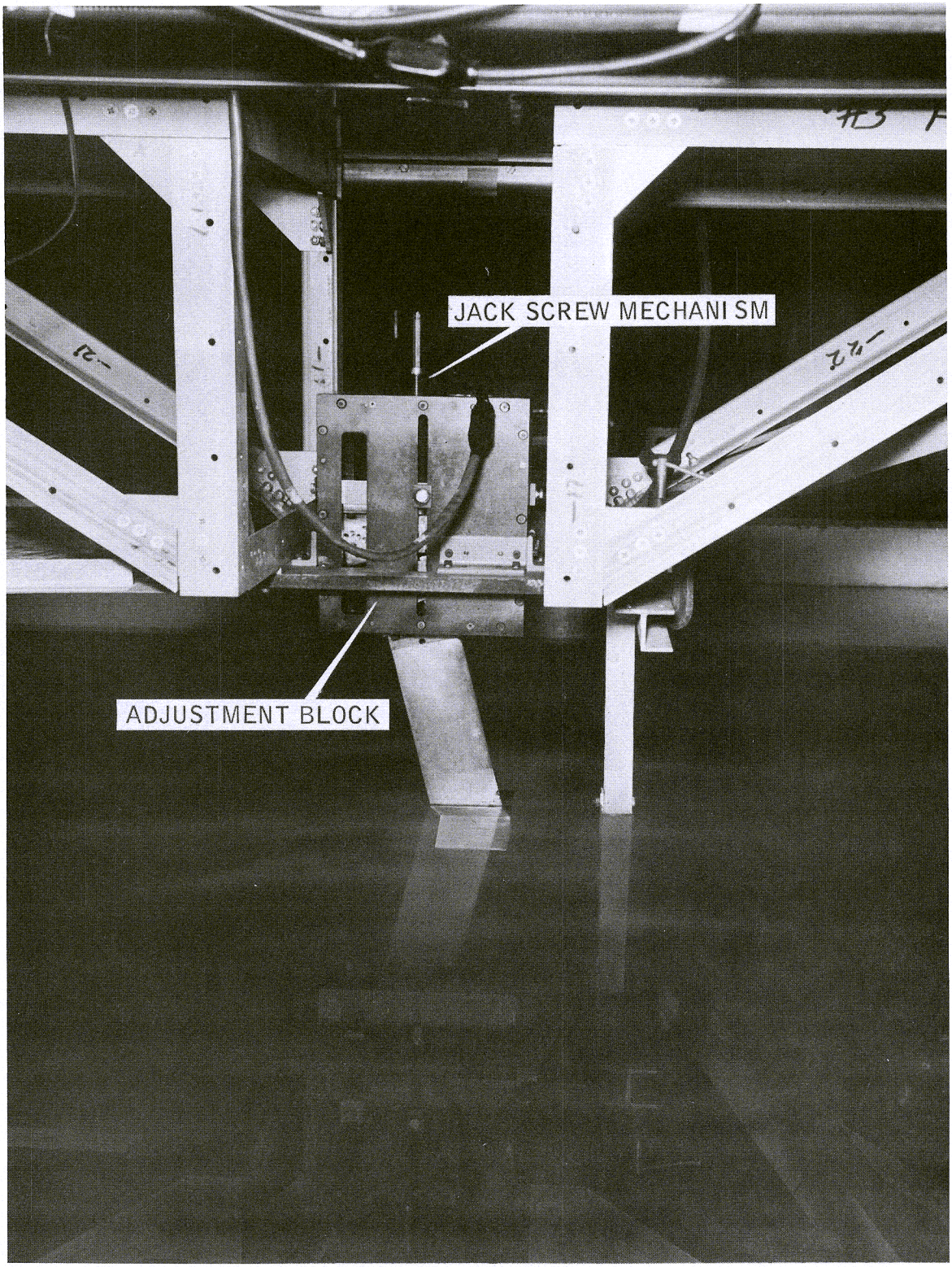

Figure 6. Combined Depth and Angle of Attack Assembly Box

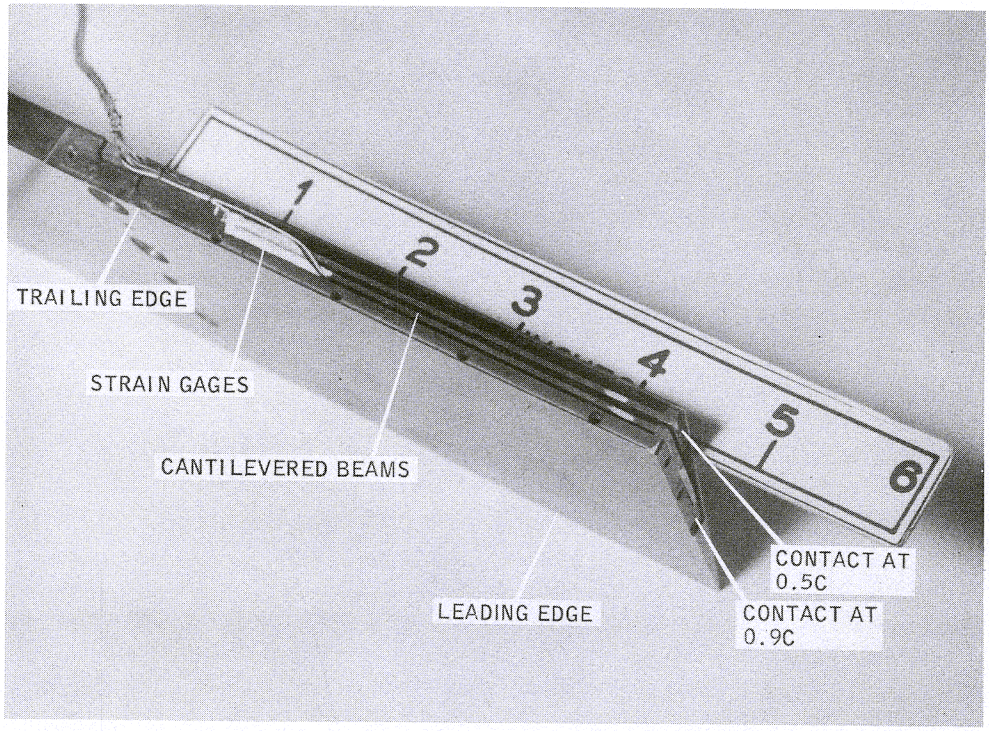

Figure 7. Foil Deflection Gages

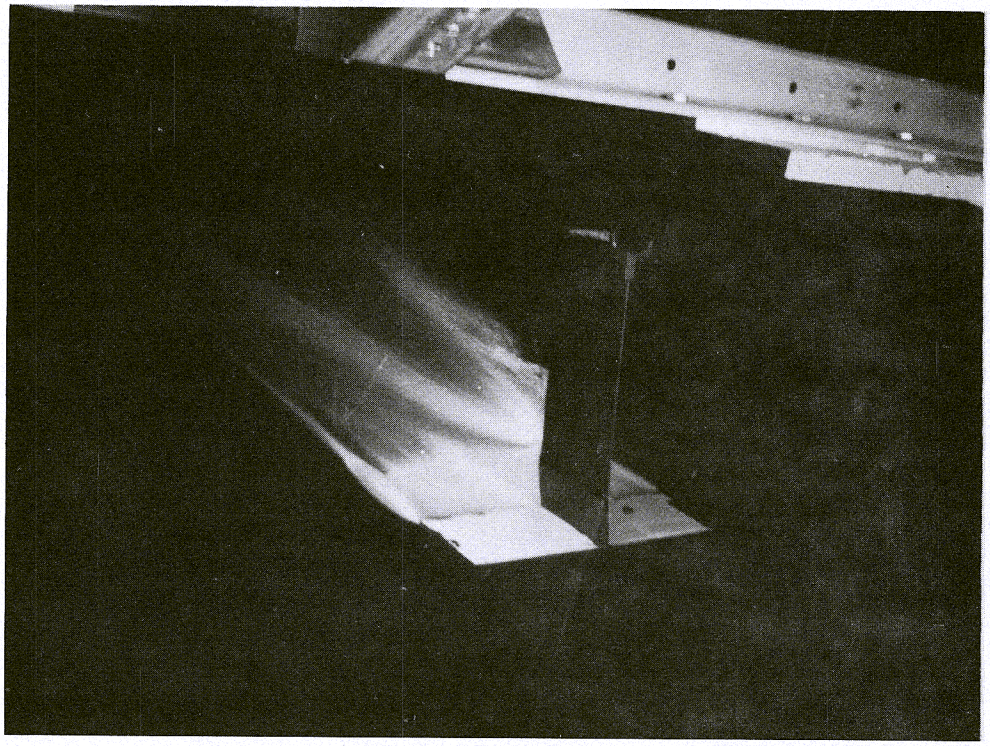

Figure 8. Two-Term Foil in Non-Cavitating Flow
$\alpha = 7.76°$, $U_\infty = 60$ ft./sec., $h/c = 1.0$

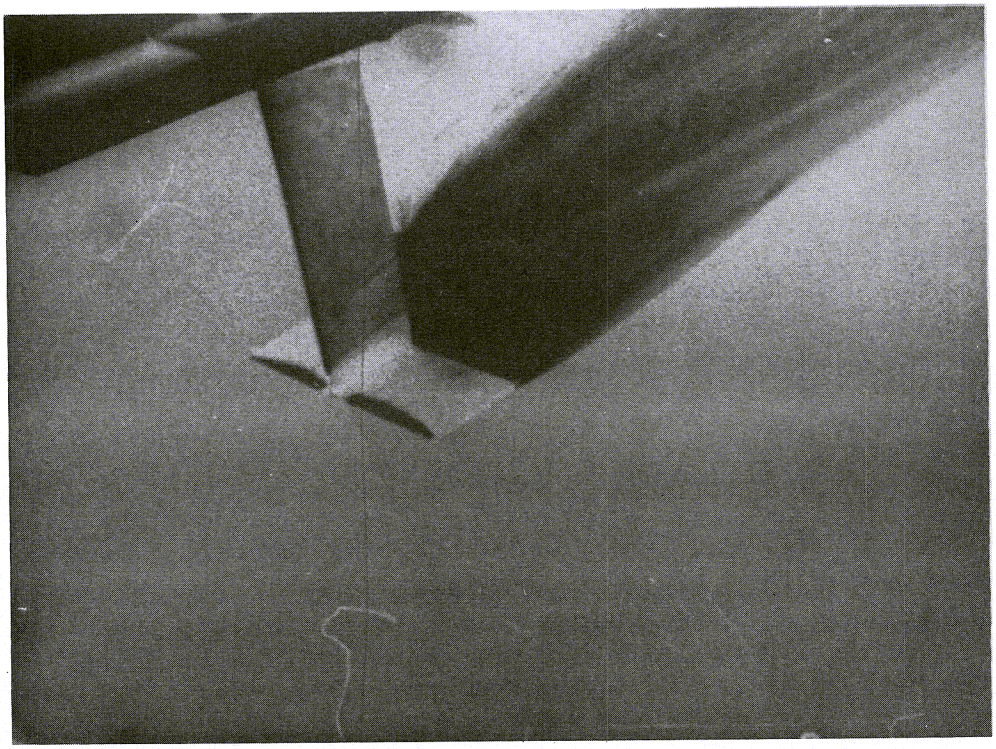

Figure 9. Flat Plate Foil in Non-Cavitating Flow
$\alpha = 7.8°$ h/c = 1.000 $U_\infty = 60.6$

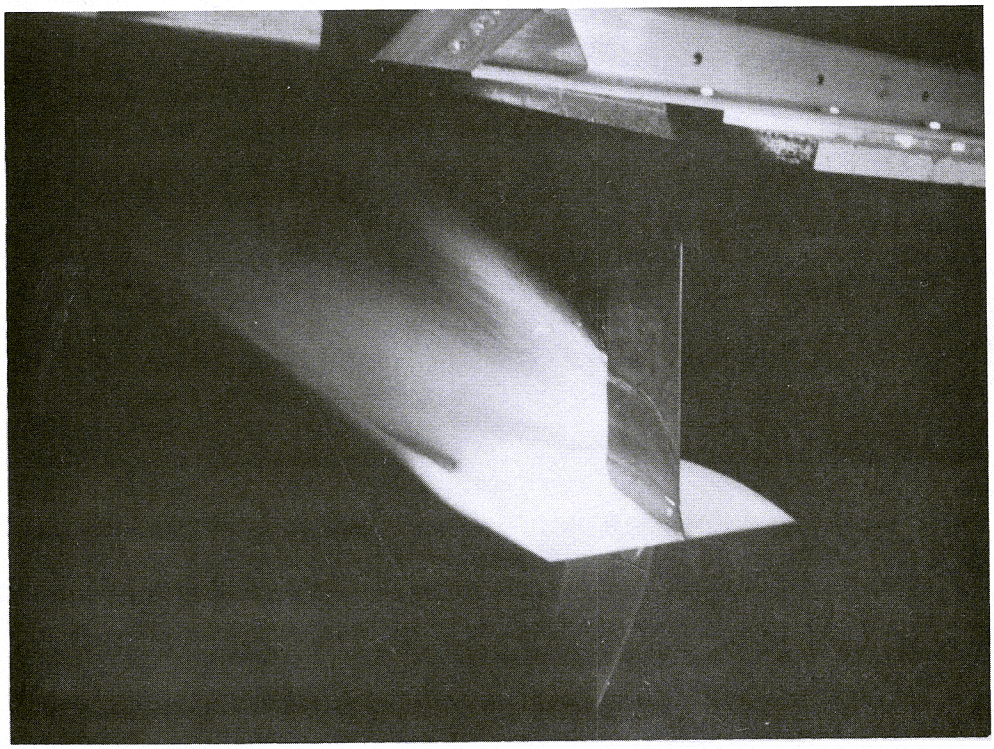

Figure 10a.

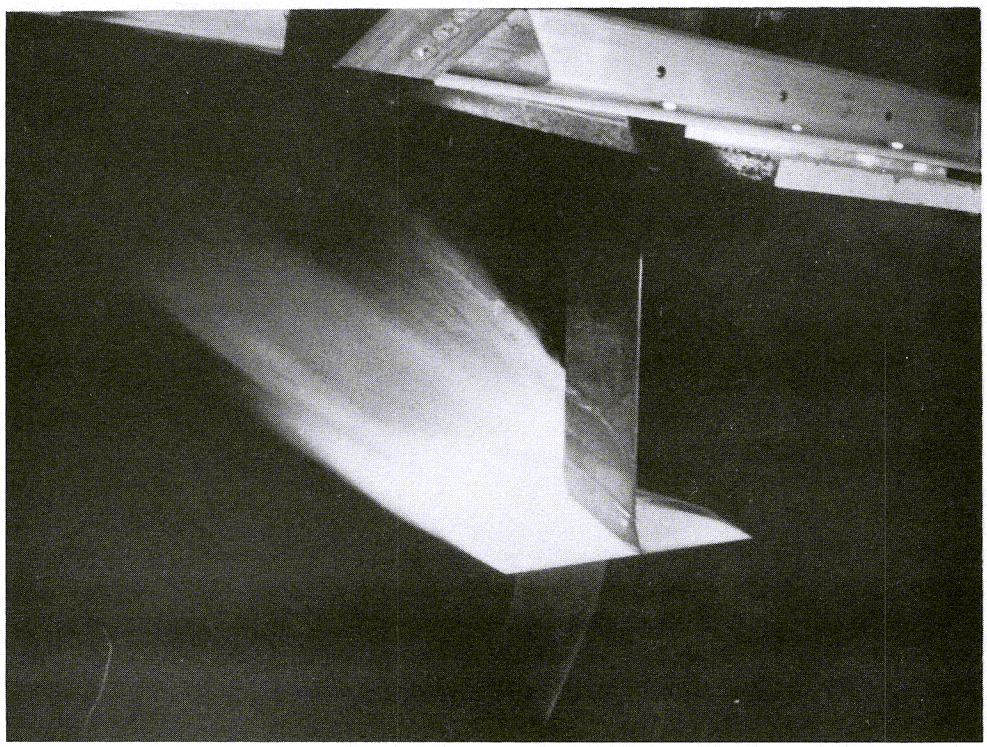

Figure 10b.

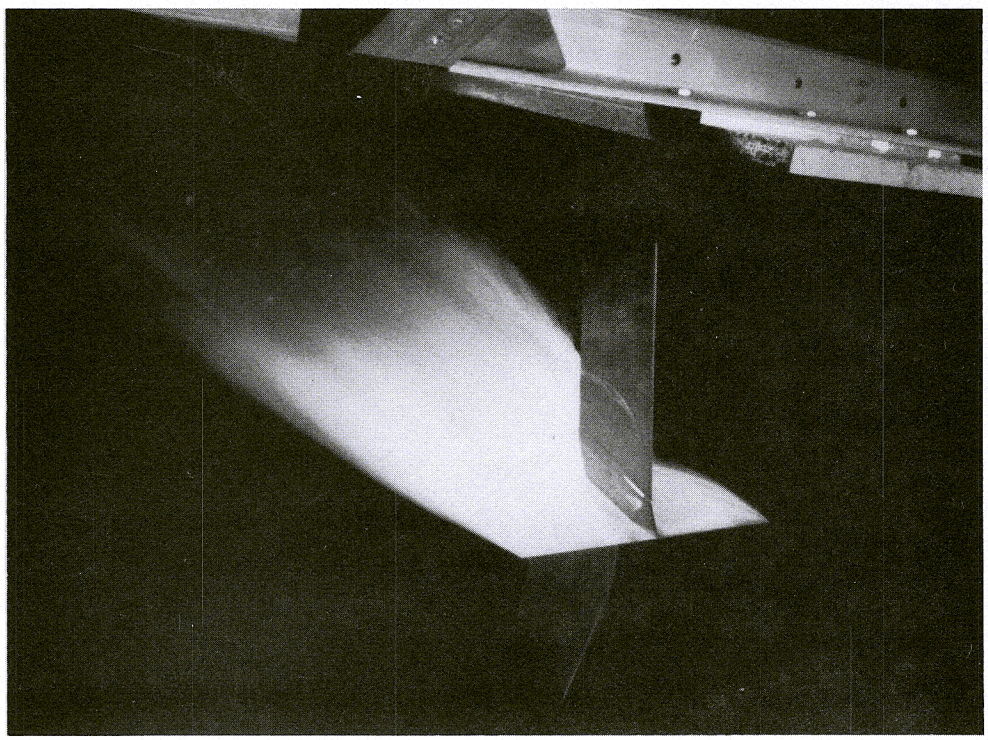

Figure 10c.

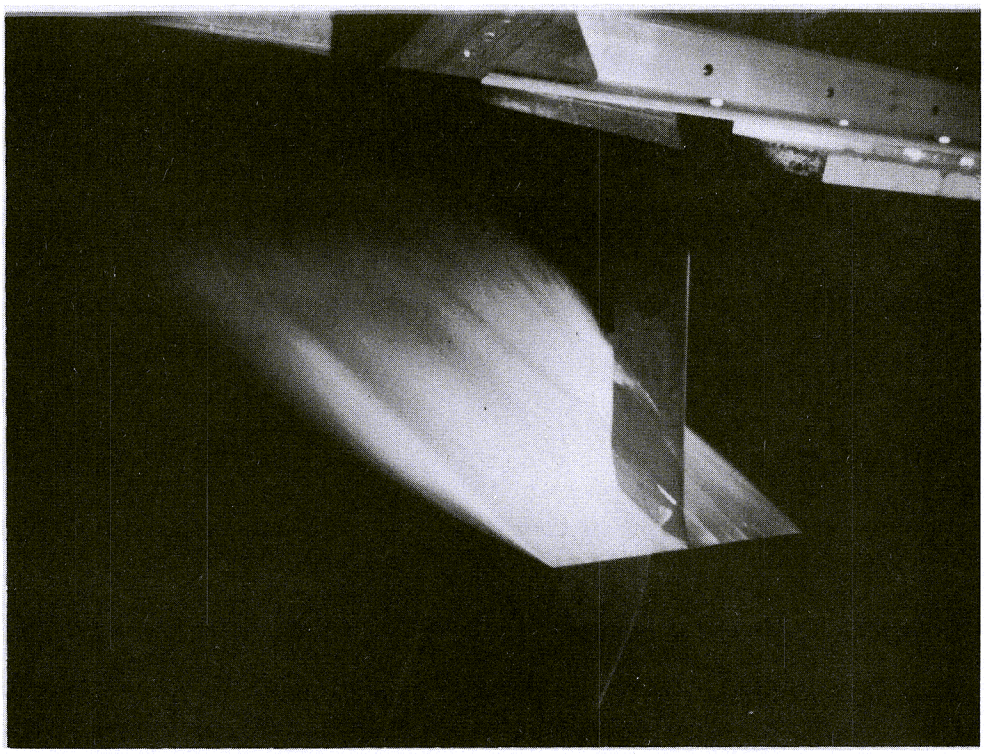

Figure 10d.

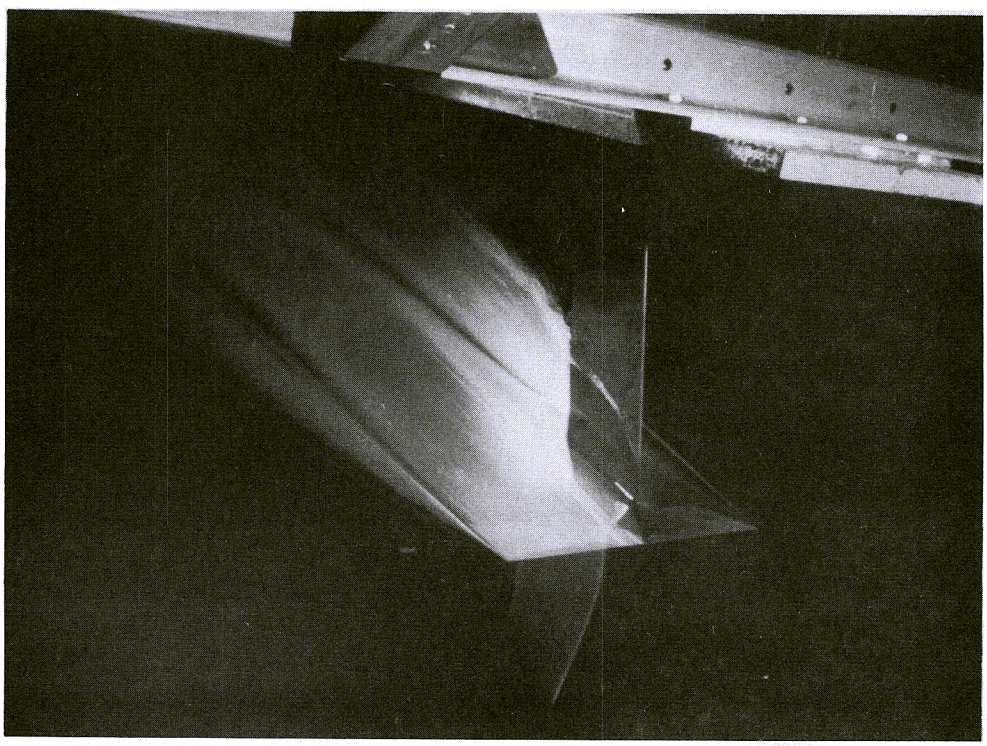

Figure 10e.

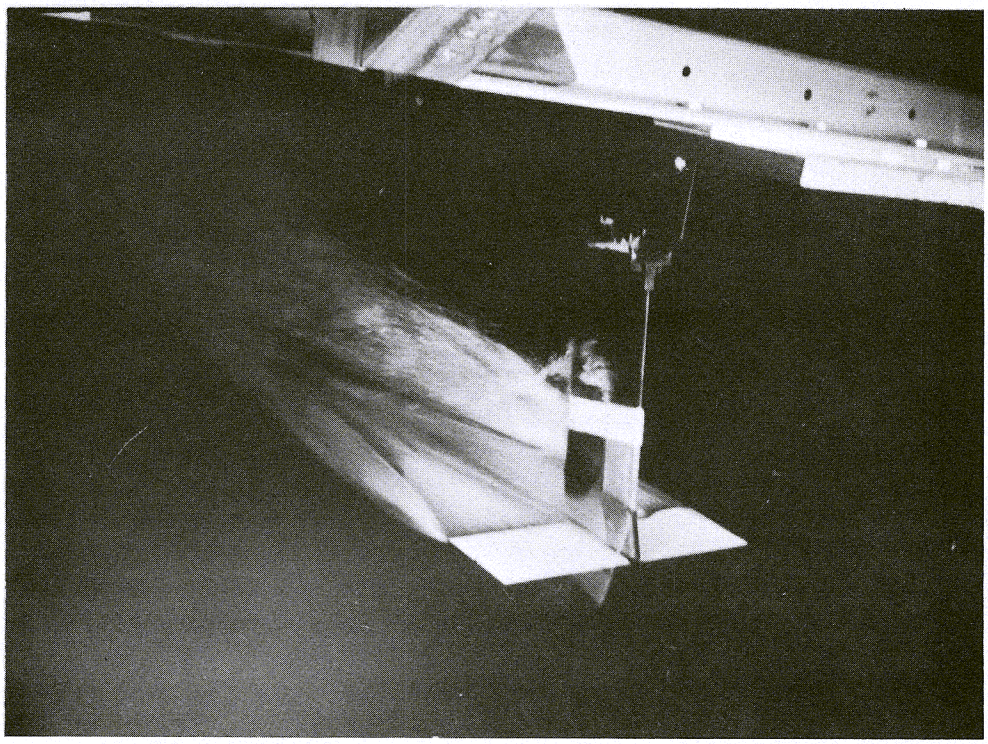

Figure 11. Glove Mounted Over Strut Leading Edge

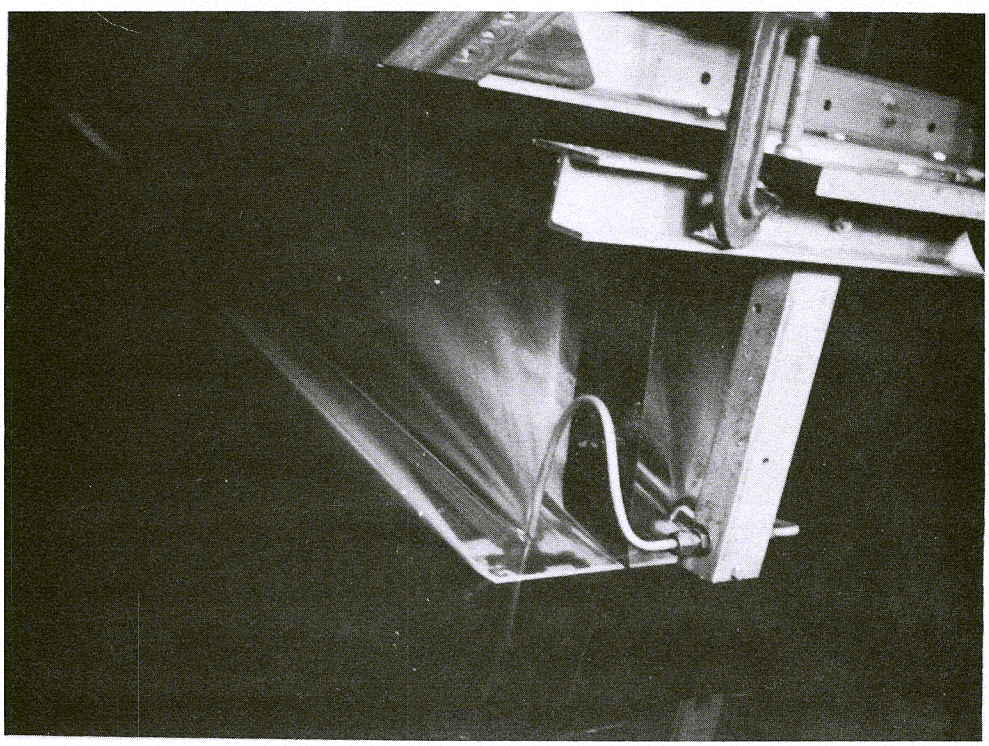

Figure 12. Test With Air Probes and Trip Wire

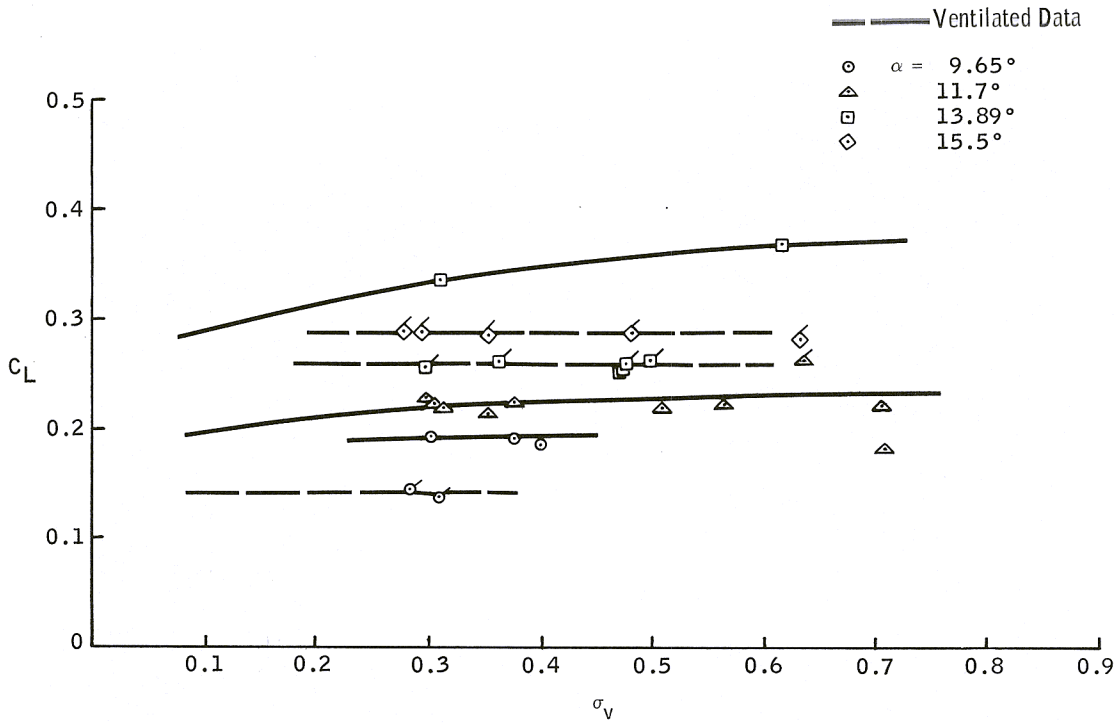

Figure 13. Lift Coefficient, h/c = 0.333, Flat-Plate Foil

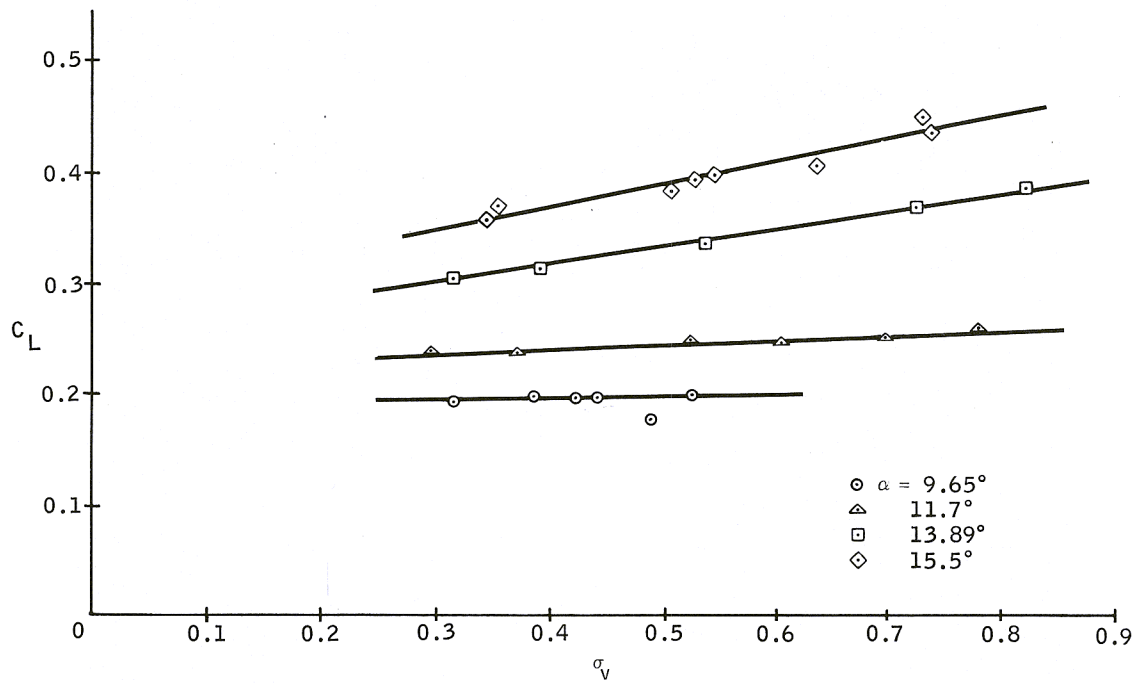

Figure 14. Lift Coefficient, h/c = 0.666, Flat-Plate Foil

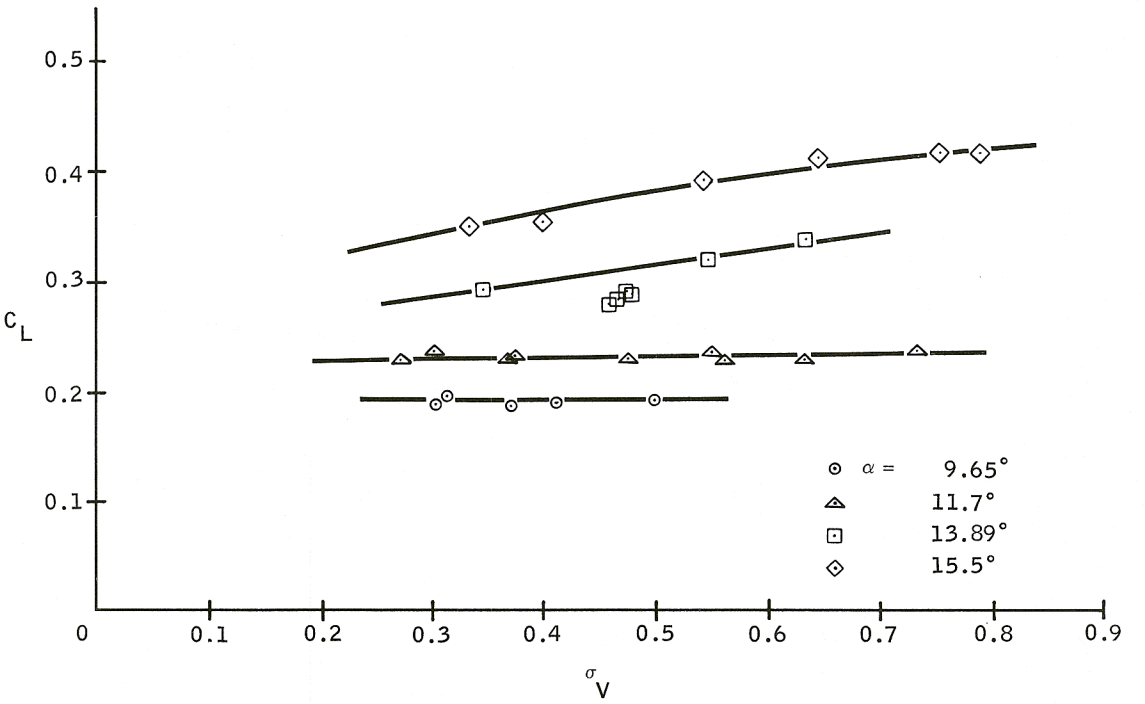

Figure 15. Lift Coefficient, h/c = 1.000, Flat-Plate Foil

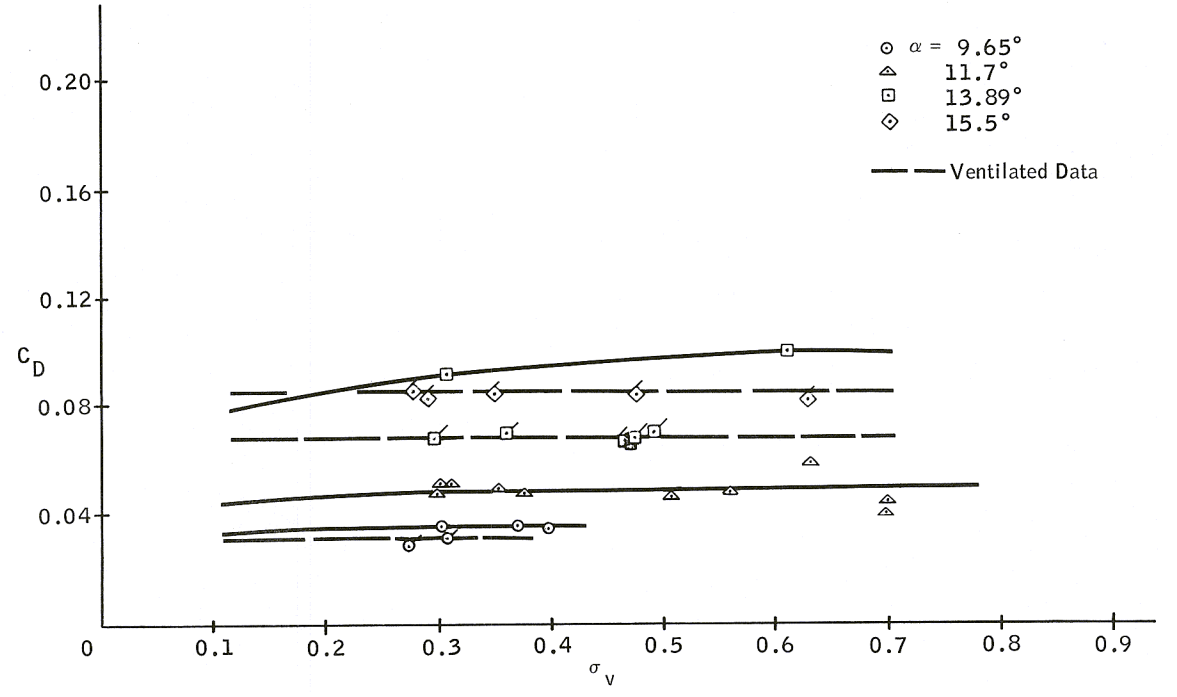

Figure 16. Drag Coefficient, h/c = 0.333, Flat-Plate Foil

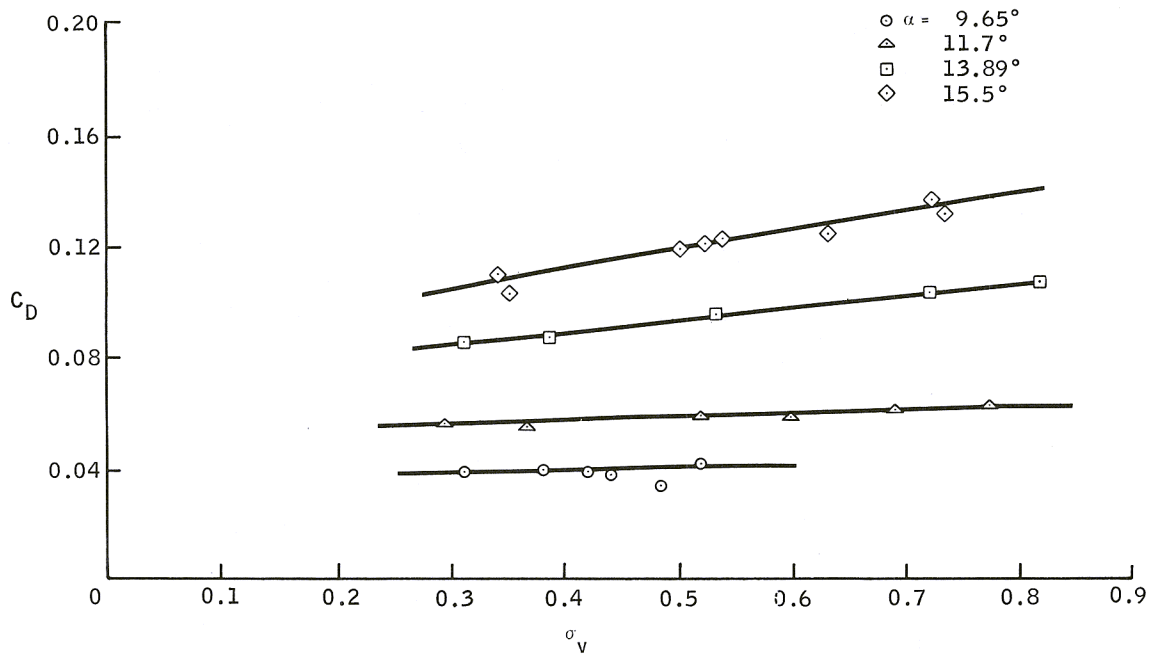

Figure 17. Drag Coefficient, h/c = 0.666, Flat-Plate Foil

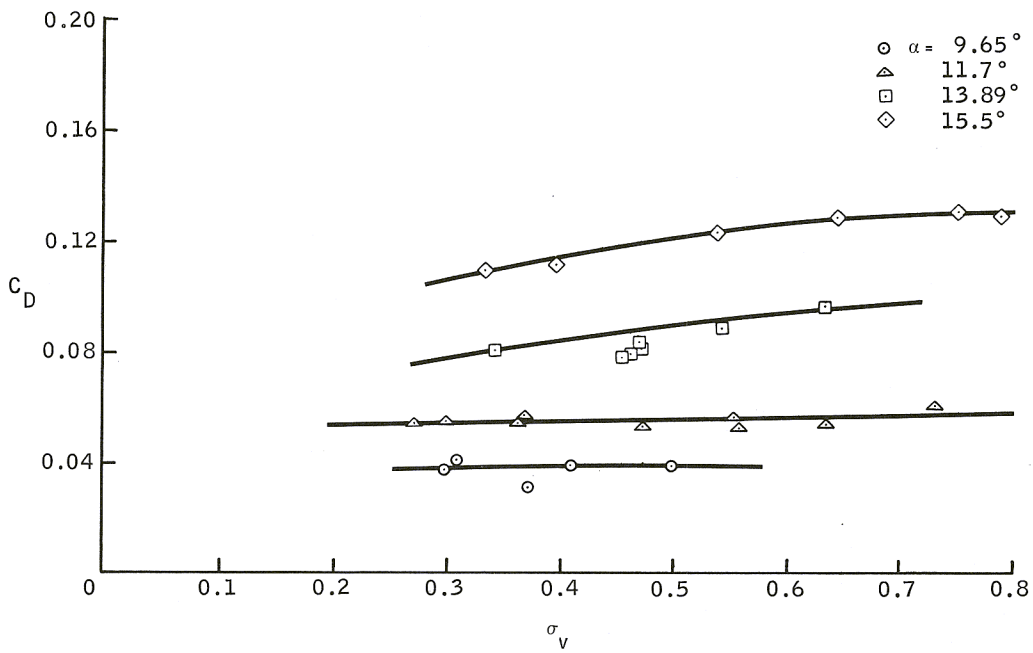

Figure 18. Drag Coefficient, h/c = 1.000, Flat-Plate Foil

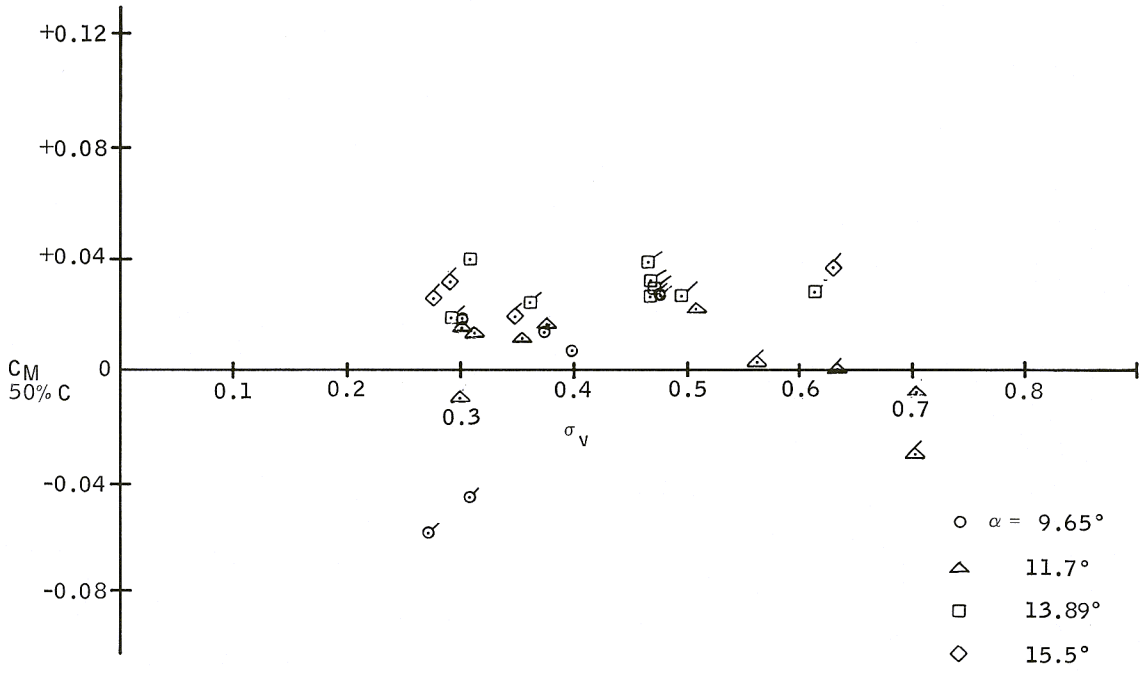

Figure 19. Pitching Moment Coefficient, h/c = 0.333, Flat-Plate Foil

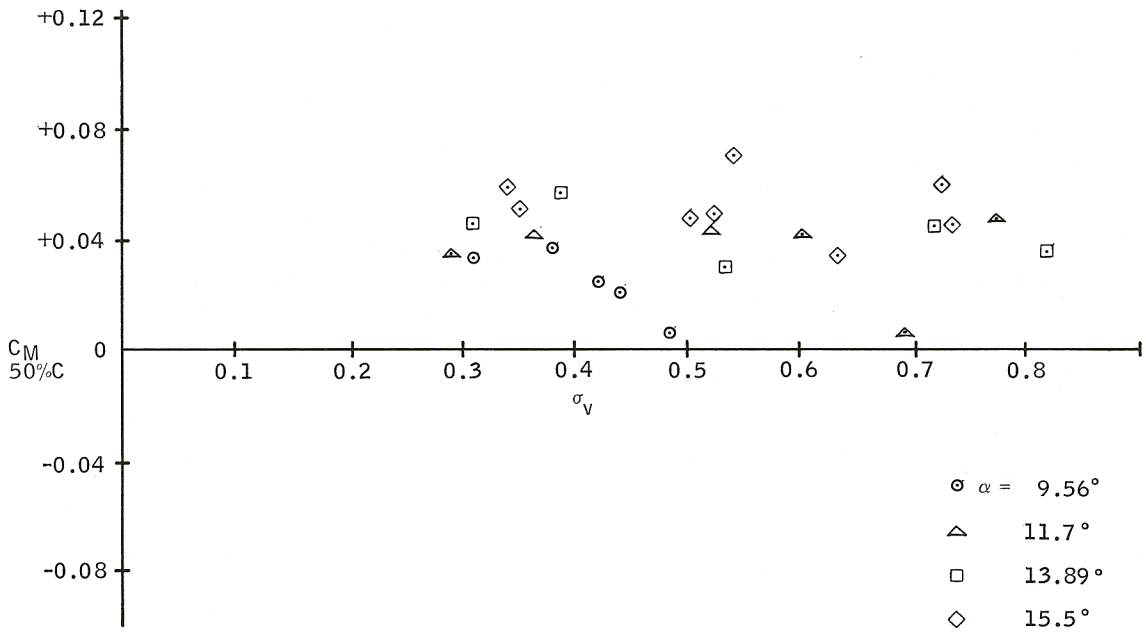

Figure 20. Pitching Moment Coefficient, h/c = 0.666, Flat-Plate Foil

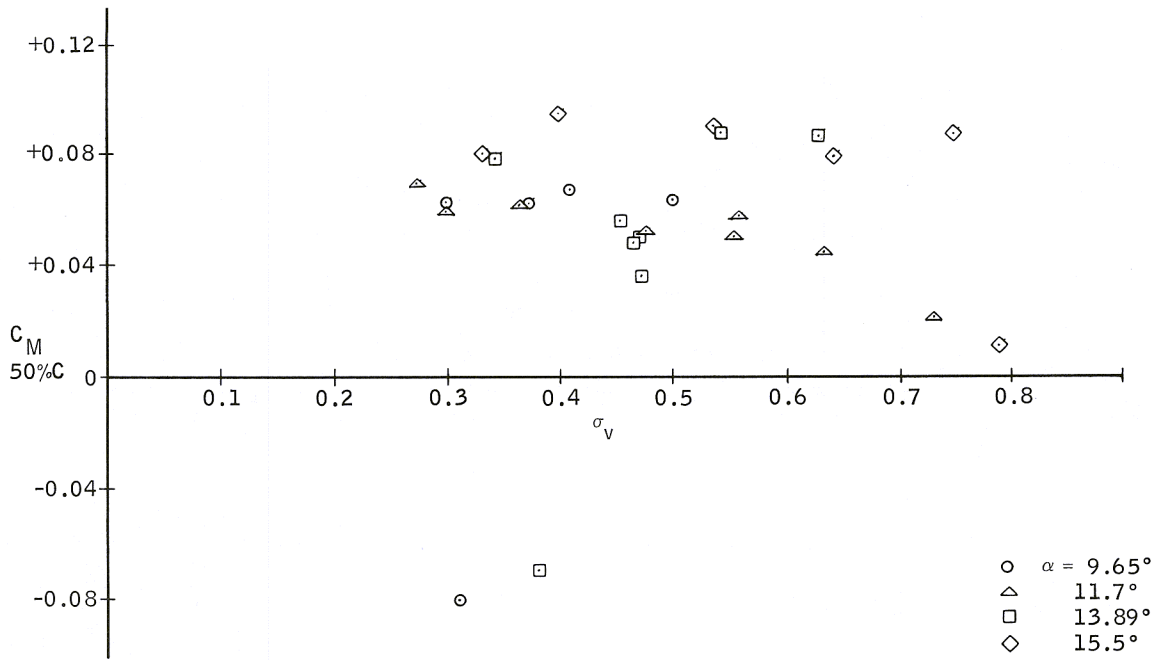

Figure 21. Pitching Moment Coefficient, h/c = 1.000, Flat-Plate Foil

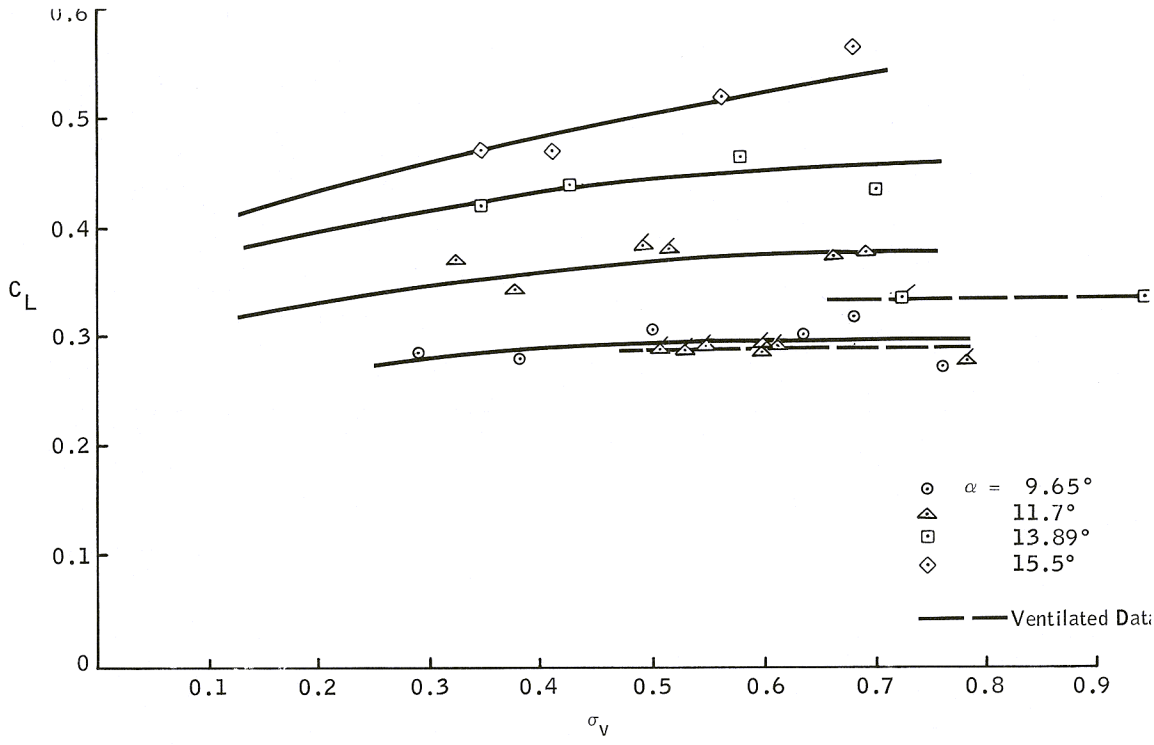

Figure 22. Lift Coefficient, h/c = 0.333, Two-Term Foil

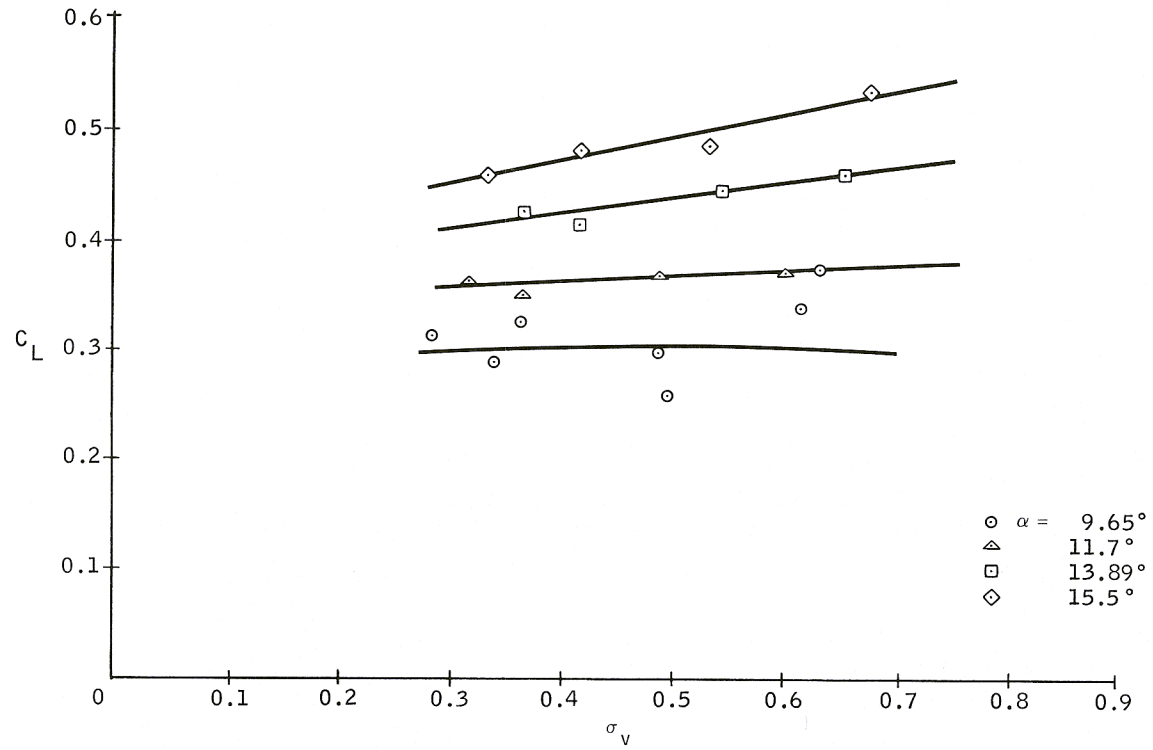

Figure 23. Lift Coefficient, h/c = 0.666, Two-Term Foil

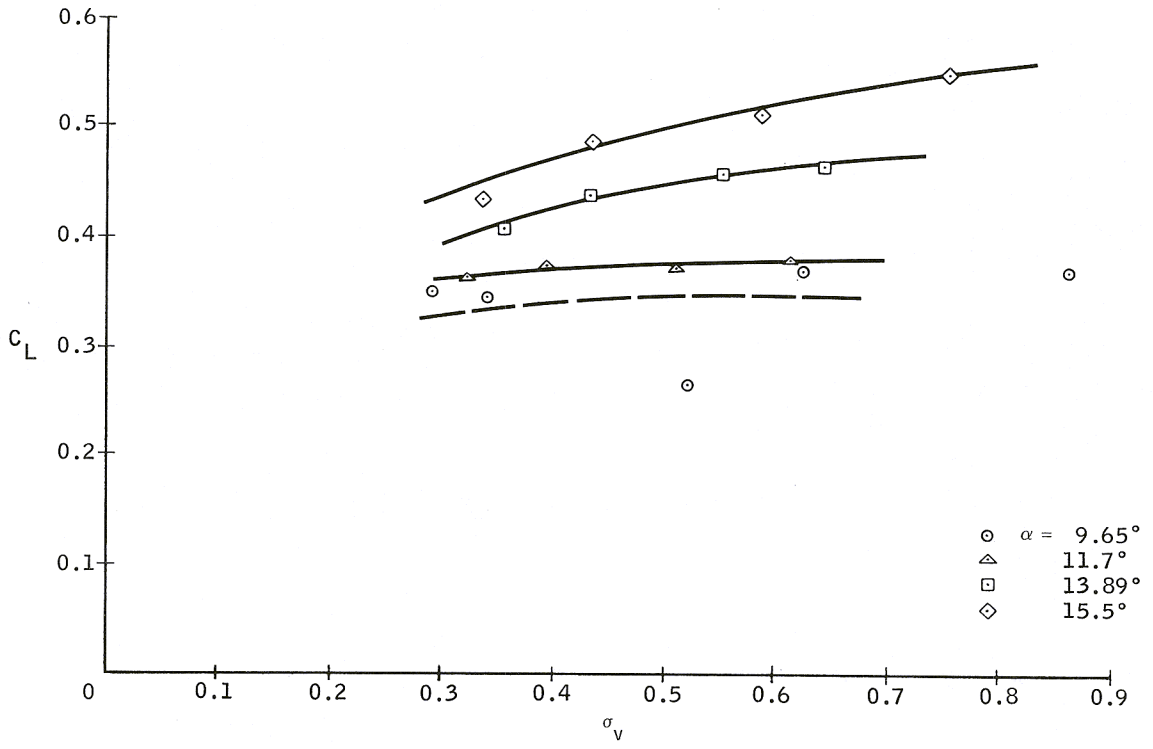

Figure 24. Lift Coefficient, h/c = 1.000, Two-Term Foil

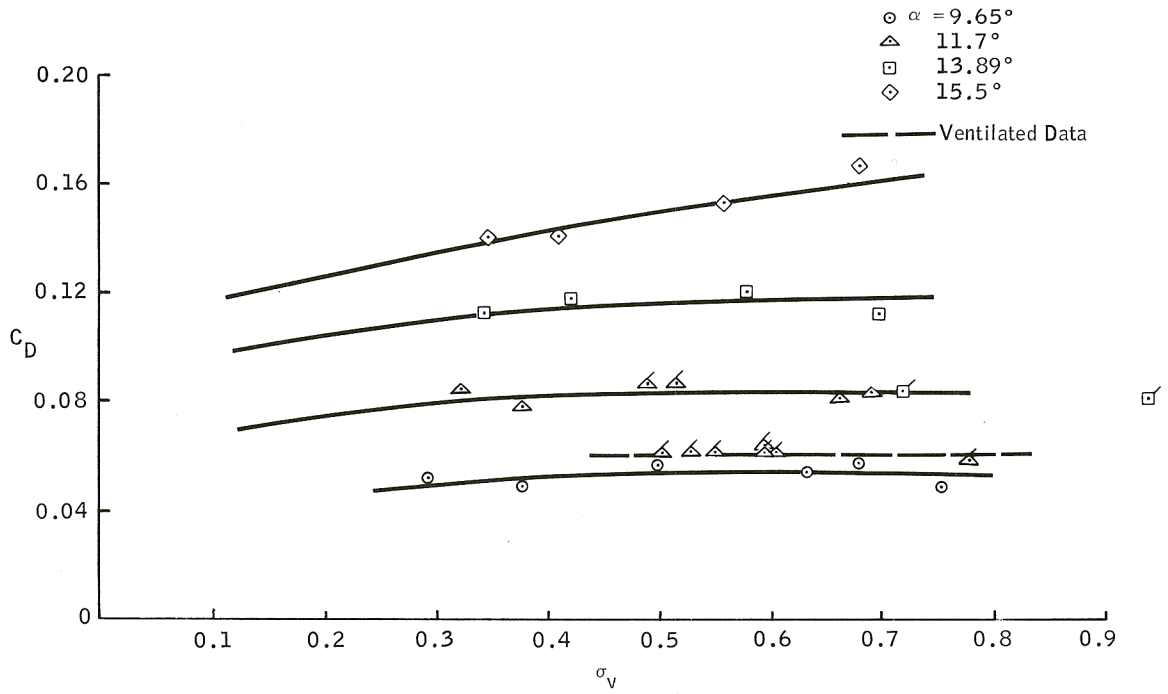

Figure 25. Drag Coefficient, h/c = 0.333, Two-Term Foil

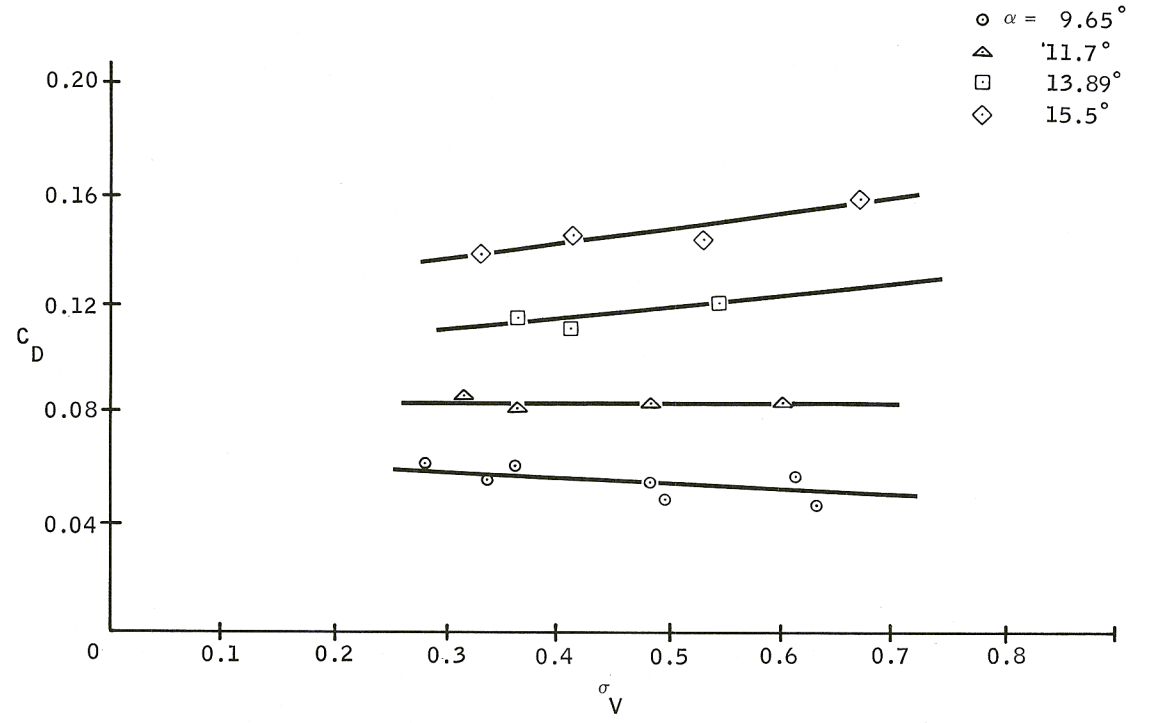

Figure 26. Drag. Coefficient, h/c = 0.666, Two-Term Foil

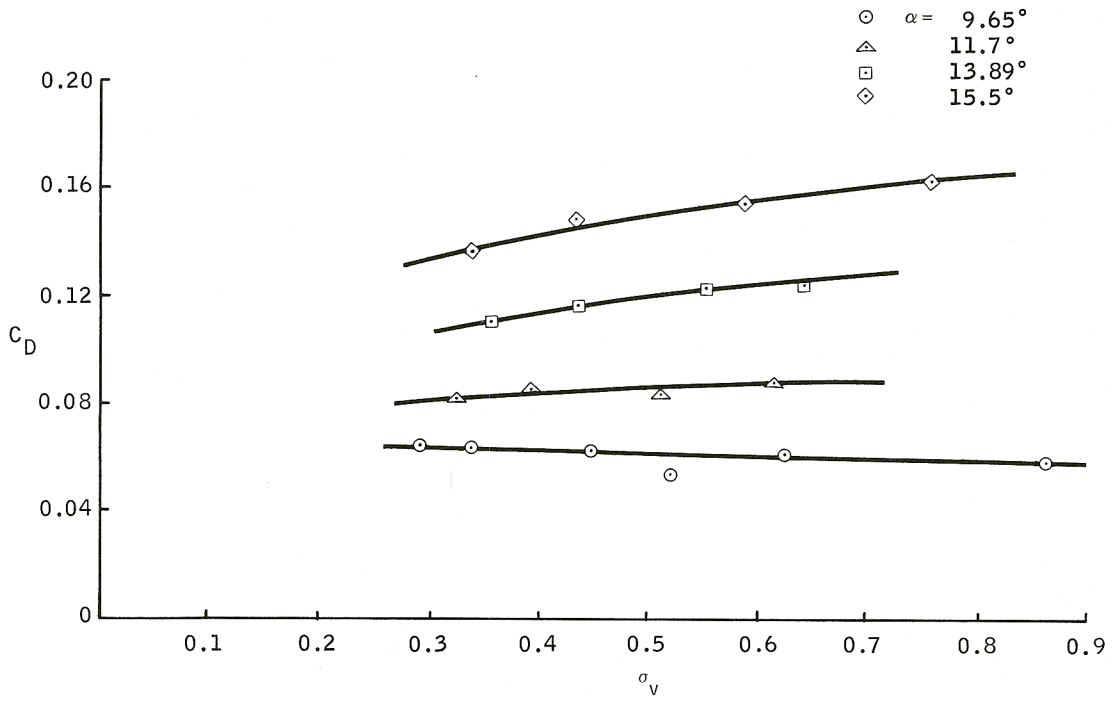

Figure 27. Drag Coefficient, h/c = 1.000, Two-Term Foil

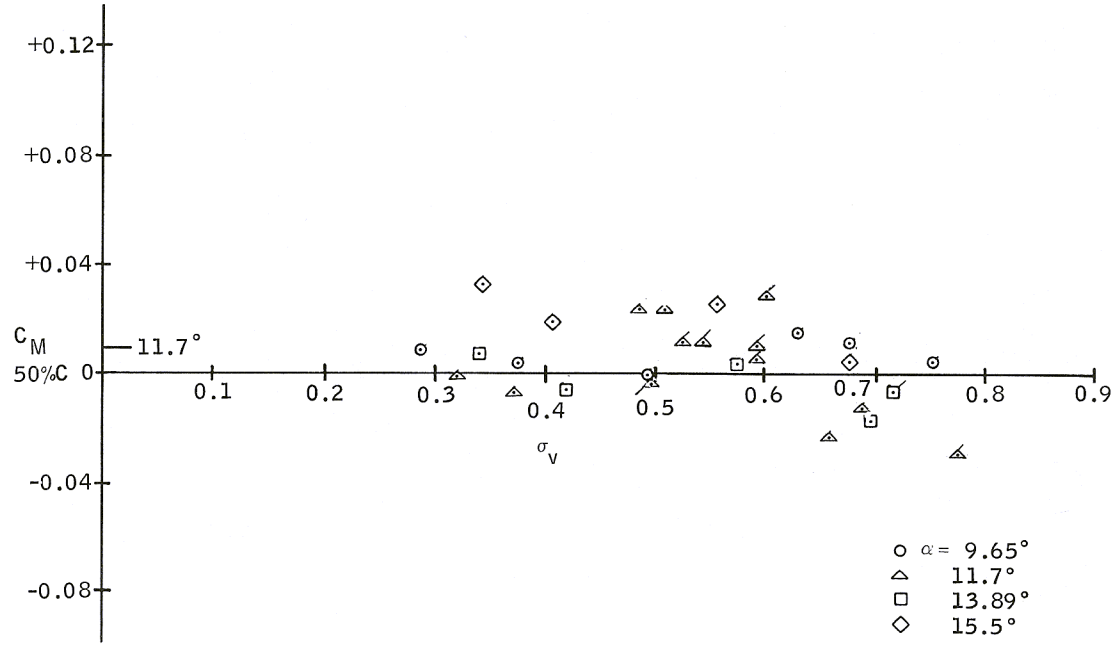

Figure 28. Pitching Moment Coefficient, h/c = 0.333, Two-Term Foil

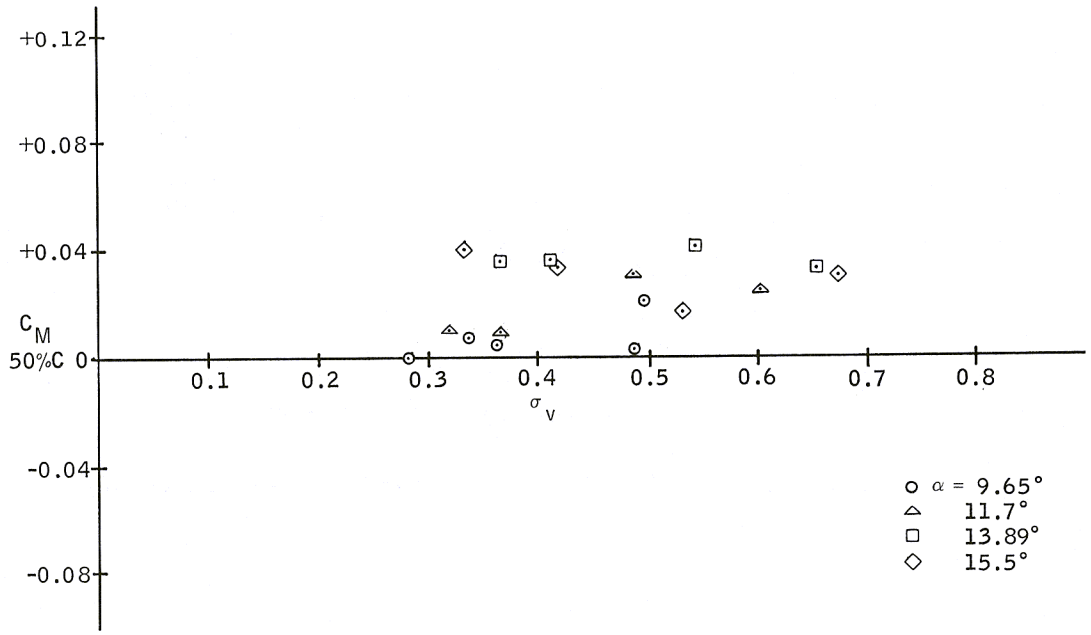

Figure 29. Pitching Moment Coefficient, h/c = 0.666, Two-Term Foil

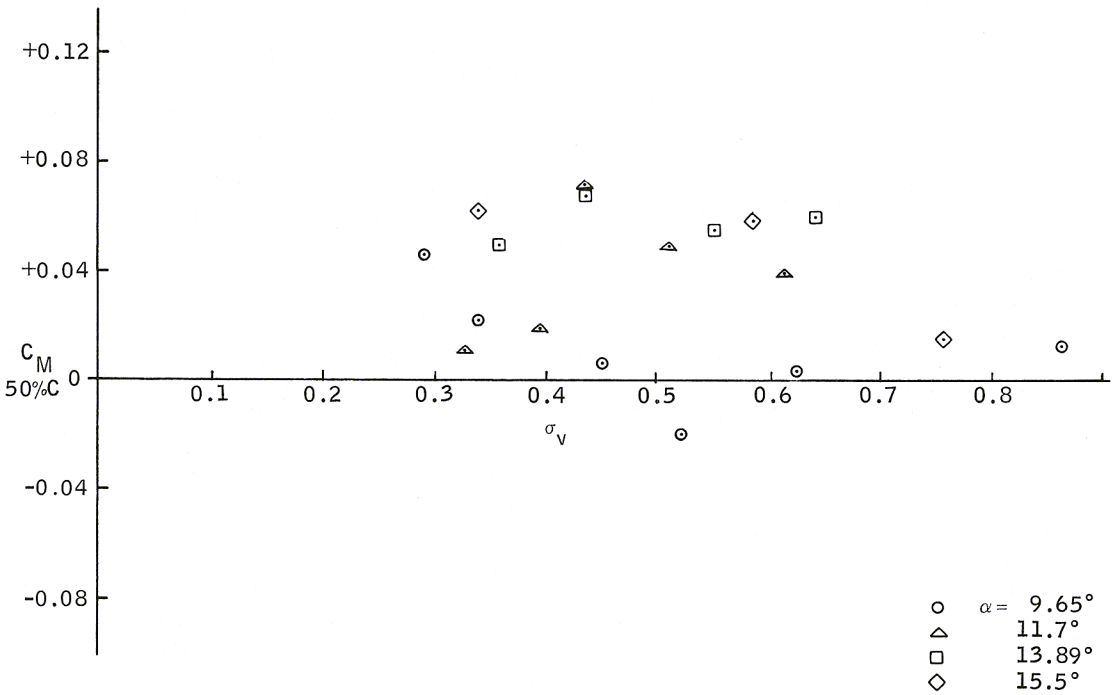

Figure 30. Pitching Moment Coefficient, h/c = 1.000, Two-Term Foil

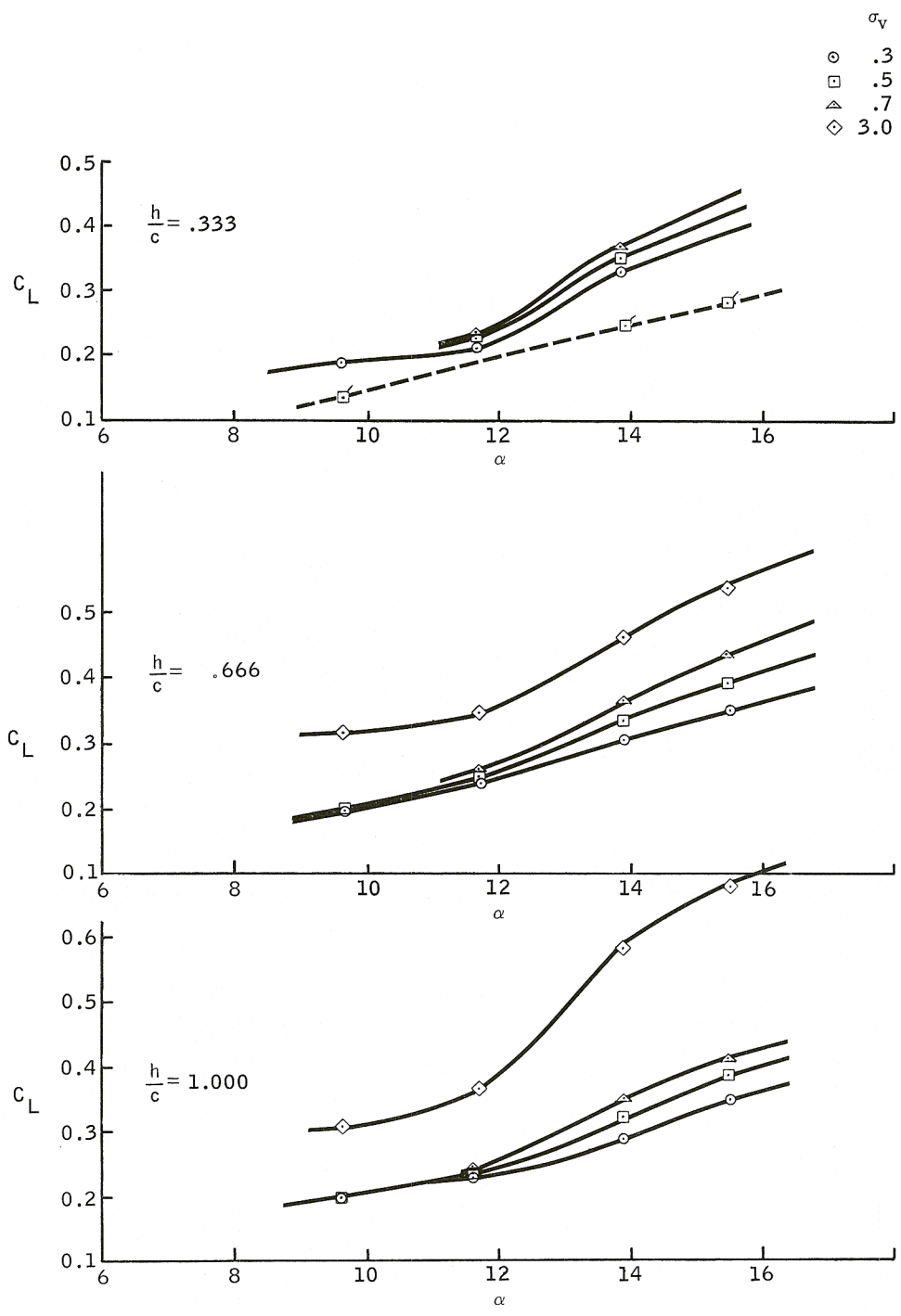

Figure 31. Variation of Lift Coefficient With Angle of Attack at Constant Cavitation Number, Flat-Plate Foil

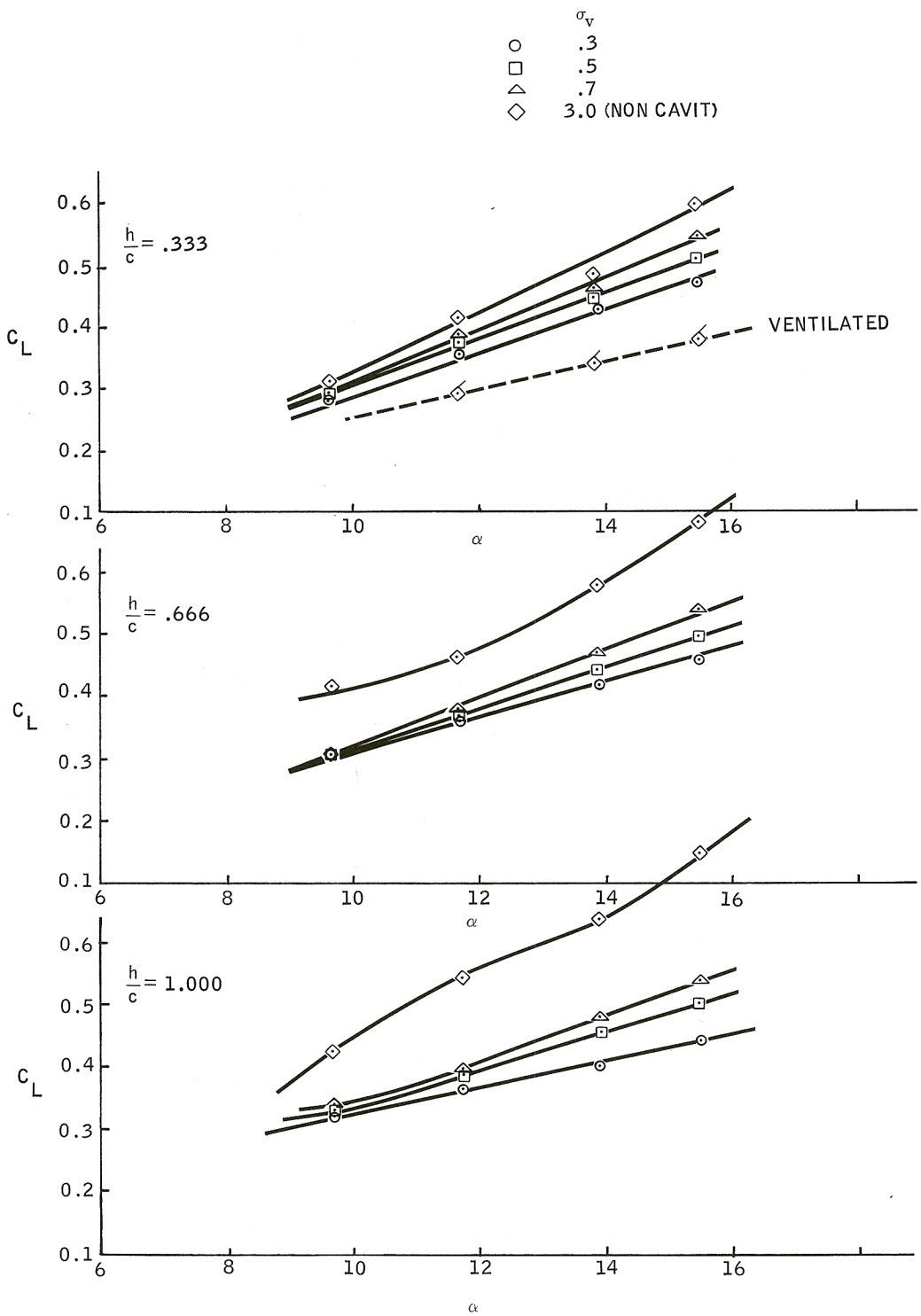

Figure 32. Variation of Life Coefficient With Angle of Attack at Constant Cavitation Number, Two-Term Foil

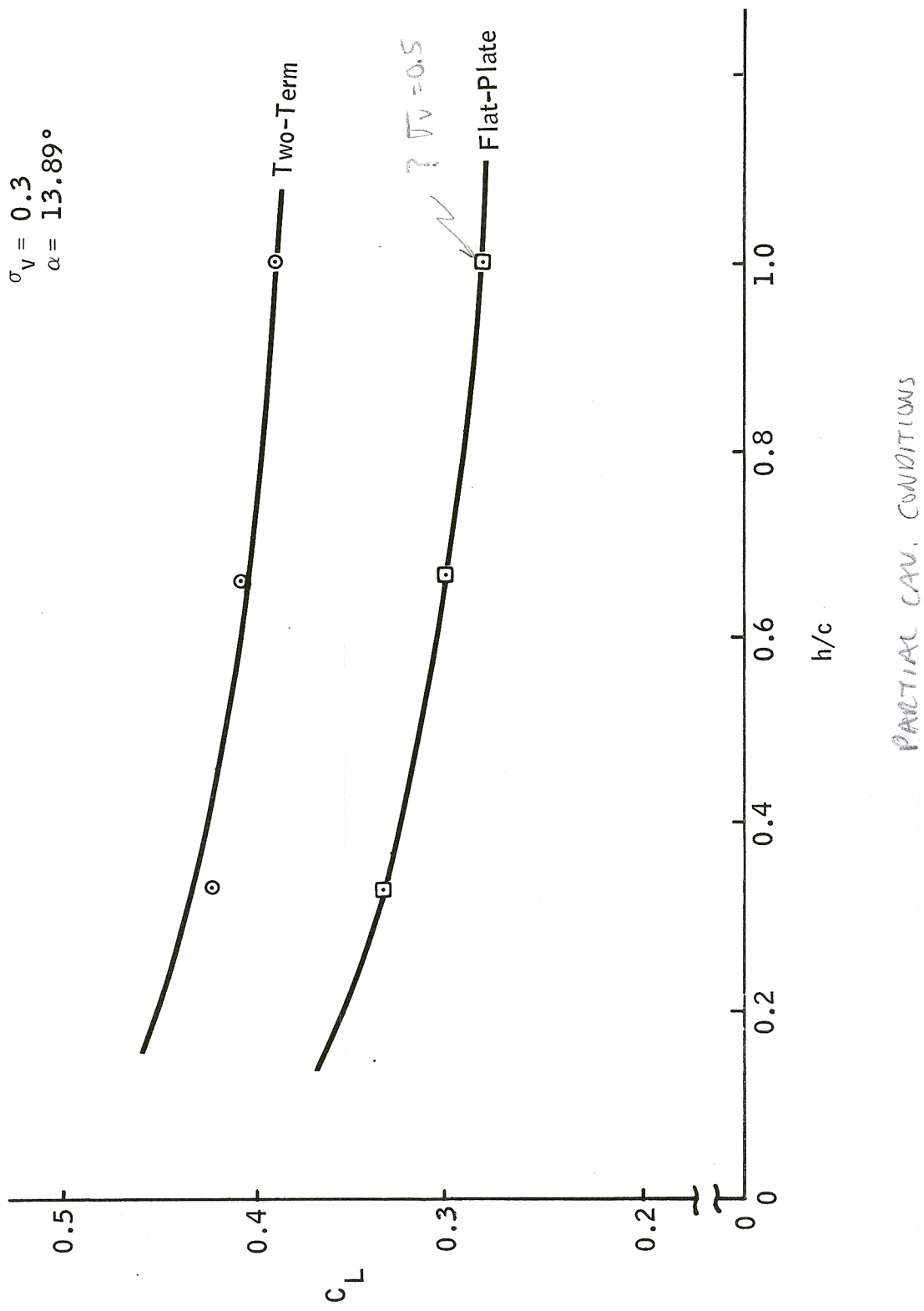

Figure 33. Variation of Lift Coefficient With Submergence Ratio

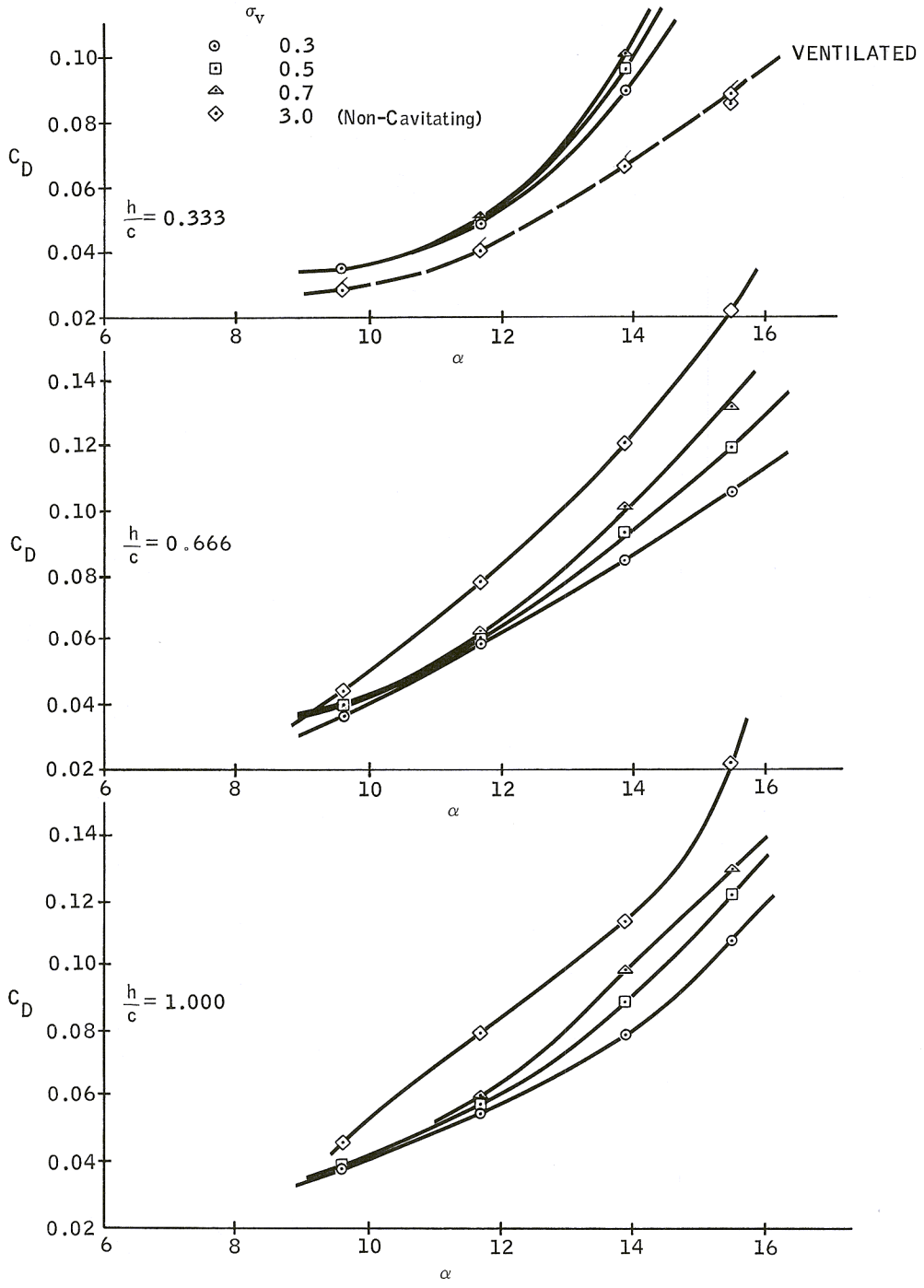

Figure 34. Variation of Drag Coefficient With Angle of Attack at Constant Cavitation Number, Flat-Plate Foil

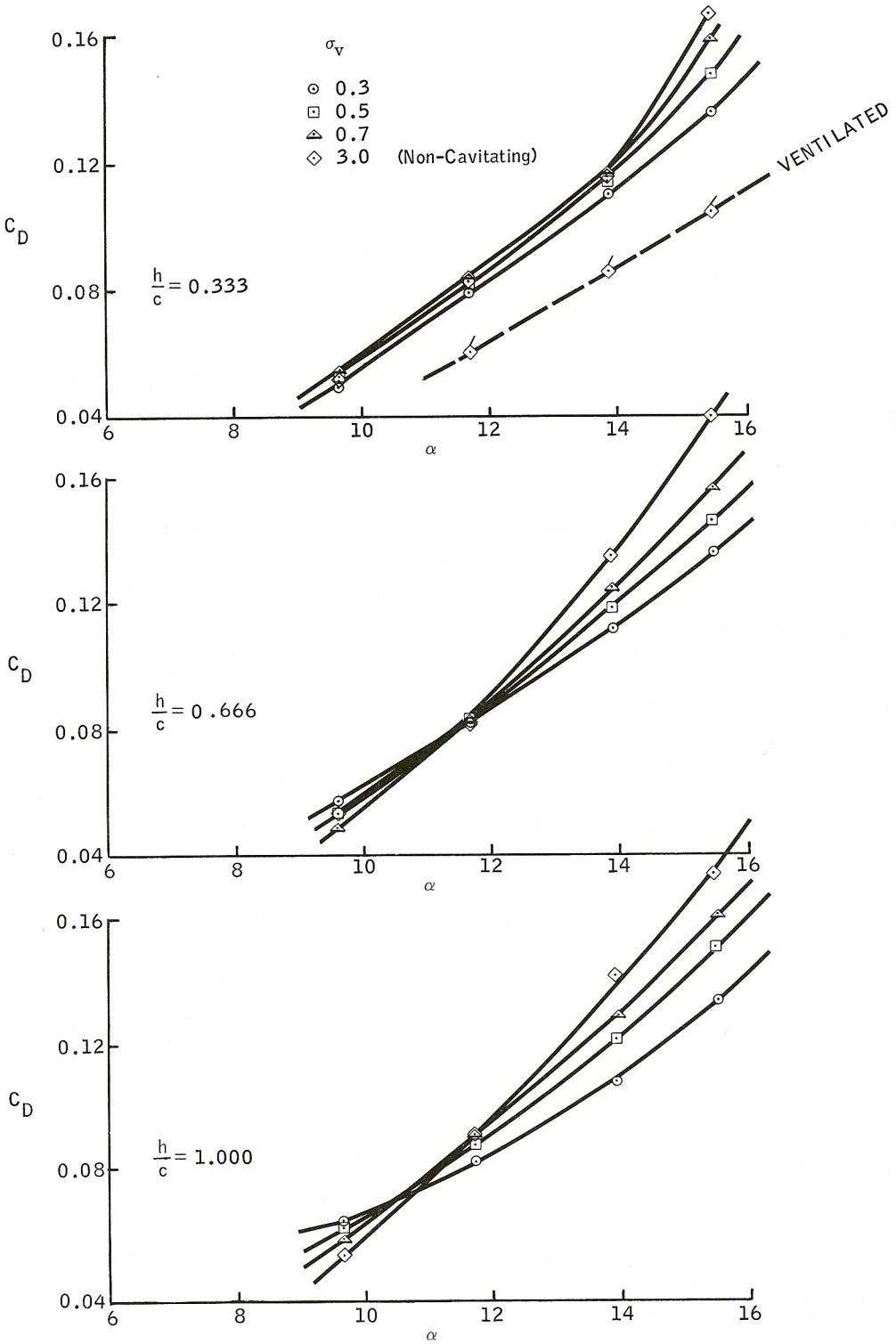

Figure 35. Variation of Drag Coefficient With Angle of Attack at Constant Cavitation Number, Two-Term Foil

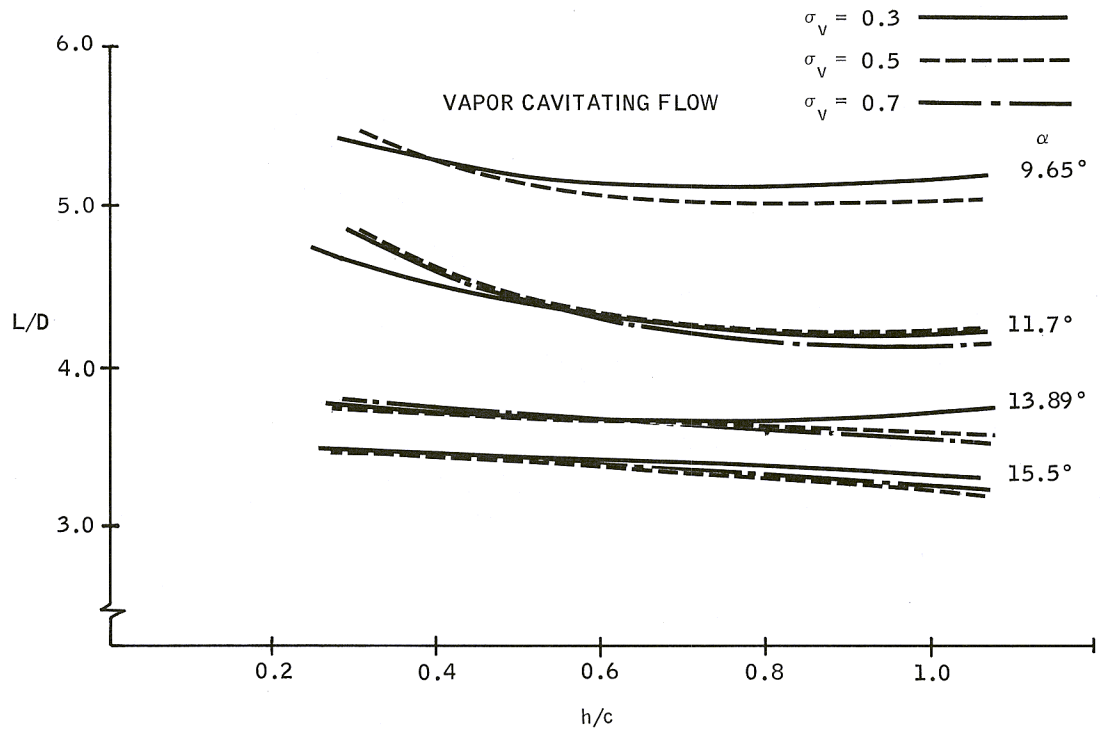

Figure 36. Variation of Lift-Drag Ratio With Submergence Ratio at Constant Cavitation Number, Flat-Plate Foil

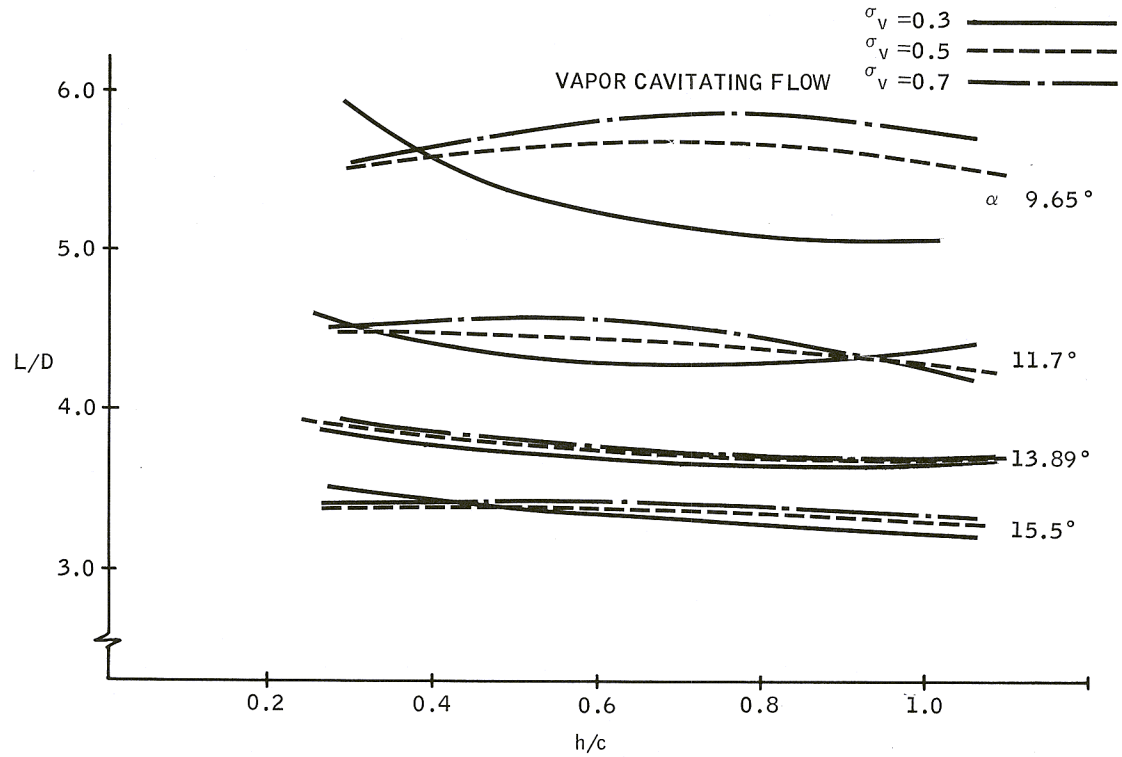

Figure 37. Variation of Lift-Drag Ratio With Submergence Ratio at Constant Cavitation Number, Two-Term Foil

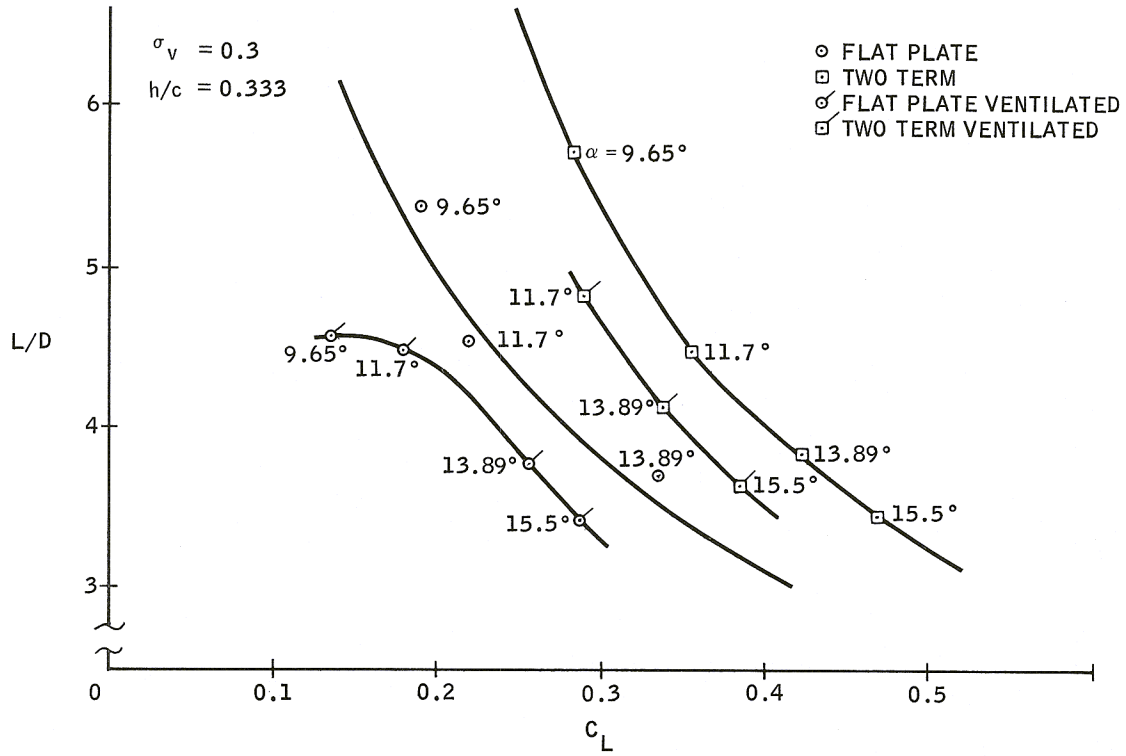

Figure 38a. Variation of Lift-Drag Ratio With Lift Coefficient at σ_V = 0.3 and h/c = 0.333

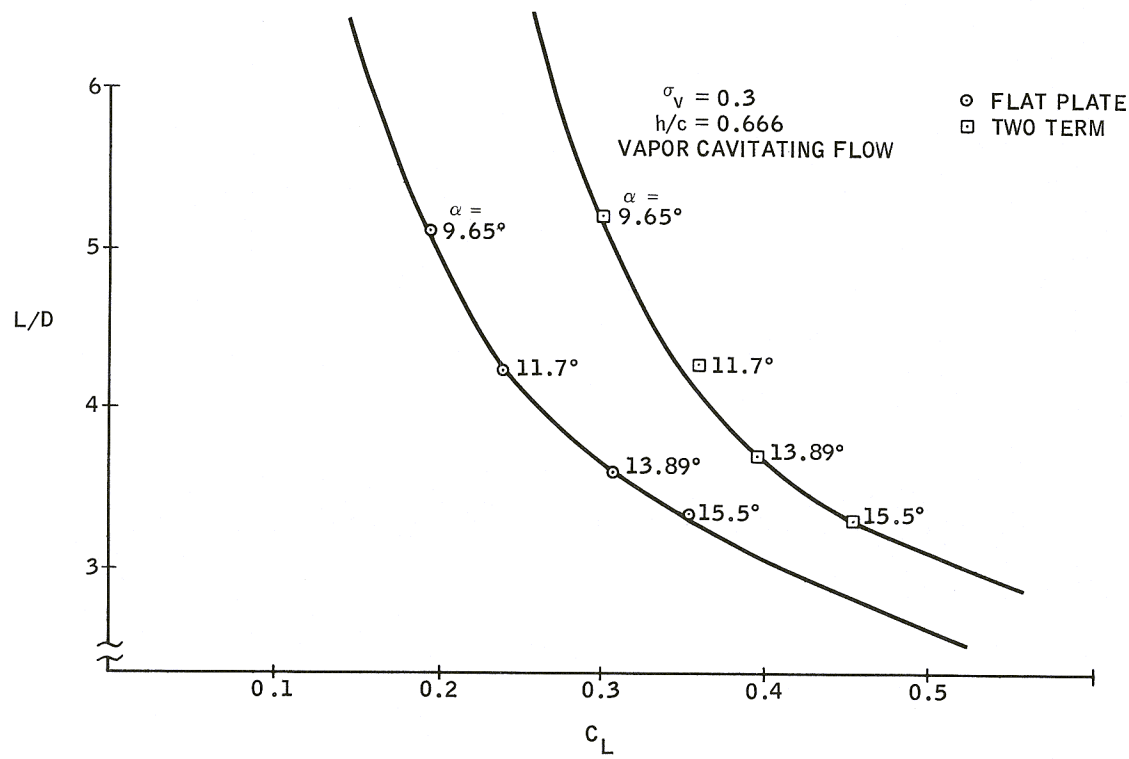

Figure 38b. Variation of Lift-Drag Ratio With Lift Coefficient at σ_V = 0.3 and h/c = 0.666

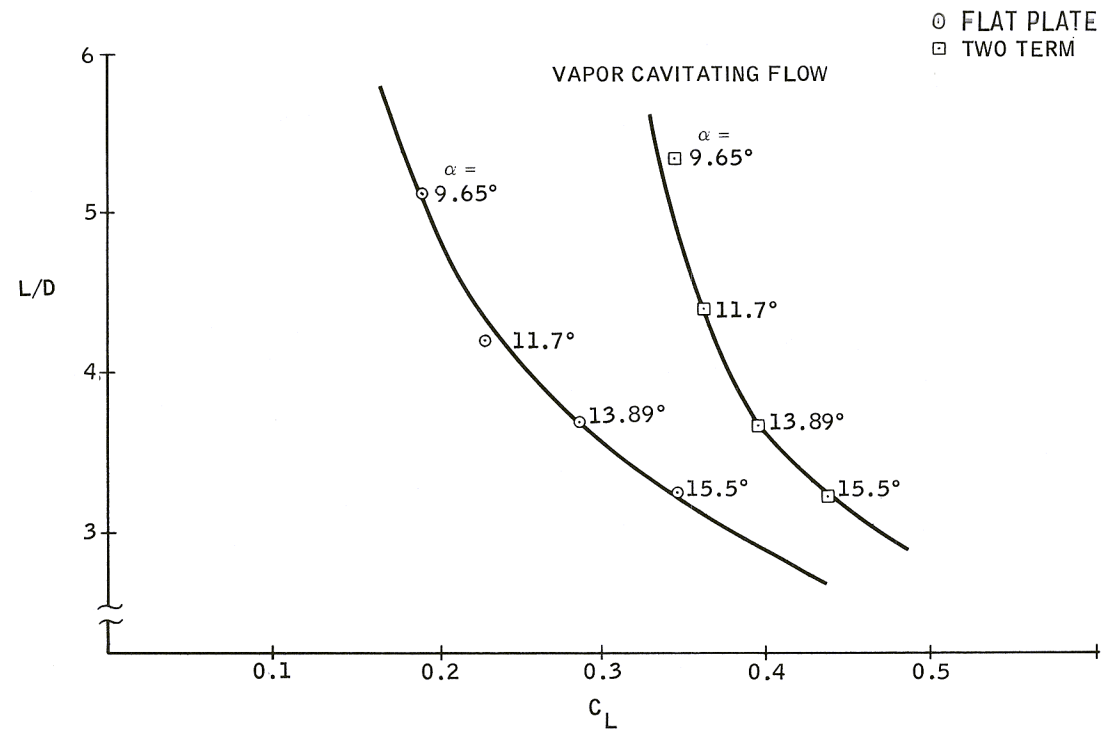

Figure 38c. Variation of Lift-Drag Ratio With Lift Coefficient at σ_v = 0.3 and h/c = 1.000

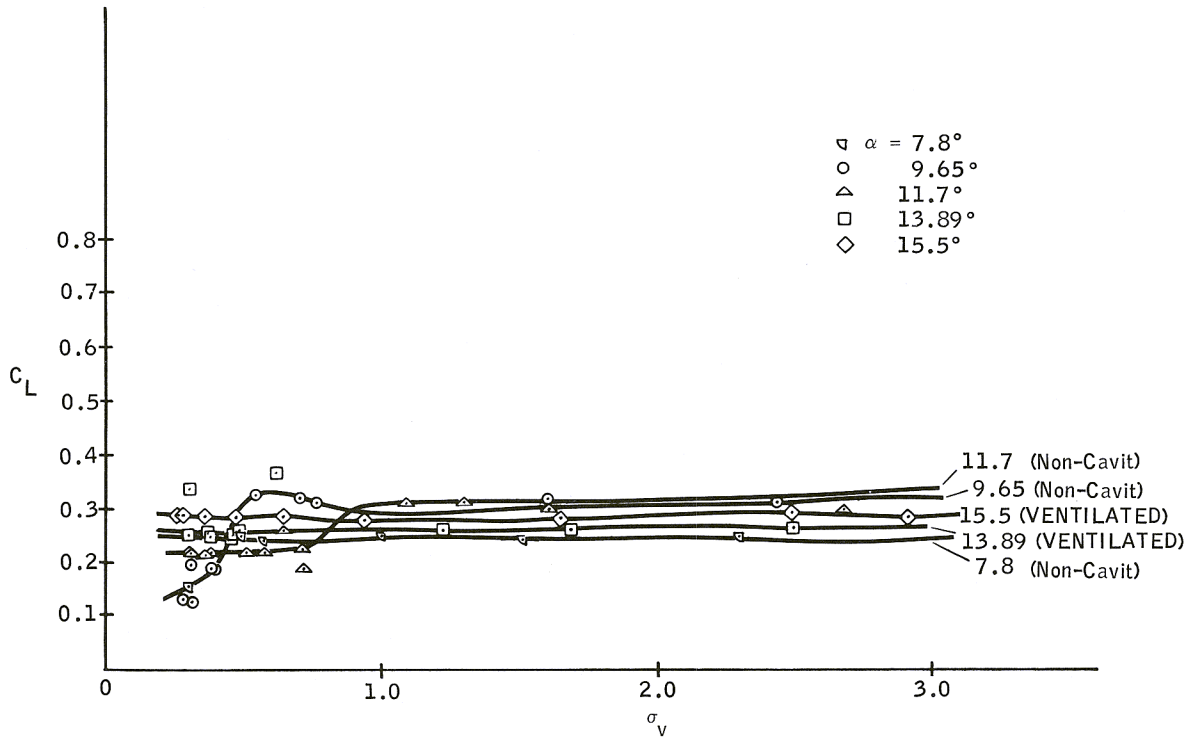

Figure 39. Lift Coefficient, h/c = 0.333, Flat-Plate Foil

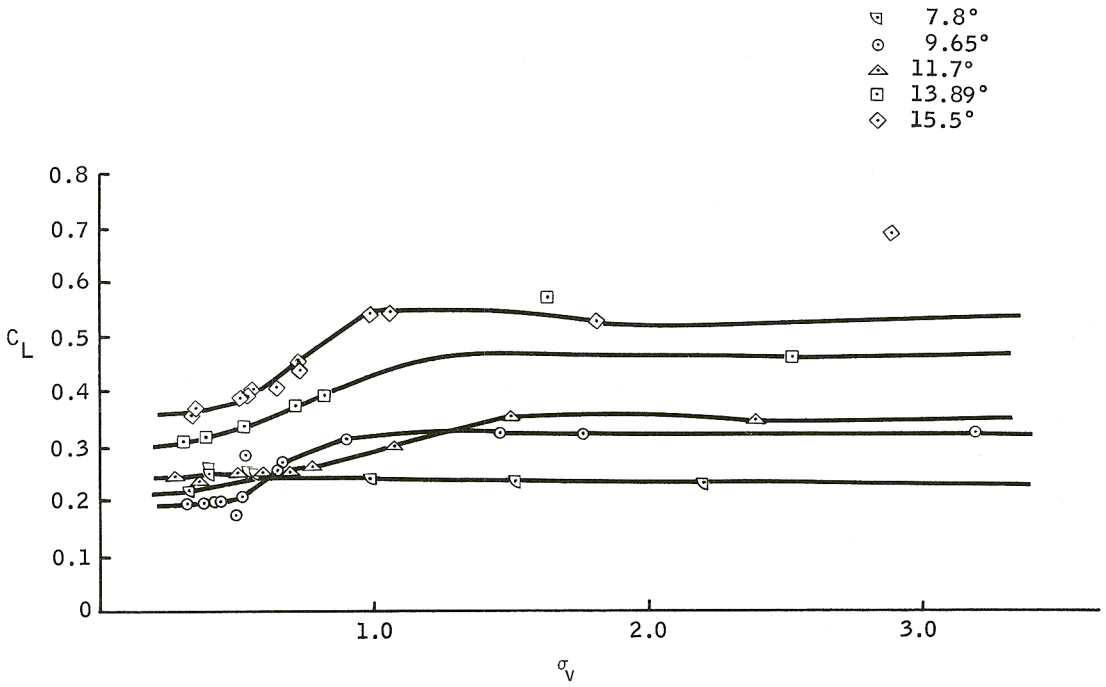

Figure 40. Lift Coefficient, h/c = 0.666, Flat-Plate Foil

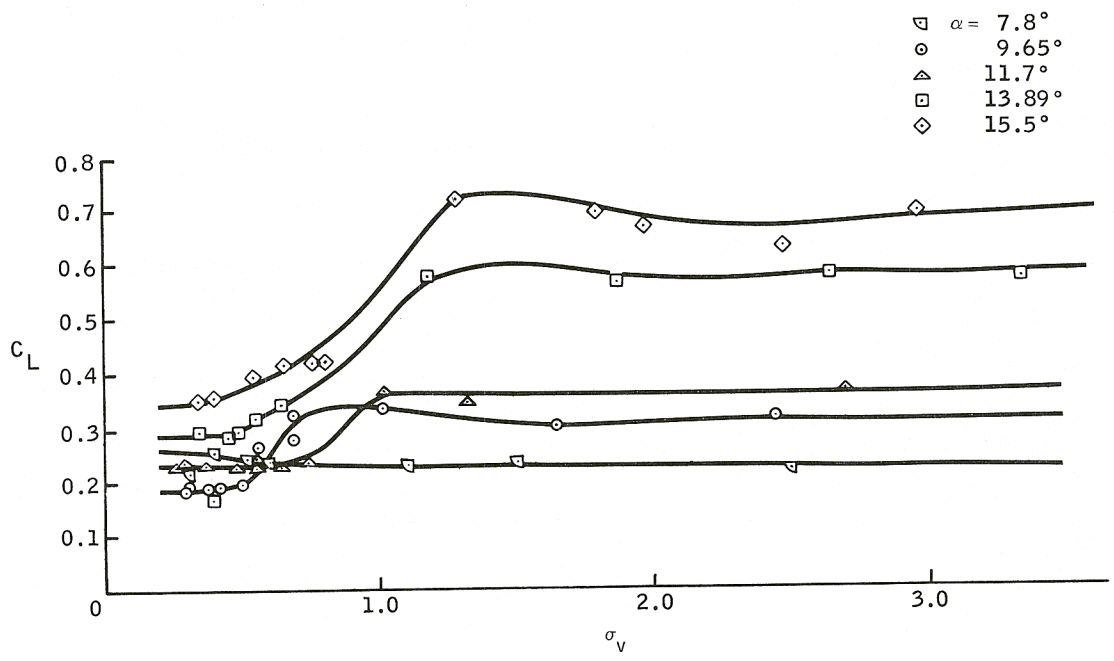

Figure 41. Lift Coefficient, h/c = 1.000, Flat-Plate Foil

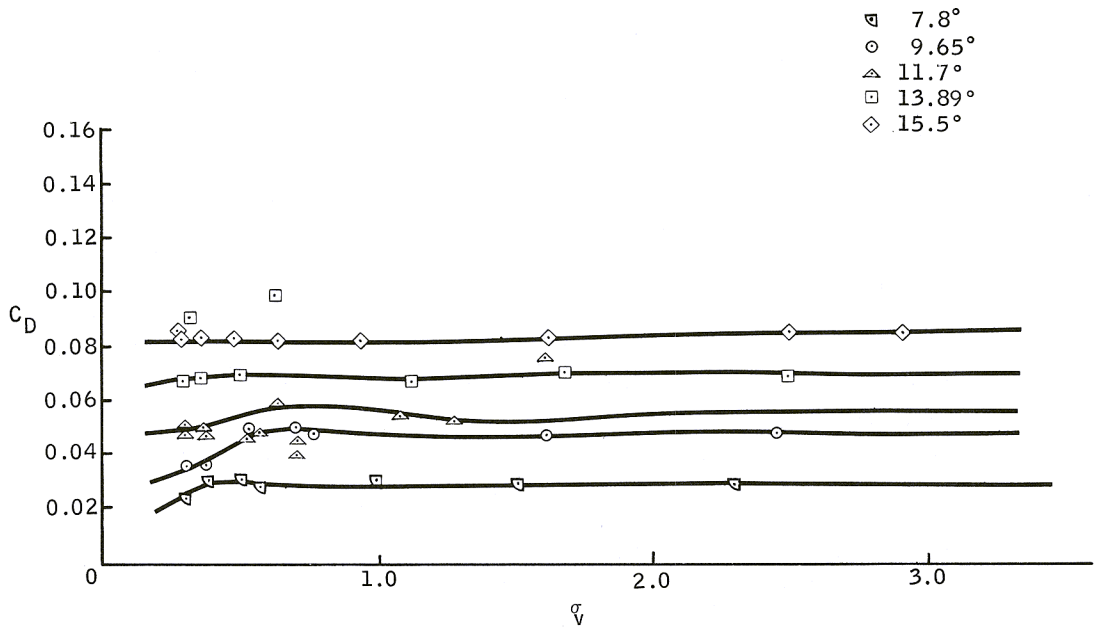

Figure 42. Drag Coefficient, h/c = 0.333, Flat-Plate Foil

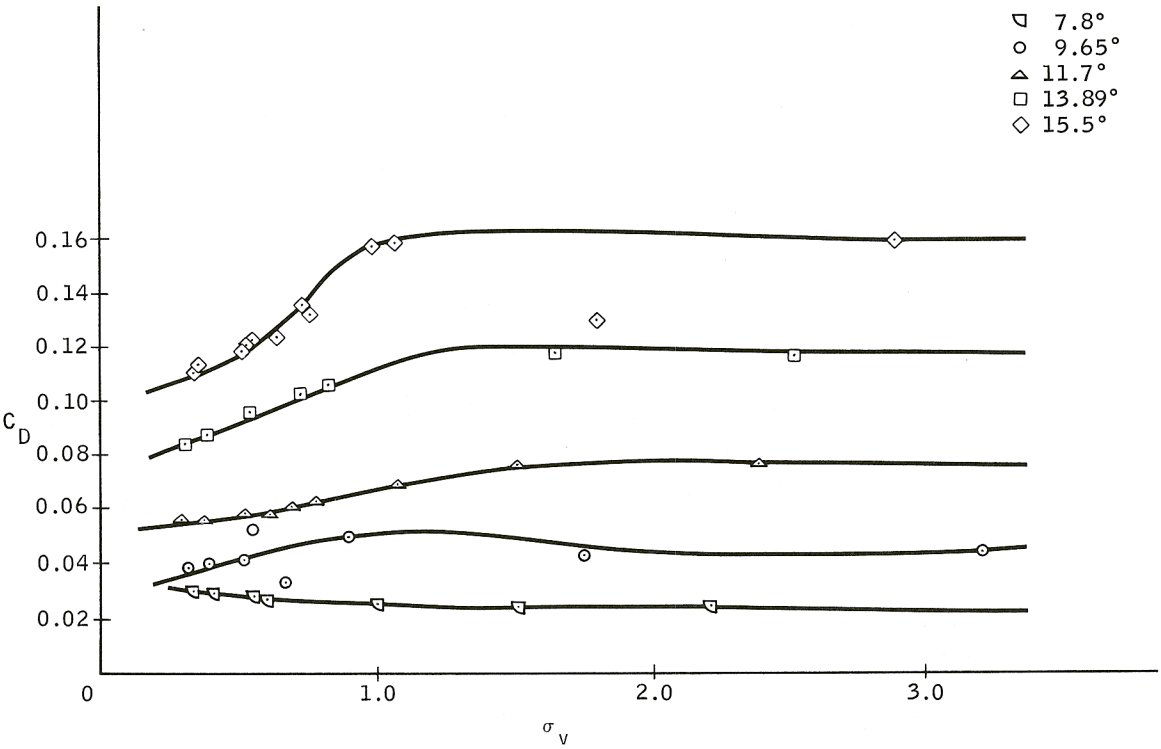

Figure 43. Drag Coefficient, h/c = 0.666, Flat-Plate Foil

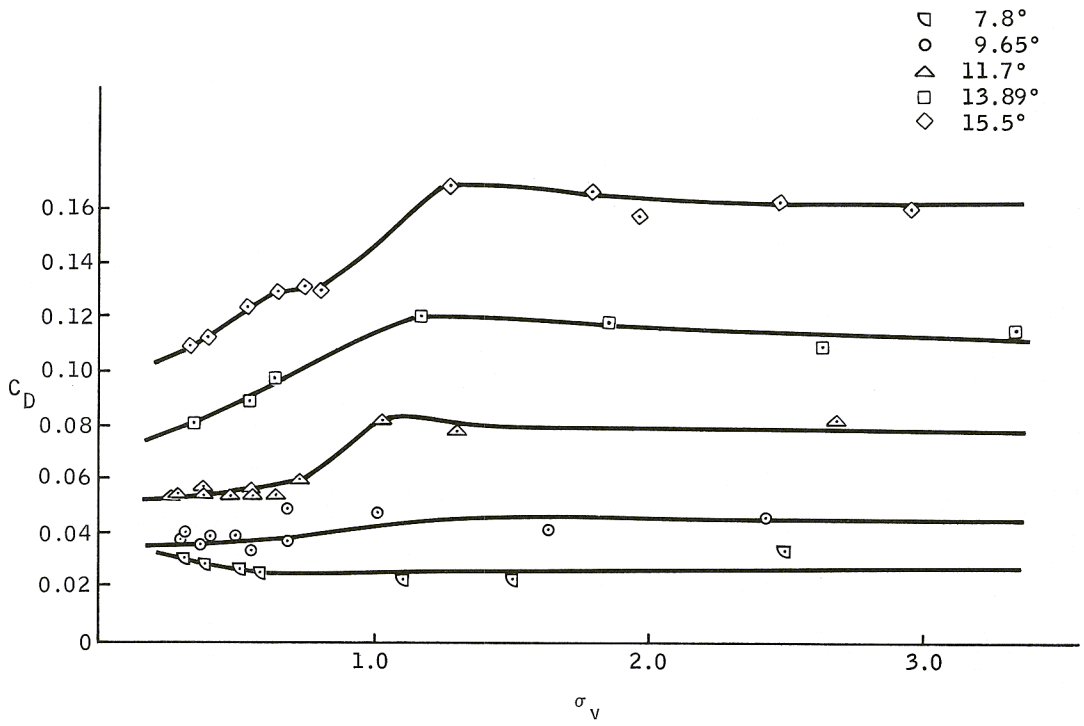

Figure 44. Drag Coefficient, h/c = 1.000, Flat-Plate Foil

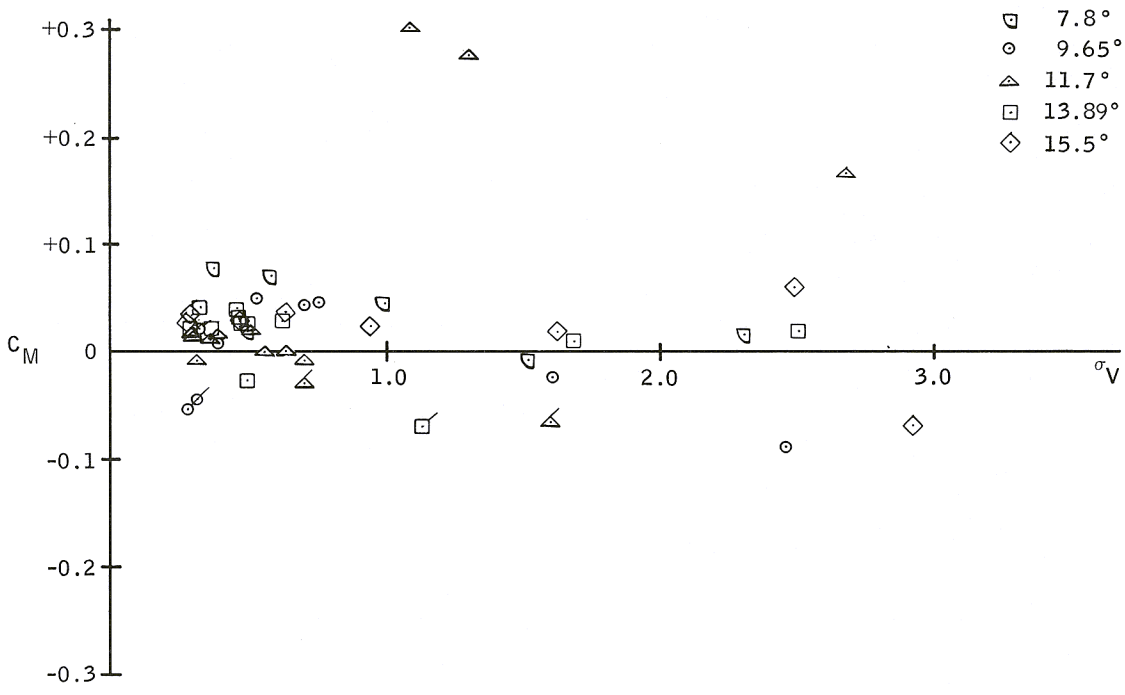

Figure 45. Pitching Moment Coefficient, h/c = 0.333, Flat-Plate Foil

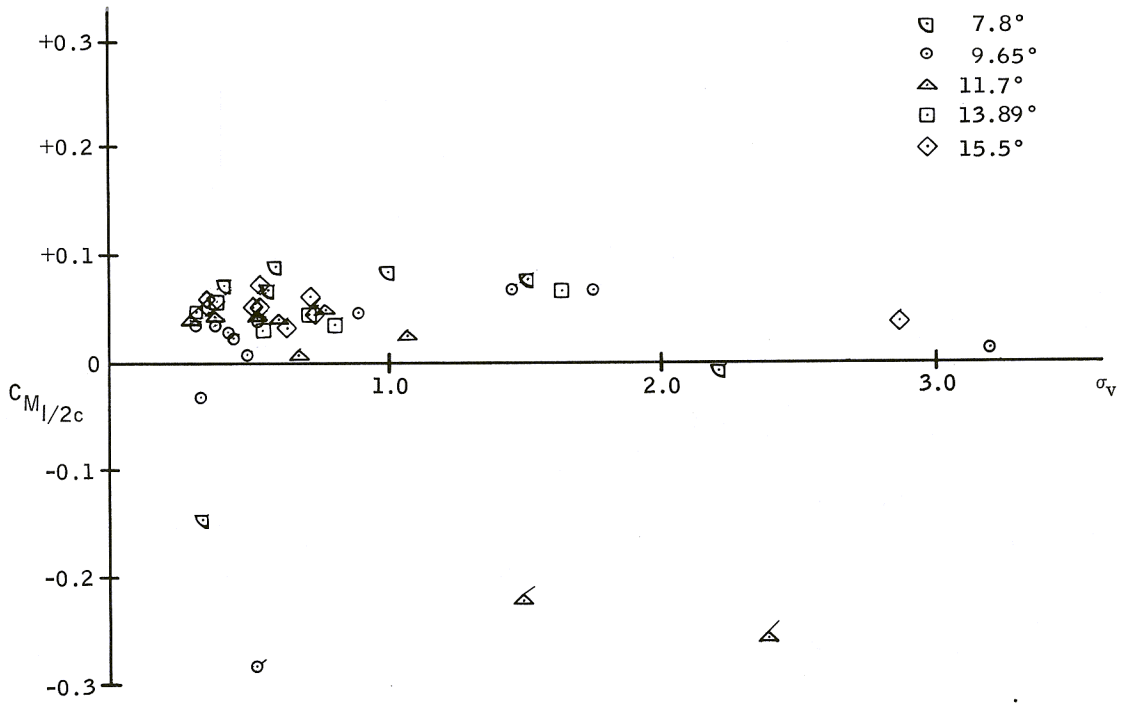

Figure 46. Pitching Moment Coefficient, h/c = 0.666, Flat-Plate Foil

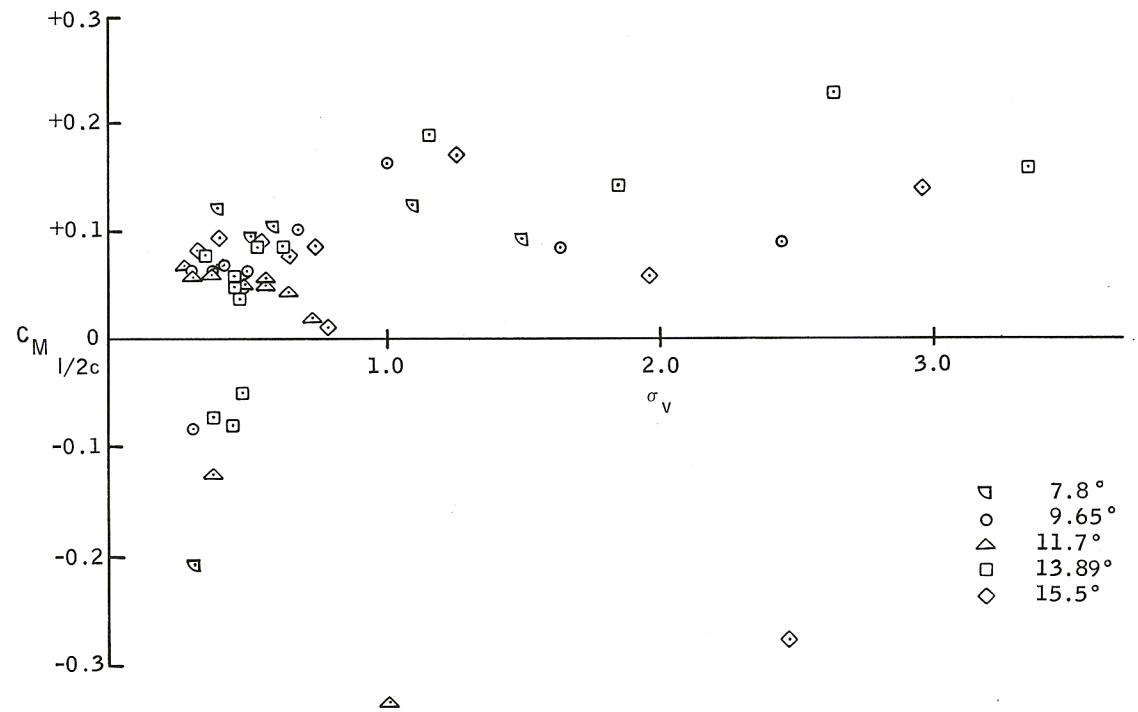

Figure 47. Pitching Moment Coefficient, h/c = 1.000, Flat-Plate Foil

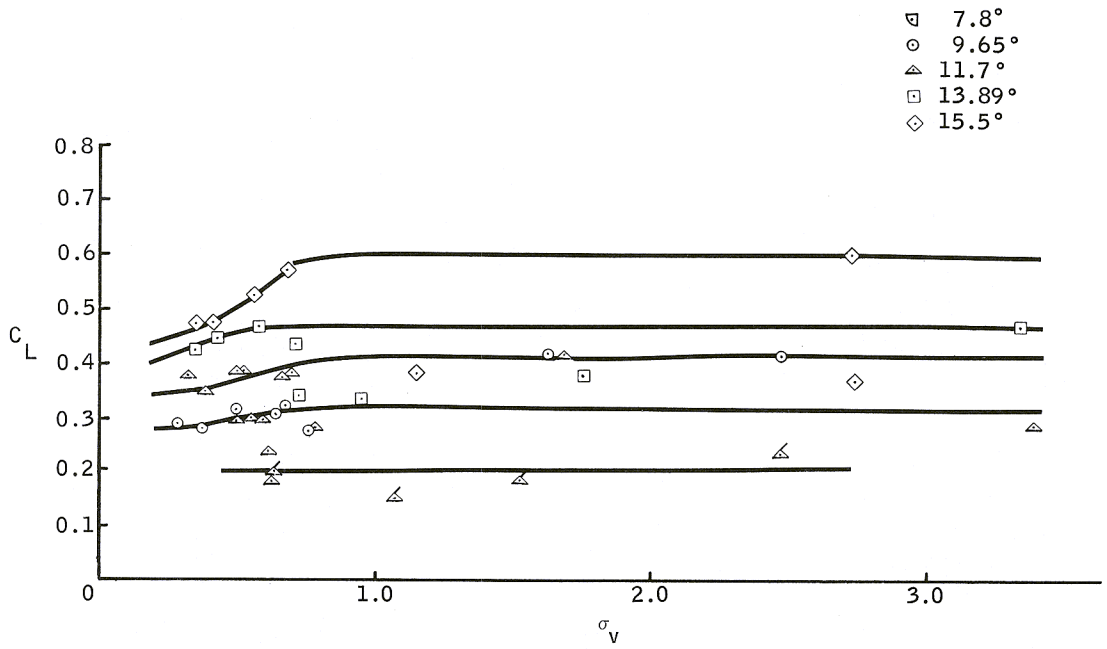

Figure 48. Lift Coefficient, h/c = 0.333, Two-Term Foil

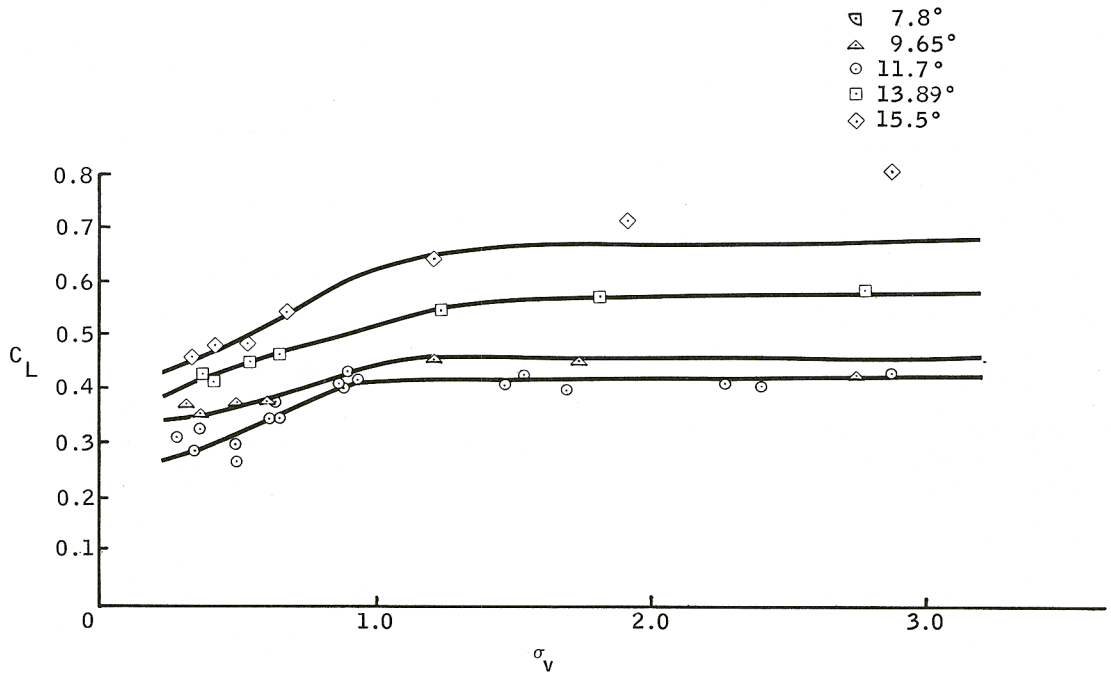

Figure 49. Lift Coefficient, h/c = 0.666, Two-Term Foil

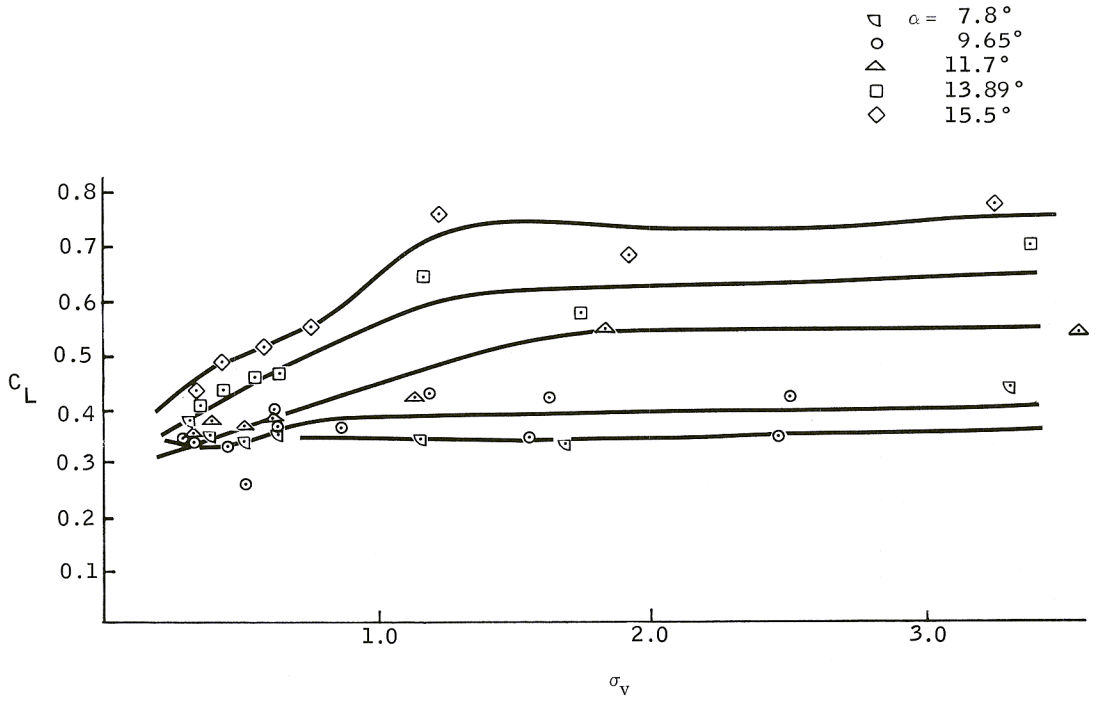

Figure 50. Lift Coefficient, h/c = 1.000, Two-Term Foil

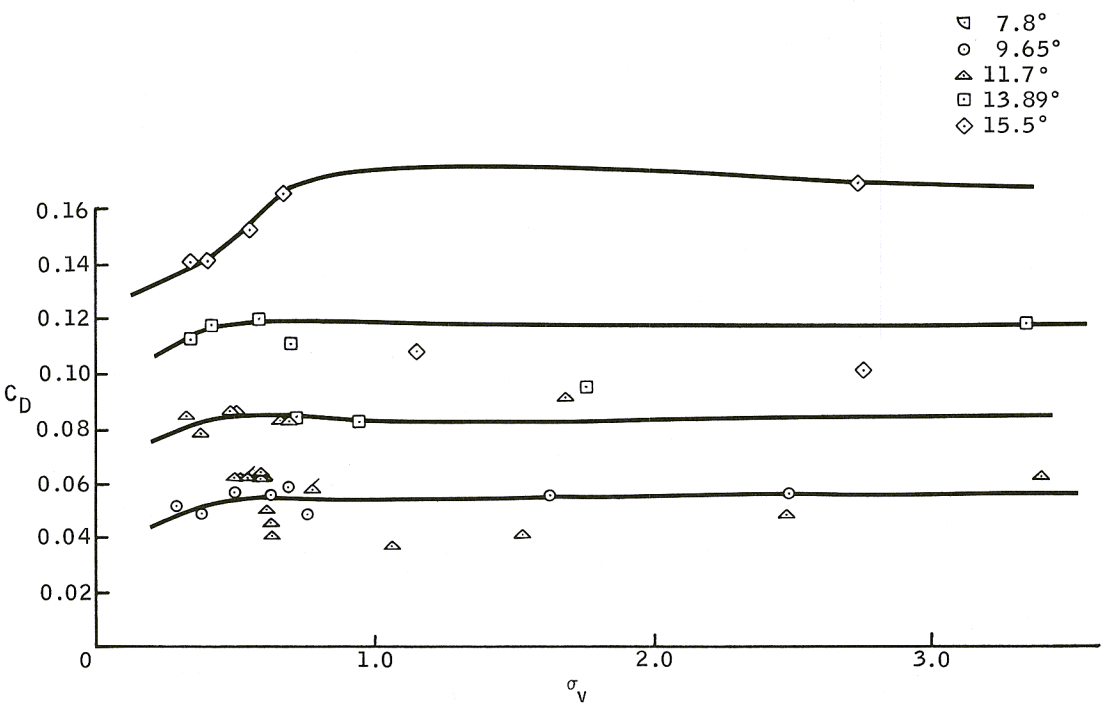

Figure 51. Drag Coefficient, h/c = 0.333, Two-Term Foil

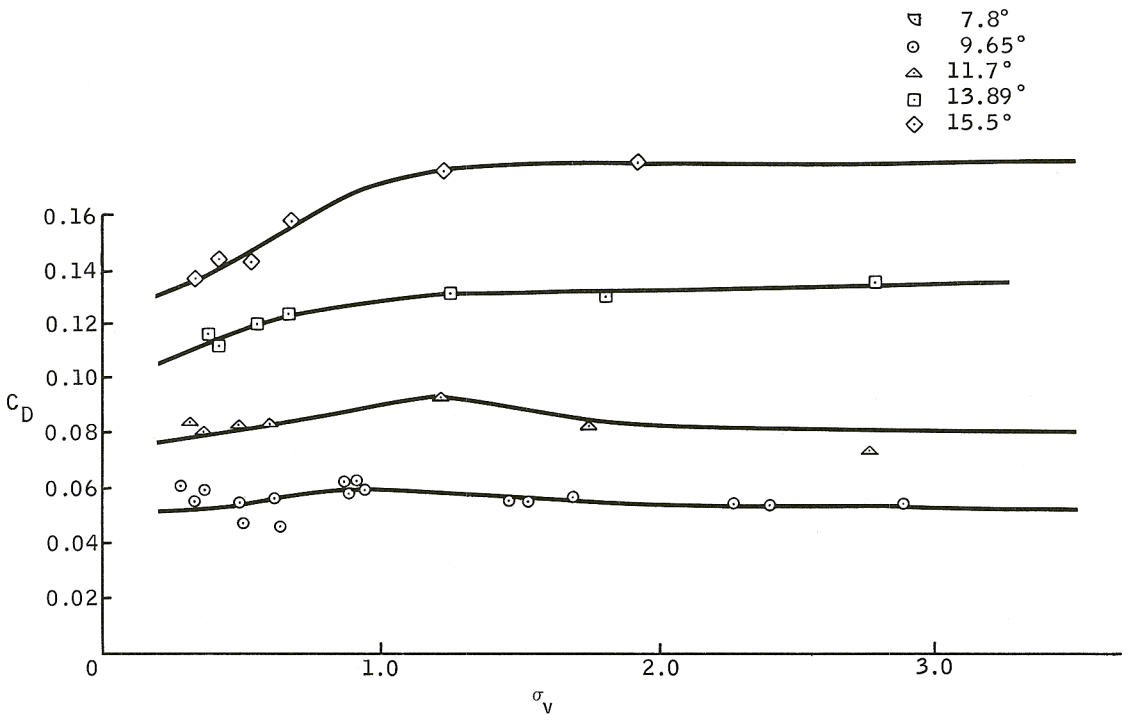

Figure 52. Drag Coefficient, h/c = 0.666, Two-Term Foil

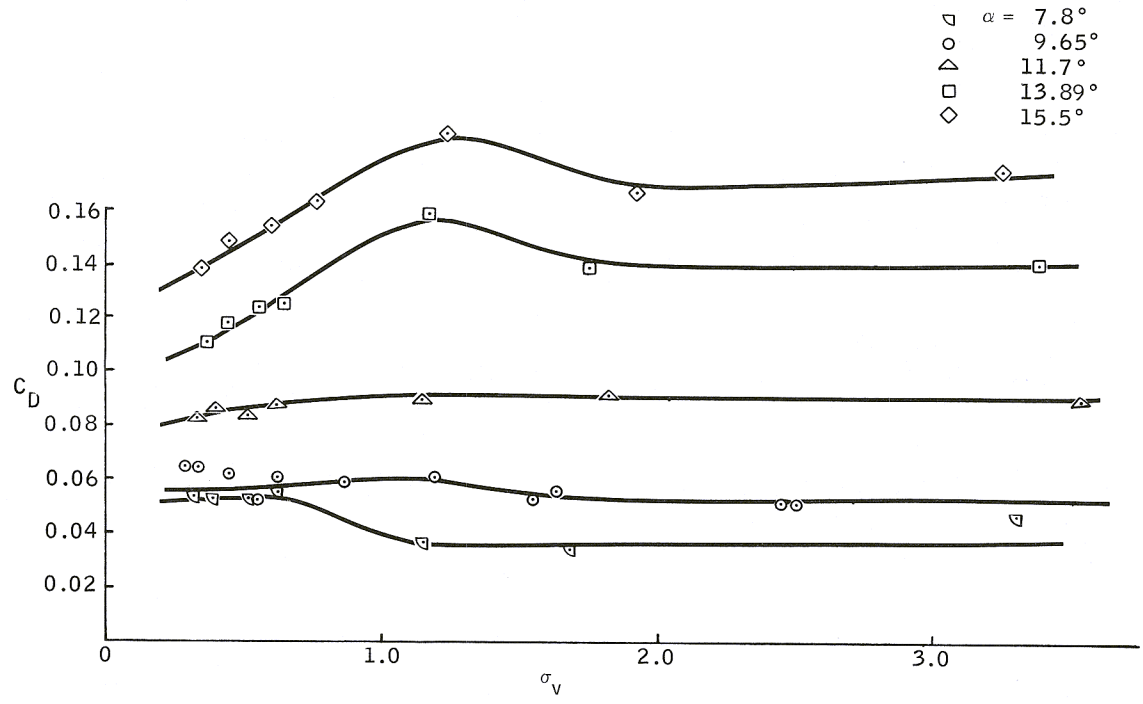

Figure 53. Drag Coefficient, h/c = 1.000, Two-Term Foil

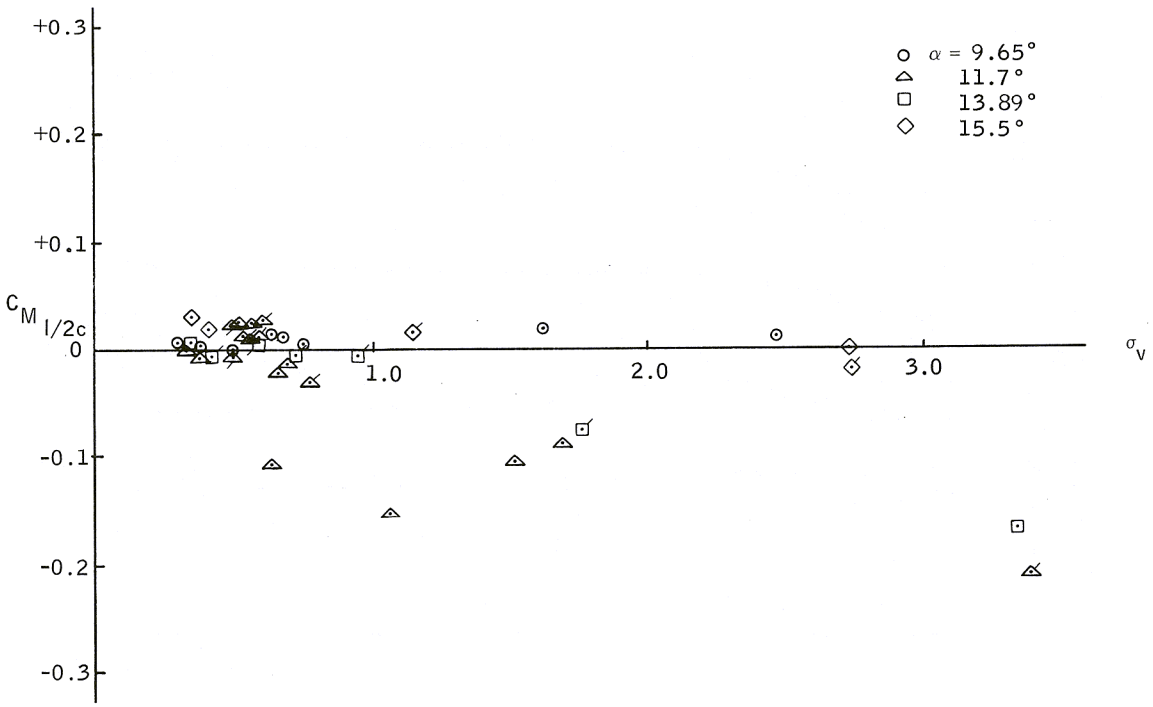

Figure 54. Pitching Moment Coefficient, h/c = 0.333, Two-Term Foil

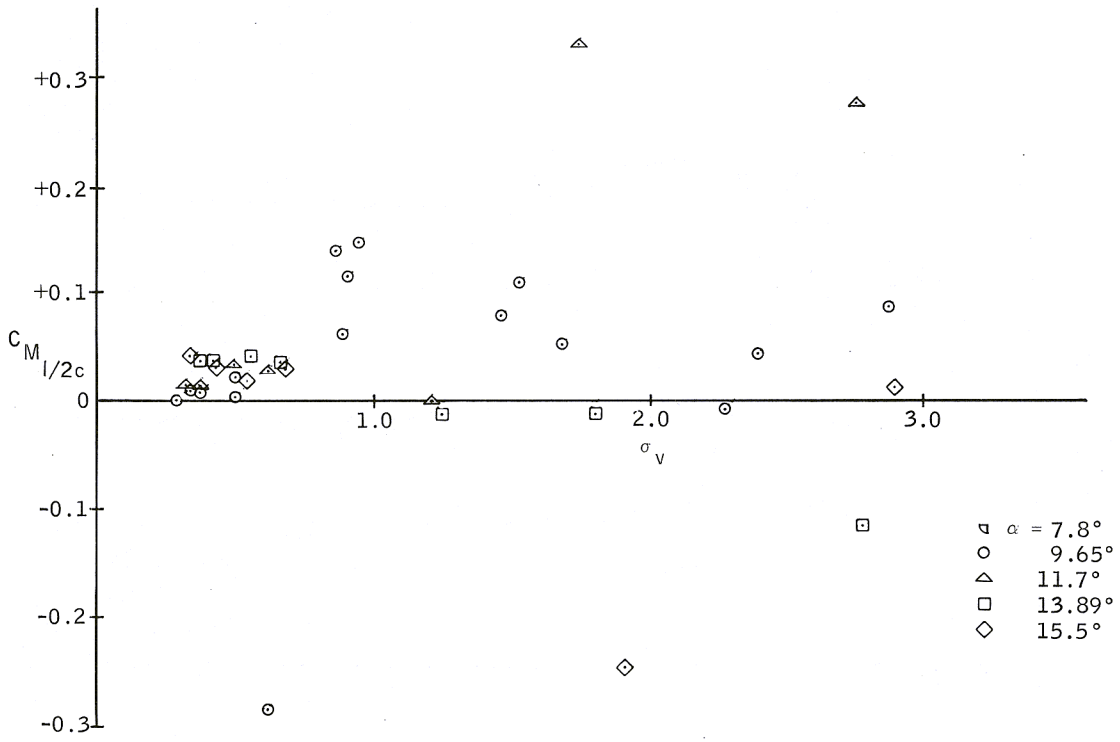

Figure 55. Pitching Moment Coefficient, h/c = 0.666, Two-Term Foil

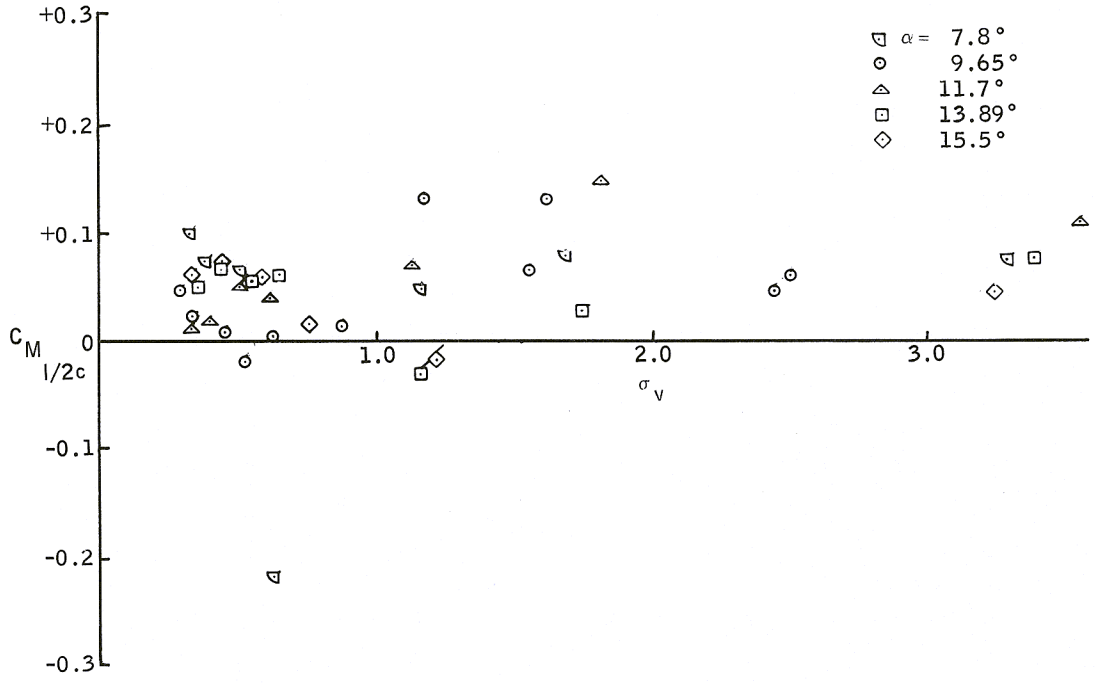

Figure 56. Pitching Moment Coefficient, h/c = 1.000, Two-Term Foil

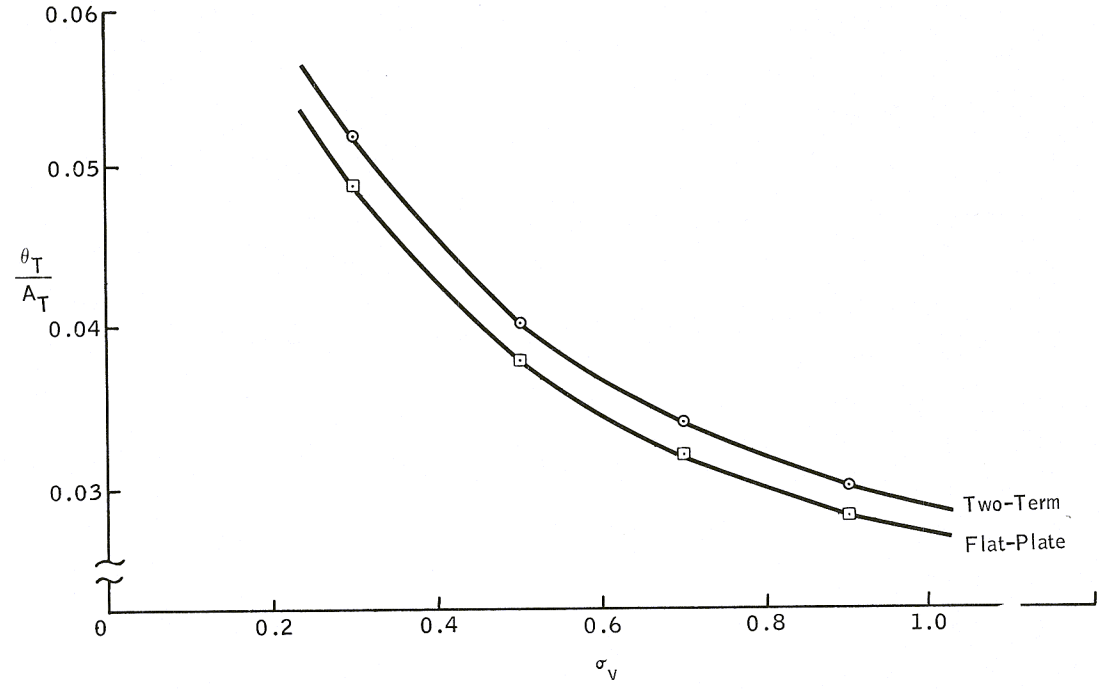

Figure 57. Variation of Θ_T/A_T With Cavitation Number

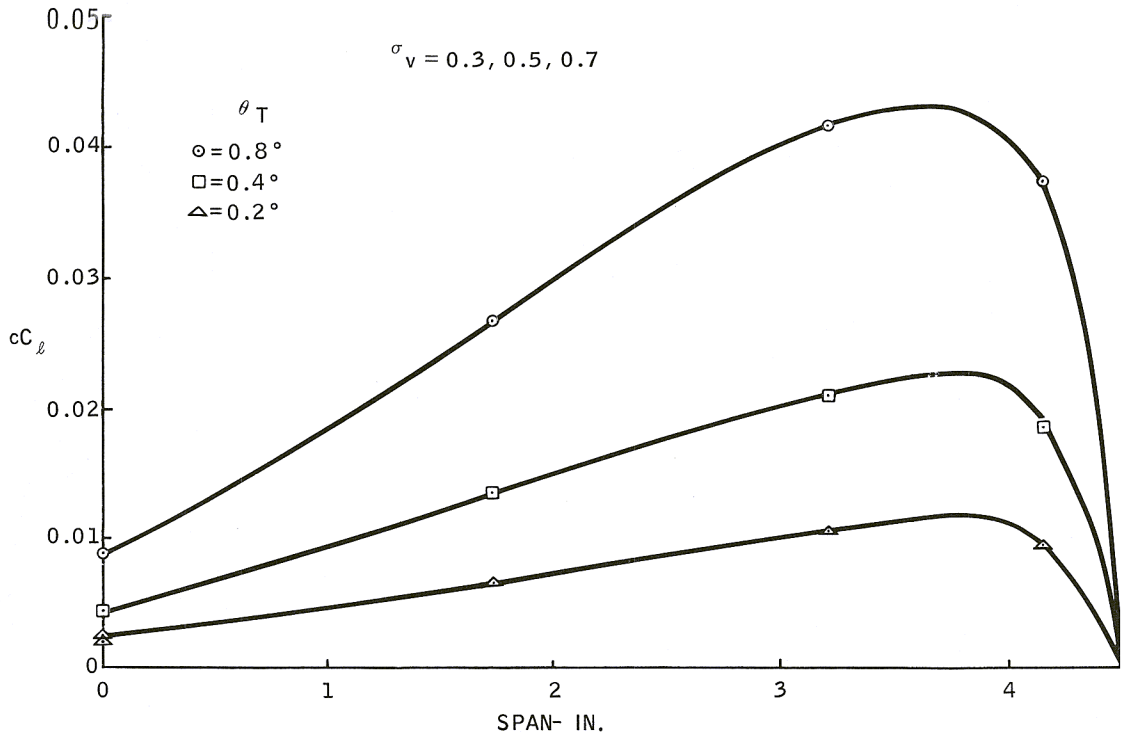

Figure 58. Incremental Lift Distribution Due to Twist

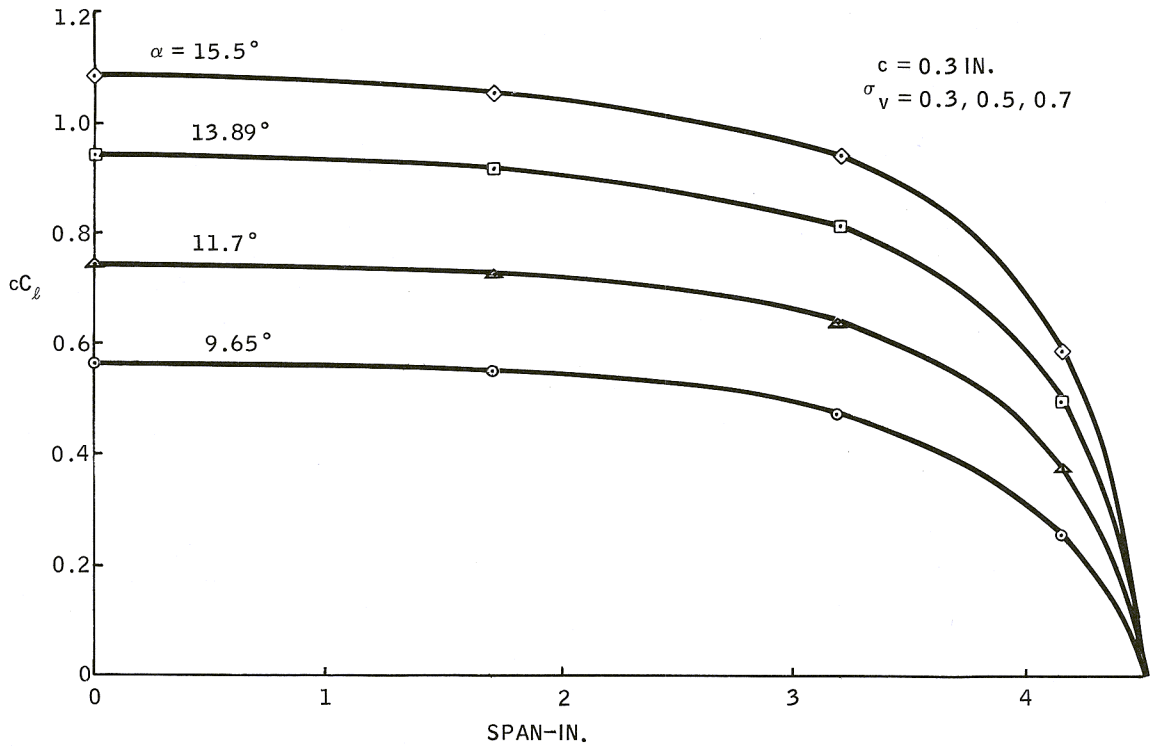

Figure 59. Basic Calculated Lift Distribution Curves for the Flat-Plate Foil

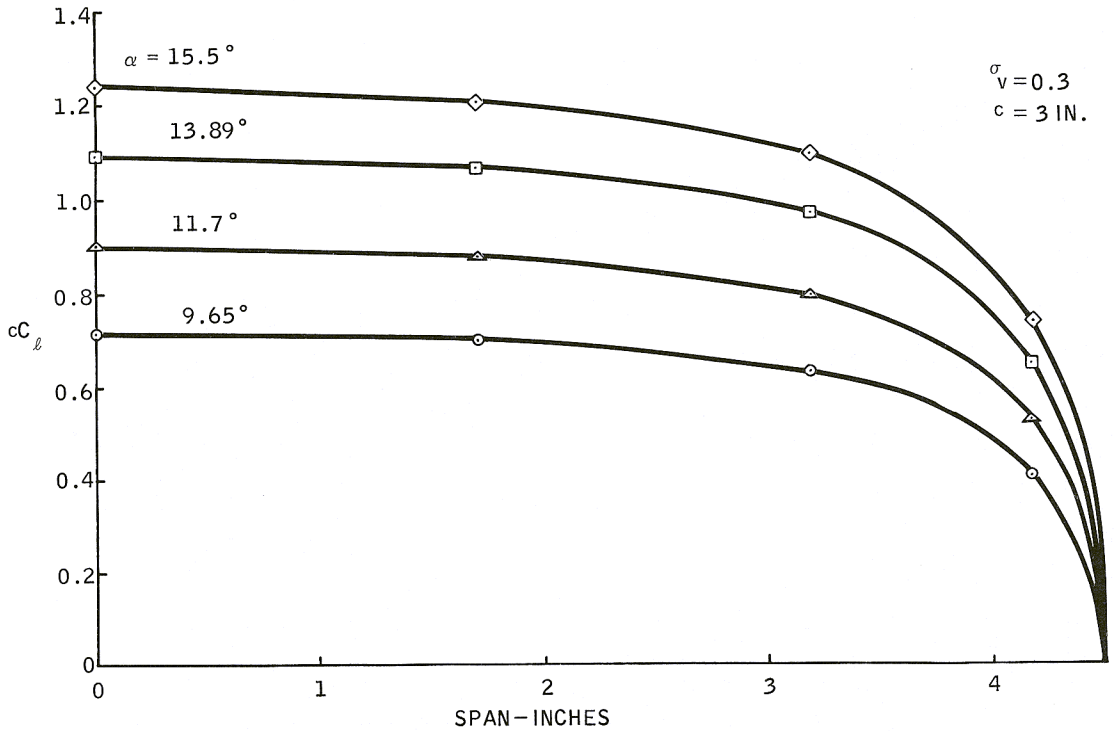

Figure 60. Basic Lift Distribution Curves for the Two-Term Foil

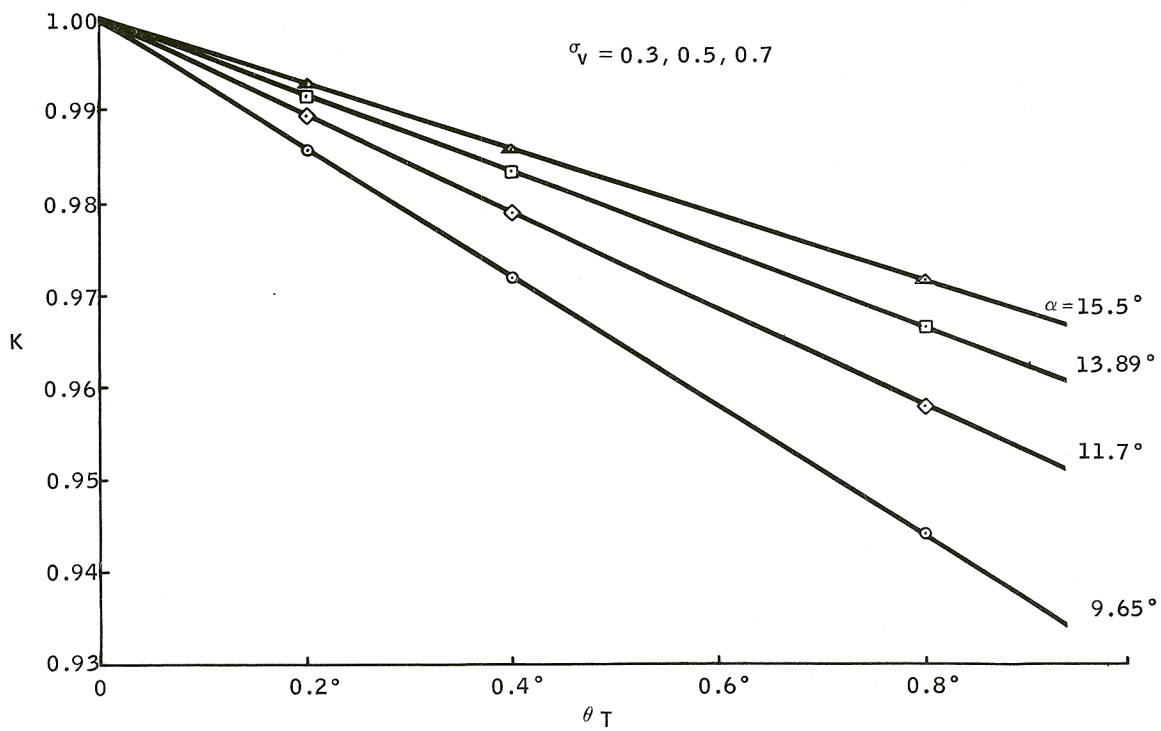

Figure 61. Variation of K With Tip Twist, Flat-Plate Foil

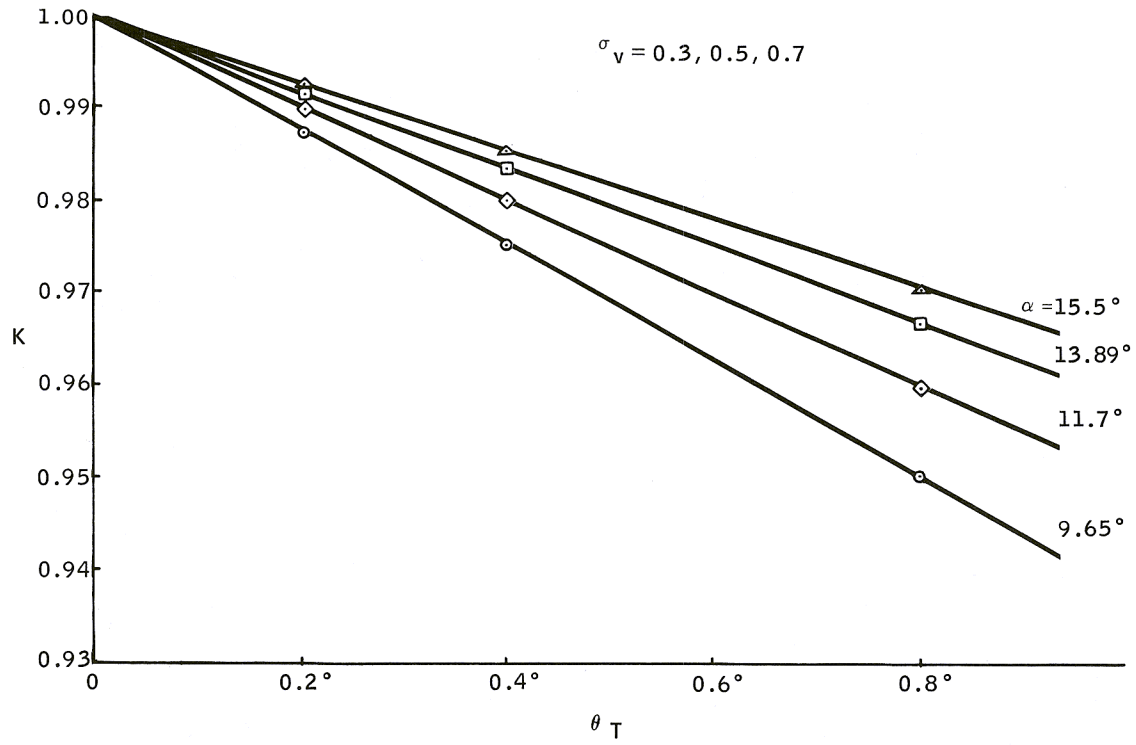

Figure 62. Variation of K With Tip Twist, Two-Term Foil

Chief, Bureau of Ships (44)
Navy Department
Washington 25, D. C.
Attn: Code 106 (1)
Code 335 (13)
Code 410 (1)
Code 420 (27)
Code 442 (1)
Code 449 (1)

Chief, Office of Naval Research
Navy Department
Washington 25, D. C.
Attn: Code 438 (2)

Commanding Officer and Director (6)
David Taylor Model Basin
Carderock, Maryland
Attn: Code 500 (1)
Code 513 (1)
Code 520 (1)
Code 526 (1)
Code 530 (1)
Code 580 (1)

Chief, Bureau of Naval Weapons (2)
Navy Department
Washington 25, D. C.
Attn: Code RAAD-334 (1)
Code RRSY-1 (1)

Mr. John B. Parkinson (1)
Langley Aeronautical Laboratory
National Aeronautics and Space Administration
Langley Field, Virginia

Boeing Airplane Company (1)
Aero-Space Division
Box 3707
Seattle, Washington

California Institute of Technology (1)
Pasadena, California
Attn: Hydrodynamics Laboratory

Director, Stevens Institute of Technology (1)
Davidson Laboratory
Castle Point Station
Hoboken, New Jersey

Hydronautics, Incorporated (1)
200 Monroe Street
Rockville, Maryland

Sperry Piedmont Company (1)
Charlottsville, Virginia
Attn: Mr. V. E. Williams

Massachusetts Institute of Technology (1)
Department of Naval Architecture and Marine Engineering
Cambridge 39, Massachusetts

Director, University of Minnesota (1)
St. Anthony Falls Hydraulic Laboratory
Hennepin Island,
Minneapolis 14, Minnesota

Technical Research Group, Inc. (1)
2 Aerial Way
Syosset, New York

Chief of Naval Operations, (1)
Navy Department
Washington 25, D. C.
Attn: Capt. N. H. Fisher, OP-712

David Taylor Model Basin (1)
High Speed Phenomena Division
Langley Field, Virginia
Attn: Mr. R. E. Olsen

Aerojet General Corporation (1)
Azusa, California
Attn: Mr. J. Levy

U. S. Naval Ordnance Test Station (1)
Oceanic Research Group
3202 E. Foothill Blvd.
Pasadena, California

Lockheed Aircraft Corporation
Hydrodynamic Group
Sunnyvale, California
Attn: Mr. R. W. Kermeen

Radio Corporation of America (1)
Aerospace Communications and Controls Division
Burlington, Massachusetts
Attn: Mr. D. Wellinger

Autonetics (1)
9150 E. Imperial Highway
Downey, California
Attn: Mr. J. M. Johnson, Jr.
Dept. 3441-12

Avco Corporation (1)
Lycoming Division
550 South Main Street
Stratford, Connecticut

FMC Corporation (1)
Ordnance Division
1125 Coleman Avenue
San Jose, California

Grumman Aircraft Engineering Corporation (1)
Marine Engineering Section
Bethpage, Long Island, New York

Dynamic Developments, Inc. (1)
Midway Avenue
Babylon, Long Island, New York

University of California (1)
Institute of Engineering Research
Berkeley, California
Attn: Prof. R. Paulling

C 1924(100)